International Journal of Coal Geology 237 (2021) 103691

Contents lists available at ScienceDirect

International Journal of Coal Geology

journal homepage: www.elsevier.com/locate/coal

A multidisciplinary study and palaeoenvironmental interpretation of middle Miocene Keles lignite (Harmancık Basin, NW Turkey), with emphasis on syngenetic zeolite formation

Yakup Çelik [a], Ali Ihsan Karayigit [b,*], R. Görkem Oskay [c], Mine Sezgül Kayseri-Özer [d], Kimon Christanis [e], James C. Hower [f], Xavier Querol [g]

[a] İstanbul University-Cerrahpaşa, Department of Geological Engineering, 34500, Büyükçekmece, İstanbul, Turkey
[b] Hacettepe University, Department of Geological Engineering, 06800, Ankara, Turkey
[c] Hacettepe University Başkent OSB Technical Sciences Vocational School, Ankara, Turkey
[d] Dokuz Eylül University, Institute of Marine Science and Technology, İnciraltı, 35340 İzmir, Turkey
[e] University of Patras, Department of Geology, Rio-Patras, Greece
[f] University of Kentucky, Center for Applied Energy Research, 2540 Research Park Drive, Lexington, KY 40511, United States
[g] Institute of Environmental Assessment and Water Research, IDAEA-CSIC, C/Jordi Girona 18-26, 08034 Barcelona, Spain

ARTICLE INFO

Keywords:
Coal facies
Boron
Vegetation
Diatomite
Zeolite
Miocene
Turkey

ABSTRACT

The Harmancık Basin, in the north-easternmost Miocene graben in western Anatolia, hosts a 12.6-m-thick coal seam located in the Keles coalfield, in which coals are being exploited by open-cast mining methods. Syngenetic clinoptilolite/heulandite-type zeolite formation in the upper part of coal seam and carbonaceous clayey diatomite as a roof rock have been identified for the first time, and the palaeoenviromental reconstruction of the coal seam was conducted using a multidisciplinary approach. The coal facies and palynological data show that vegetation and depositional changes took place during the middle Miocene, which resulted in vertical variations in elemental and mineralogical compositions. During the initial stages of mire development woody vegetation (e.g. pollen with affinity to Cupressaceae) prevailed, telmatic conditions were common, and preservation of organic matter was high due to anoxic conditions. Thus, relatively low-ash yield was observed in the lower and middle parts of the coal seam. Furthermore, the presence of kaolinite and smectite-type clay mineral aggregates in these parts of the coal seam suggests that alteration of synchronous volcanic inputs took place under weak acidic to neutral conditions. In contrast, limnotelmatic conditions prevailed during the late stages of peat-accumulation, and macrophytes coinciding with herbaceous peat-forming vegetation (e.g. Osmundaceae, Polypodiaceae, and Nymphaeaceae) were dominant. The elevated Gelification Index (GI) values in the uppermost parts of the coal seam could be related to development of alkaline conditions in the palaeomires, which also caused formation of syngenetic clinoptilolite/heulandite-type zeolite from the alkaline activations of synchronous volcanic inputs. Even though palynological data points to the prevalence of freshwater conditions during peat-accumulation, B enrichments along Sr/Ba ratio higher than 1.0 could point to possible marine influence; however, no Neogene marine deposits have been identified in the Harmacik Basin. Nevertheless, the SEM-EDX data show the presence of traceable Ba and Sr in clinoptilolite/heulandite grains, and Sr-bearing barite around feldspar grains in the studied samples from the upper parts of the coal seam. This implies K-feldspars and K-rich alkali-feldspars, derived from synchronous volcanic ash fall, altered under alkaline conditions. Moreover, alginite proportions increased towards the upper parts of the seam, while relatively high Hydrogen Index (HI) values were reached in the uppermost part of coal seam and carbonaceous clayey diatomite roof-rock sample. Furthermore, palynolgical data imply that vegetation changes towards the roof of the coal seam reflect the progressive development of more humid conditions and nutrient-rich surface waters, which favoured increased algal activity.

* Corresponding author.
E-mail address: aik@hacettepe.edu.tr (A.I. Karayigit).

https://doi.org/10.1016/j.coal.2021.103691
Received 6 November 2020; Received in revised form 22 January 2021; Accepted 22 January 2021
Available online 12 February 2021

1. Introduction

The elemental composition of coal has been widely studied by a number of researchers, particularly for environmental studies and more recently as a source for critical elements (e.g. Dai and Finkelman 2018; Dai et al. 2012, 2020a; Eskenazy et al. 1994; Finkelman et al. 1999, 2018; Hower et al., 1999, 2020a, b; Seredin et al. 2013; Spears and Zheng 1999). These studies show that potentially hazardous elements are mainly located in minerals contained in coal, and to a lesser extent in the organic fraction of coal. With the determination of elemental affinities in coal, suitable coal beneficiation and combustion methods can be designed. Besides sedimentological and palaeontological data, mineralogical compositions and elemental enrichments can help to deduce depositional conditions (e.g. redox, salinity, and hydrological conditions (e.g. Christanis et al. 1998; Dai et al., 2020b; Goodarzi and Swaine 1994; Hower et al. 2002; Karayigit et al., 2020a, b; Li et al., 2019; Spiro et al., 2019). Furthermore, mineralogical composition of cleat/fracture infilling in coal could allow to predict composition of infiltrated solutions into coal seams during the late syngenetic and diagenetic stages. For instance, the B contents of coal and Sr/Ba ratios may indicate marine influence in the palaeomire and/or saline water penetration into peat beds post-deposition, while syngenetic carbonate minerals mostly imply neutral to alkaline conditions during peat accumulation (Goodarzi and Swaine 1994; Hower et al. 2002; Karayigit et al., 2017a; Korisidis et al., 2019; Querol et al. 1996). Nevertheless, high B content as an indicator for marine influence should be supported by palaeontological evidence since high B contents were reported from non-marine sequences too (Celik et al., 2017; Karayigit et al. 2000, 2017a; Kear and Ross, 1961; Lynskey et al., 1984; Mackay and Wilson, 1978; Moore et al., 2005; Newman et al., 1997). Moreover, synchronous volcanic inputs (e.g. airfall ash/tephra) into the palaeomire can deposit distinct layers, which during diagenesis may result in altered tuff layers (e.g. tonstein). The alteration of these inputs, particularly volcanic glass, may result in the formation of various by-products dependant on redox conditions and hydrogeological regime within palaeomires (Arbuzov et al. 2016; Bohor and Triplehorn 1993; Dai et al., 2017; Spears and Arbuzov 2019; Whateley et al. 1996). Syngenetic kaolinite formation is mostly related with acidic conditions and an open hydrogeological system, whereas zeolite minerals are mostly formed under alkaline conditions during peat accumulation (Querol et al. 1997). Moreover, the geochemical composition of synchronous volcanic inputs could also control syngenetic kaolinite and zeolite formation (Querol et al. 1997). Therefore, elemental and mineralogical compositions of coal and former tuff layers could be useful parameters for better understanding conditions during peat accumulation and post-depositional alteration.

The estimated total coal resources of Turkey are around 16 Gt; and is mainly composed of low-rank coals with high ash yields, high total S contents, and low net calorific values; and the resource are mostly hosted in Cenozoic basins in western and central Turkey (Oskay et al. 2013). Additionally, Turkish Cenozoic coals are characterized by elevated concentrations of B, Cr, V, As, Ni, Mo, and U (Esenlik et al. 2006; Gürdal 2011; Karayigit et al. 2000, 2017b, 2019a, 2019b, 2020a, 2020b; Palmer et al. 2004; Querol et al. 1997). Furthermore, regional extensional tectonic regime, which caused formation of graben basins, and climate conditions (subtropical and humid climatic conditions) allowed peat accumulation under fluvio-lacustrine conditions during the early-middle Miocene (Ersoy et al. 2014; Kayseri-Özer 2017). Regional volcanic activities have also resulted in the formation of altered tuff layers within coal seams, and also several borate, zeolite, and clay deposits (e.g. Bigadiç and Emet Basins) (Gündoğdu et al., 1989, 1996; Helvacı and Alanso, 2000). Previous studies from coal seams and altered tuff layers within coal seams show that the parent Miocene age volcanic matter was mostly high-K calc-alkaline and alkaline in composition (Baş 1986; Ercan et al. 1997; Ersoy and Helvacı, 2016; Helvacı et al. 2017; Okay et al. 1998); however, there are distinct mineralogical differences among coal-bearing basins in the western and north-western central Turkey (Bechtel et al., 2014; Erkoyunlu et al. 2017, 2019; Karayigit et al., 2017a, b, 2020a; Oskay et al., 2019a; Querol et al. 1997; Toprak et al. 2015; Whateley and Tuncali 1995; Whateley et al., 1996). For instance, syngenetic kaolinite is dominant clay minerals in coal beds and altered tuff layers in western Anatolia (e.g. Soma Basin), while zeolite minerals are mostly reported in coal beds from north-western central Anatolia (e.g. Çayırhan, Koyunağılı, and Alpu Basins). The difference in mineralogical composition is presumably related to the establishment of different redox conditions and hydrogeological systems which allowed flushing ions and/or caused enrichment of certain ions into the palaeomires.

Although the majority of low-rank coal resources are hosted in the Plio-Pleistocene sedimentary basins (e.g. Afşin-Elbistan/K.Maras, Karapınar/Konya, and Kangal/Sivas) in central Turkey, several important Miocene coal seams are located within graben basins in western Anatolia (Karayigit and Gayer 2000; Karayigit et al. 2000, 2017a, 2019a; Oskay et al. 2016; Palmer et al. 2004). The Harmancık, Seyitömer, and Domaniç-Tunçbilek basins, are examples of Miocene coal-bearing fluvio-lacustrine sequences interlayered with volcanic rocks in western Anatolia (Celik 2005; Helvacı et al. 2017; Oskay et al. 2013) (Fig. 1). The Keles coalfield is located in the Harmancık Basin (Fig. 1), and the initial mineable coal reserves total ca. 70 Mt. This resource has been exploited since the late 1980's, applying open-cast mining techniques in order to support the nearby Orhaneli power plant and, in the near future, the under-construction Keles power plant. The Neogene coal seams have been known since the 1960's; to date, the limited number of studies have been focused on regional geology, tectonic evolution, and geochemistry of volcanic units in the adjacent areas of the Keles coalfield (Baş 1986; Ersoy and Helvacı, 2016; Helvacı et al. 2017). No coal petrography, mineralogy and geochemistry, or palynological and sedimentological studies of the Keles coal-bearing sequence have been reported to date. The aim of this study is (1) to identify coal petrographical, mineralogical, geochemical, and sedimentological characteristics of the Keles coalfield, (2) to ascertain controlling factors on elemental enrichments, (3) to elucidate the evolution of the palaeoclimate and the development of palaeovegetation during peat-accumulation, and (4) to reconstruct depositional conditions in the palaeomires in the Keles coalfield. Since the Keles coalfield has similar geological background with Tunçbilek (Domaniç Basin) and Seyitömer (Seyitömer Basin) coalfields, the specific purpose of the study is to compare mineralogical and geochemical features of all these coalfields.

2. Geological Setting

The Harmancık Basin, the north-easternmost of the Miocene grabens in western Anatolia, is a NE-SW-trending basin (Celik 2005; Helvacı et al. 2017) (Figs. 1 and 2a). The pre-Neogene basement and margins of the basin are exclusively composed of metamorphic rocks of the Tavşanlı Zone on the northern margins, while ophiolites are widely exposed in the southern margins (Fig. 1), as in the Domaninç-Tunçbilek and Seyitömer Basins (Celik and Karayigit 2004a, 2004b; Karayigit and Celik 2003). In contrast with coalfields in the Tunçbilek and Seyitömer basins, the pre-Neogene basement and marginal rocks in the Keles coalfield are composed of metamorphic rocks of the Tavşanlı Zone (Fig. 2a). The Miocene basinal infillings of the Harmancık Basin are about 600-m thick. Deposition commenced with alluvial fan sediments represented by reddish and poor-sorted basal conglomerates with mudstone intercalations; the clastic sediments are transitional laterally and vertically to fluvial deposits, which are mainly cross-bedded sandstone, channel fill conglomerate, and mudstone with thin coal layers (Unit 1) (Figs. 2b and 3). The basal conglomerate of this unit widely outcrops near the margins of the Harmancık Basin, while fluvial sediments outcrop mostly in the central and eastern parts (Fig. 2a). Lacustrine conditions during the early-middle Miocene became dominant within grabensin western Turkey (Baş 1986; Ersoy et al. 2014; Celik and Karayigit et al., 2004a, b; Helvacı et al. 2017; Karayigit et al., 2017a, b,

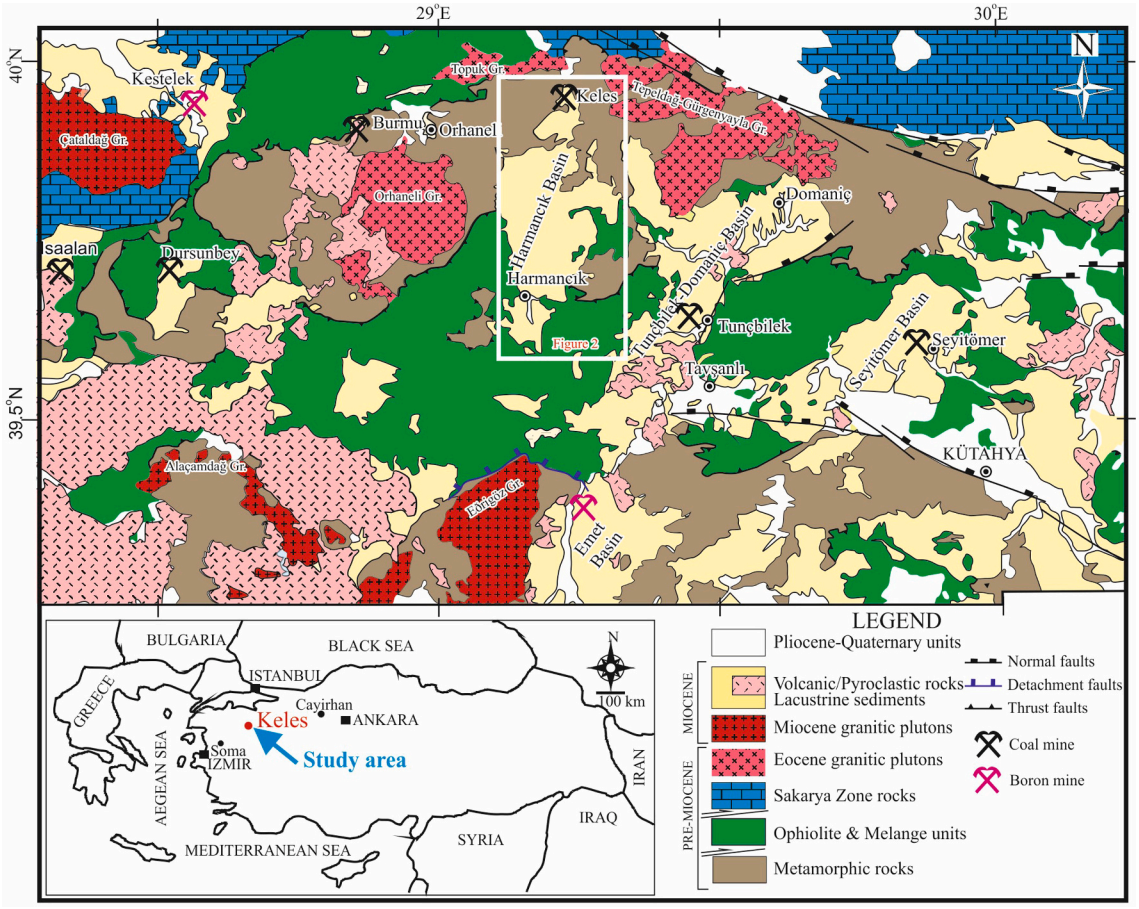

Fig. 1. Geological map of the Harmancık Basin and its surroundings (quadrilateral area is representing Fig. 2a; modified from Celik and Karayigit, 2004a, b, and Helvacı et al. 2017).

2020a). Similarly, in the Harmancık Basin, Unit-1 transitions to coal-bearing lacustrine and deltaic sediments (Unit-2). Unit-2 commences with claystone, coal, diatomite, and mudstone, overlain by marl and limestone (Figs. 2b and 3). The upper parts of this Miocene basinal infilling sequence transitions to an alternation of fan delta (conglomerate-sandstone-mudstone) and lacustrine sedimentary rocks (clayey limestone-marl with tuffite-claystone) (Fig. 2b). In the southern parts of the Harmancık Basin, Miocene andesite and basalts are also observed within sediments of Unit-2 (Fig. 2a). The Miocene coal-bearing basinal infilling of the basin is overlain unconformably by Quaternary unconsolidated sediments (Fig. 2b).

3. Material and methods

A total of eighteen (thirteen coal, one roof rock and one floor rock, and three intercalation (claystone)) samples were taken from a 14-m high face with a 12.5 m thick seam (Figs. 2c and 4). The coal lithotype were logged according to the nomenclature adopted by the International Committee for Coal and Organic Petrology (ICCP, 1993). For lithotype definition, macroscopically idenitified features (e.g. colour, gelification and structure) of 10 cm widths were noted, and low-rank coal lithotypes (e.g. matrix) were applied in the studied coal seam. The standard sedimentary facies are described based on Miall's classification (Miall 1977, 1978, 1985, 1996). Sedimentary facies are grouped into associations representing distinct depositional environments.

The proximate and ultimate analyses, as well as the determination of the gross calorific values of the coal samples were conducted following the related American Society for Testing and Materials (ASTM) (D3175, 2020; D3174, 2012; D3302, 2019; D5373, 2016) at Hacettepe University (Ankara, Turkey) using LECO TGA-601, SC-144DR, TruSpec, and AC 350 instruments. Polished blocks were prepared from crushed coal samples (Ø < 1 mm) according to ASTM D2797/D2797M (2011) and examined using a Leica DM4000M microscope under both white incident light and blue-light excitation at Hacettepe University. The maceral nomenclature followed the ICCP System 1994 (ICCP, 2001; Pickel et al., 2017; Sýkorová et al. 2005). The random huminite reflectance was measured on ulminite B according to the International Organization for Standardization (ISO) 7404–5 (2009) standard. The mineralogical compositions of raw coal samples and low temperature (450°C) coal ashes, and inorganic samples were determined using X-ray powder diffraction (XRD) with a Cu anode tube at at both İstanbul and Hacettepe Universities. The scanning area covered the 2θ interval between 4° and 70°, with a scanning angle step of 0.015°, and a time step of 1 s. The clay fraction analysis (XRD-CF) was also determined on selected raw coal and inorganic samples at İstanbul University following the methodology proposed by Poppe et al. (2001). Thirteen coal samples and one roof rock sample (K-18) were analyzed applying FT-IR (Fourier transform-infrared spectrometry; raw samples for FT-IR measurements were ground to less than 250 μm, and measurements were carried out using a PerkinElmer Spectrum Two FT-IR equipment. Absorbance data were collected in a spectral range of 4000-400 cm-1. The software of FT-IR machine does not allow evaluation of absorbance peak integration areas; thus, limited identifications can be applied on the sample spectra. More information about the applied method can be found in Chen et al. (2015). Furthermore, for better additional information regarding to mineralogical composition, eight selected coal samples (K-2, -3, -4, -6, -8, -11, -14, -15 and -17) coated with carbon and one roof rock sample (K-18) coated with palladium were examined under a Carl Zeiss EVO-50

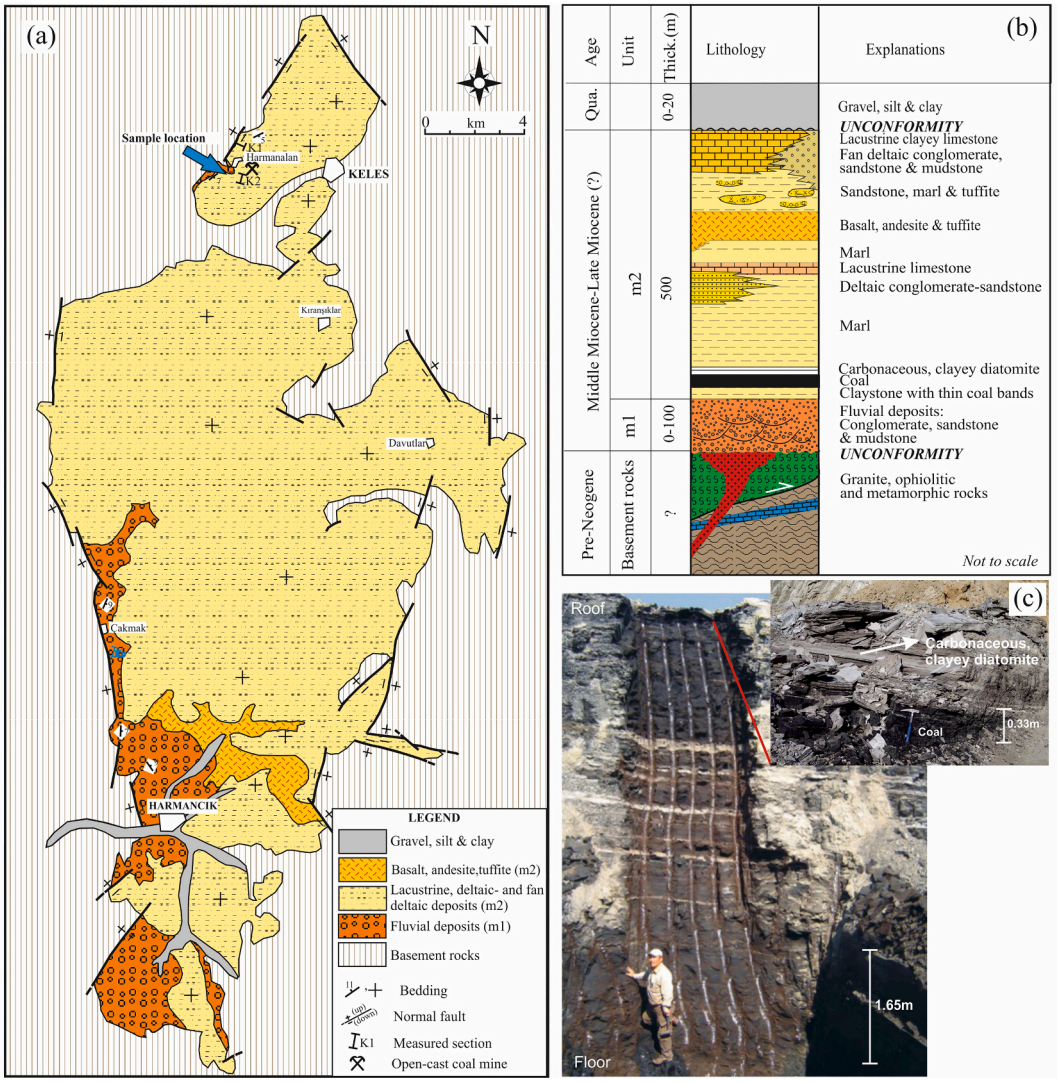

Fig. 2. (a) Geological map and (b) stratigraphic column of the study area, and (c) General view of the working coal seam.

EP type SEM-EDX.

The Rock-Eval pyrolysis of the studied roof rock and coal samples was performed in order to determine the total organic carbon (TOC), T_{max}, hydrogen index (HI), oxygen index (OI), residual carbon (RC), pyrolyzed carbon (PC), and mineral carbon (MINC) values using the Rock-Eval 6 analyzer at the Research and Development Laboratory of the Turkish Petroleum Co. (TPAO) according to the procedure described by Espitalié et al. (1977a, b). The IFP 160000 standard material was also used to determine the accuracy of the pyrolytical analyses.

The Si content of the coal samples was determined from ashed coal samples at 750°C using X-ray fluorescence (XRF) equipment according to ASTM D4326 (2011) standard at University of Kentucky (Lexington, USA), and the results converted to whole coal basis. The contents of Ti, Al, Fe, Mg, Ca, Na, and K were determined using inductively coupled plasma atomic emission spectrometry (ICP-AES) at the Institute of Environmental Assessment and Water Research (IDAEA) (Barcelona, Spain). The minor and trace element compositions of coal samples were determined applying an inductively coupled plasma mass spectrometry (ICP-MS) at the IDAEA. The whole-coal samples were digested following a two-step acid-digestion method described in detail by Querol et al. (1997). The accuracy of analysis and digestion method were checked using reagent blanks and standard reference materials SARM 19 (South African coal, Council for Mineral Technology). The Hg contents of coal samples were determined using an AMA254 Advanced Mercury Analyzer at the University of Kentucky.

In this study, nine selected coal samples (K-3, 4, -5, -6, -9, -11, -15, -16 and -17) were palynologically studied (Fig. 4). Taxonomic identifications of the fossil spores and pollen were based on published atlases and sporomorph keys (Akgün et al. 2007; Biltekin et al. 2015; Bouchal et al. 2017; Bruch and Gabrialyan, 2002; Bruch et al. 2002, 2004, 2006; Güner et al. 2017; Ivanov and Lazarova, 2005; Ivanov and Lazarova, 2019; Ivanov et al. 2002, 2007a, 2007b; Ivanov et al., 2010; Kayseri and Akgün 2008; Kayseri-Özer et al., 2014b, a; Kayseri-Özer 2014, 2017; Mosbrugger and Utescher 1997; Uhl et al. 2003; Utescher et al., 2007a, b, 2009a, 2009b, 2014; Yavuz et al., 2017). The studied samples were prepared based on the standard technique (hydrochloric acid (HCl), hydrofluoric acid (HF), potassium hydroxide (KOH), and heavy liquid separation ($ZnCl_2$) and were stored in glycerin) for disintegrating Neogene sediments (Erdtman 1966). The TGView 2.0.2 (Grimm 2004) and TILIA 2.0.b.4 (Grimm 1991) software programs were used to construct the diagrams (Grimm 1987). Cluster analysis was obtained with CONISS (Grimm 1987). Palaeoclimatic interpretation was based on the climate preferences of plants (Bruch et al., 2004; Mosbrugger and Utescher 1997). Moreover, the fossil plants were grouped based on their ecological preferences following Jiménez-Moreno (2005, 2006), Jiménez-Moreno et al. (2005, 2007a, b, 2008), Nix (1982), and Suc

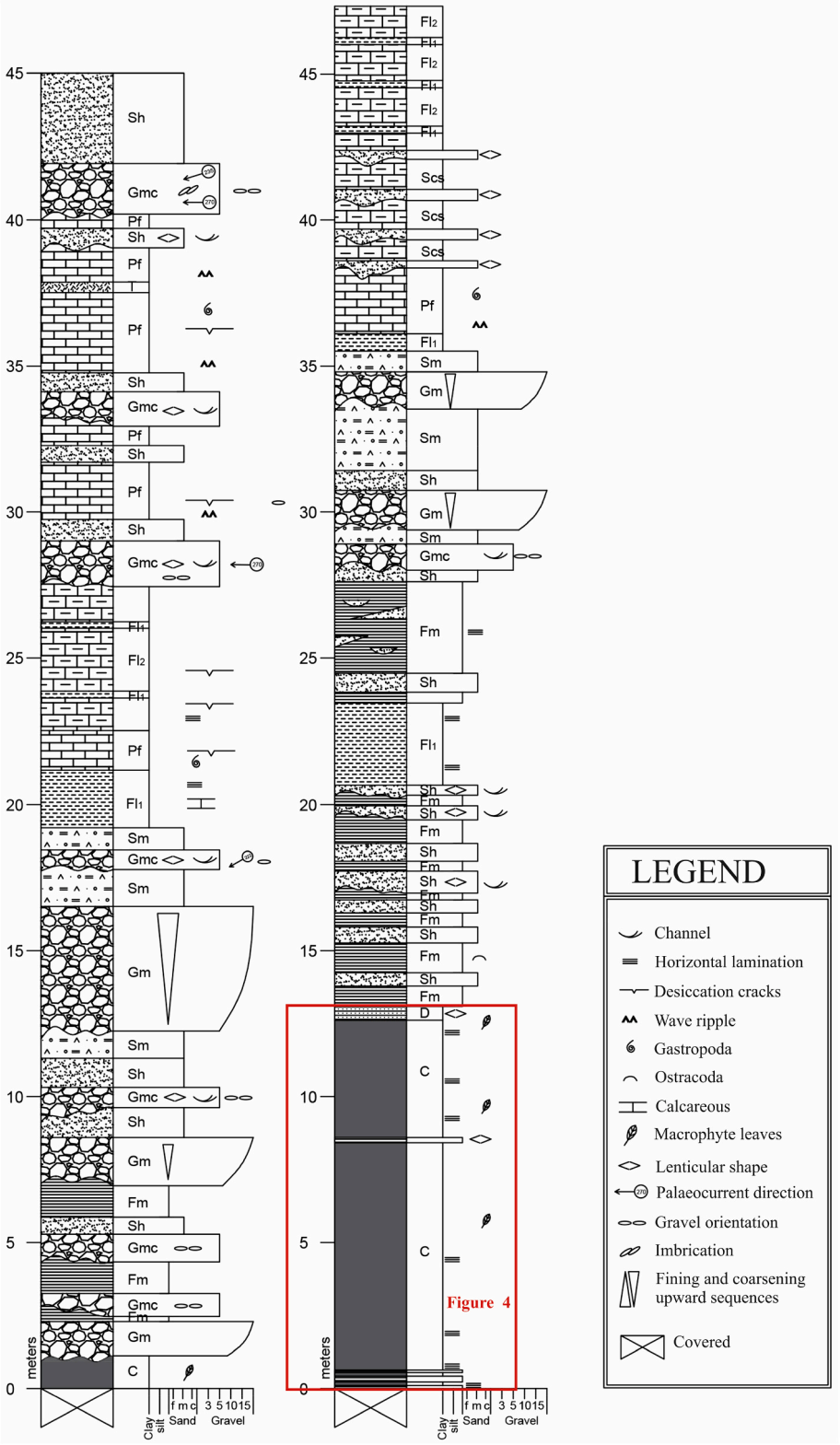

Fig. 3. Measured stratigraphic sections from the Keles coalfield.

(1984), and information about vegetative change has also been obtained. For this aim, the following groups are distinguished by researchers: (1) Mega-mesothermic (subtropical) elements (Cupressaceae, Cupressaceae-Taxodioideae-*Glyptostrobus*, *Engelhardia, Myrica,* Sapotaceae, *Castanea-Castanopsis* type, and Cyrillaceae-Clethraceae); (2) Helophytes (Typhaceae-*Sparganium* and Nymphaeaceae); (3) *Cathaya* (pollen of *Cathaya* sp.); (4) Mesothermic (warm temperate) elements (*Quercus*, *Carya*, *Pterocarya, Carpinus*, *Juglans*, *Zelkova*, *Ulmus*, *Tilia*, *Acer*, *Alnus, Salix*, *Nyssa*, *Sequoia*-type and *Fagus)*; (5) *Pinus*+ Pinaceae (*Pinus diploxylon* and *haploxylon* types and undetermined Pinaceae pollen); (6) Mid-altitude trees (Meso-microthermic elements) (*Cedrus);* (7) High-altitude trees (microthermic elements) (*Abies* and *Picea*); (8)

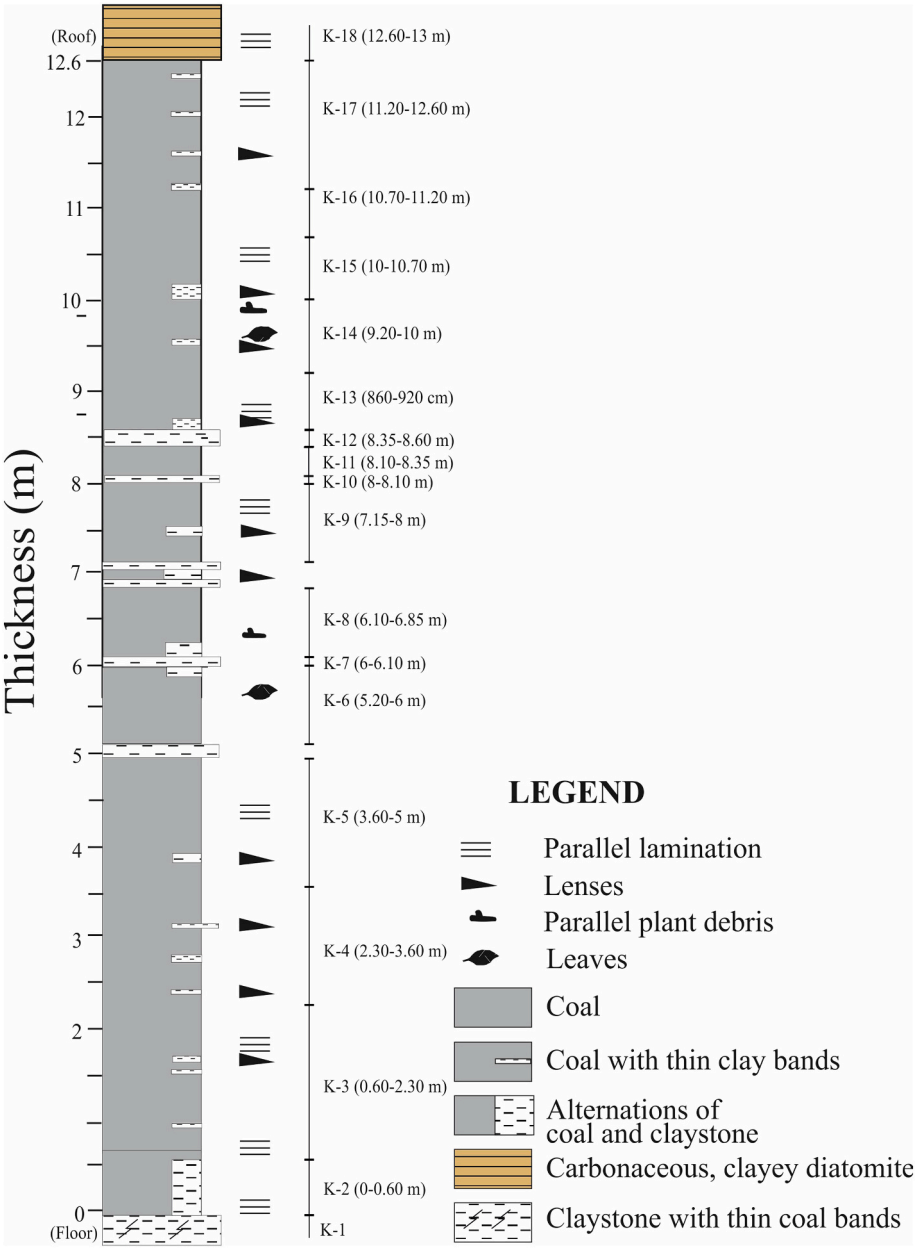

Fig. 4. The sampling profile.

Xerophytes:xerophyte taxa (e.g. *Quercus ilex-coccifera* (evergreen) type and Oleaceae-*Olea*); (9) Herbs and Shurbs (Poaceae, Onagraceae and Asteraceae-Asteroideae); (10) Steppe elements (Ephedraceae). A brief analysis of the diatom flora from one roof rock sample (K-18) was conducted using SEM-BSE images from a palladium coated polished block, with identification genus stage.

Paleoclimate reconstructions are supported by the numerical climatic values calculated by the Coexistence Approach Method (CoA) (Mosbrugger and Utescher 1997). The coexistence intervals for each climatic parameter were calculated using the software Clim-Stat 1.02 and Palaeoflora Database (Mosbrugger and Utescher, 1997; Utescher et al., 2014). The analysis of Keles coalfield palynoflora used four main climatic parameters, namely mean annual temperature (MAT), mean temperature of the coldest month (CMT), mean temperature of the warmest month (WMT), and mean annual precipitation (MAP).

4. Results

4.1. Sedimentological descriptions

On the basis of stratigraphical and sedimentological features of dominant grain-size class, texture, stratification, degree of clast rounding and sorting, twelve facies were defined in the Keles coal-bearing sequence (Table 1, Fig. 3): (1) matrix-supported blocky conglomerate (Gm); (2) clast-supported conglomerate (Gmc); (3) horizontal stratified sandstone (Sh); (4) tuffaceous sandstone (Sm); (5) sandstone and marl alternation (Scs); (6) organic-rich mudstone (Fm); (7) calcareous claystone (Fl1); (8) limestone (Pf); (9) marl (Fl2); (10) coal (C); (11) carbonaceous clayey diatomite (D); and (12) tuff (T) (Table 1 and Fig. 3). The facies were grouped into four facies associations; the concepts of facies and facies associations are according to Miall (1992), Reading (1996), and Rust (1982).

The facies association 1 (FA1) consists of the Gm, Gmc, Sh, and Sm facies (Table 1). This fining-upward sequence begins with erosive

Table 1
Facies description in this study and facies code based on Miall (1978, 1996).

Facies	Description	Interpretation
Matrix-supported blocky conglomerate (Gm)	Matrix supported, angular to subrounded, poorly sorted, irregular stratification up to 4-m thick, gravels 10-75 cm, erosive base, units up to 4.2 m, sand-silt mixture matrices, inverse grading	Cohesive debris flow deposits proximal or mid parts of alluvial fans (Reading, 1996)
Clast-supported conglomerate (Gmc)	Clast to partly matrix supported, angular to subrounded, horizontal stratification, gravels up to 5 cm, erosive base, units up to 1.5 m, normal or inverse grading, regularly imbricated	Braided channel and bar deposits middle parts of alluvial systems (Miall 1996)
Horizontal-stratified sandstone (Sh)	Laminated, fine to medium grained sandstone, well sorted, sheet-like beds, layers 5 – 10-cm thick, units up to 3 m	Down on the floodplains deposits of a distal alluvial-fan setting or delta plain deposits of a lacustrine delta system (Miall 1992, 1996; Rust, 1982)
Tuffaceous sandstone (Sm)	Fine to coarse grained, mostly tuffaceous material, massive layers, inversely or normally graded, units up to 1.5 m.	Flat alluvial or deltaic deposits, near lake margins deposits.
Sandstone and marl alternations (Scs)	Ripple and low-angle cross stratification, Sandstone layers 20 – 30-cm thick, units up to 4.5 m.	Progradation on small deltaic lobes in flat marginall lacustrine zone.
Organic-rich mudstone (Fm)	Laminated, massive to fine layers, with sandy banded, coal and plant fragments, rarely carbonate nodules.	Mire deposits or lake shore
Calcareous claystone (Fl1)	Laminated, grey-green colors, alternation with marl.	Shallow lacustrine
Limestone (Pf)	Laminated, with ripple and desiccation cracks and ostracods and gastropods, the limestone overlain or interstratified with carbonaceous claystone, 10-20 cm thick	Shallow lacustrine to palustrine
Marl (Fl2)	Laminated, gray-green, rarely with gastropod and ostracods fossils, units up to 1-2 m.	Low energy lacustrine areas with terrigenous input
Coal (C)	Lignite, 5.5-14-m thick, massive or stratified intercalating with thin claystone	Mire / swamp
Carbonaceous clayey diatomite (D)	Laminated, the diatomite overlays coal Laminated, unit up to 30 cm intercalating with limestone. It occurs locally with limestone	Diatomaceous muds were deposited during the early beginning of the lake as a fresh water system.
Tuff (T)		Tuff associated with the limestone formed during ash air-fall in lacustrine facies; air-fall ash/tephra deposits

contacts. This consists mainly of clastic facies with thickness from 50 to 420 cm (Table 1). This association occurs cyclically and suggests boulder, gravel, and sand deposition in the braided bar and channel systems of an alluvial fan that reached the lacustrine margin area. Features of the alluvial fan conglomerates include the 10- to 75-cm clast size and the local debris-flow events. Moreover, the occurrence of these deposits were observed to cut the finer facies of FA 2 on the lacustrine margin areas. They may be interpreted as a facies deposited on a rather flat area covered by alluvial fans in lake margin areas and palustrine environments. Palaeocurrents inferred from the conglomerate clast imbrication suggest that the source of alluvial sediments was located to the NE-E of the Keles coalfield. The Facies association 2 (FA-2) is composed of the Fm, C, and D facies (Table 1), and is characterized by the occurrence of coal seam alternating with claystone layers (Fig. 3). The coal seam is built of organic-rich mudstone (Fm), carbonaceous clayey diatomite (D), and coal seams. The thickness of the coal seam in this association varies from 5.5 to 14 m, and contains intercalations. *In situ* tree stumps, pyrite, as well as carbonate concretions are also observed in the Keles coalfield. The deposits of this facies association indicate a high-rate of phytogenic accumulation with a variable supply of clastic material. FA2 sequence was deposited in mires or along lake shores during the early onset of the lacustrine conditions.

The facies association 3 (FA-3), dominated by Pf and Fl2 facies (Table 1), consists mainly of horizontally laminated limestone (Pf) and marl (Fl2) with wave ripples, desiccation cracks, as well as ostracods and gastropods remains. This is a complex association formed of claystone, marl, limestone, and tuffaceous facies. It began with low-energy deposition on a lacustrine margin area. It continued with carbonate deposits which were deposited in lake marginal areas affected by waves (Pf). The sequence of FA3 represents an overall shallowing, implying a change from lacustrine-palustrine to shallow lacustrine conditions. Moreover, this facies association is closely related to the small deltaic systems environment (FA-1 and -4) and is connected with the fan deltaic facies.

The facies association 4 (FA-4) is composed of the Scs facies (Table 1), and is characterized by the occurrence of sandstone- and marl-alternations (Fig. 3). The deposits of this facies association typically cap coarsening-upward units. Marl represents evidence of a water body with carbonate deposition. Hence, this association is a progradation of the alluvial channel system as it entered a shallow lake in the form of a small delta. Overall, identified facies associations recognized in Keles coal-bearing sediments, comprise sediments deposited in braided bars and channels of alluvial fans, mires, shallow lakes, and small deltaic systems in a shallow lake.

4.2. Macroscopic features and standard coal characteristics

The studied coal samples appear greyish black and black in colour in the upper part of the seam and dark brown-brown colour in the lower parts (Fig. 2c). The mineral-rich coal samples are composed of clayey bands, with lenses thicker than 10 mm. This lithotype was identified in the lowest part of seam. The xylite-rich coal samples generally consist of brown-coloured bands with plant remains and are mainly identified in the central parts of seam. In addition, clayey bands thinner than 1 mm were identified from some xylite-rich coal samples. The matrix coal samples are black in colour with ungelified humic masses and are common in the upper part. The roof rock sample is greyish in coloured and laminated, and contains coal fragments and carbonaceous plant remains, while the floor rock sample is a black, organic-rich claystone. The intercalation samples are mostly beige-coloured, sandy-silty claystone (Fig. 4).

The studied samples are generally characterized by low ash yield (avg. 19.1%, on dry basis), and high gross calorific values (avg. 20.7 MJ/kg, db), total C (avg. 55.7%, db), and H contents (avg. 6.0%, db) (Table 2). Although ultimate analysis of coal samples does not provide evidence for significant vertical elemental changes, the ash yield follows anupward increase. In turn, the gross calorific value decreases upwards stratigraphically (Fig. 5). These differences are presumably related with the presence of a clay band-bearing xylite-rich coal lithotype in the lower seam part. Furthermore, coal samples from the upper part are depleted in S compared with the lower ones. Moreover, the ash yield, the gross calorific value, and the total C and H contents of the roof (sample K-18) are 69.3%, 6.4 MJ/kg, 16.0%, and 2.4% (on dry basis), respectively (Table 2). The relatively high gross calorific values and total C contents might be related to the presence of coal fragments and carbonaceous plant remains in this sample (Table 2).

Table 2
The results of proximateand ulimate analyses, and the calorific value determination of the Keles coal samples and roof rock sample heulandite (VM: volatile matter, GCV: gross calorific value; as-rec: as-received basis; db: dry basis; MC: matrix coal, MR: mineral-rich coal; XC: xylite-rich coal).

Sample	Thickness (m)	Lithology	Moisture (wt%, as-rec)	Ash	VM	GCV (db, MJ/kg)	C	H	N	S
				(wt%, db)				(wt%, db)		
K-18	12.6-13.0	Diatomite	4.4	69.3	26.7	6.4	16.0	2.4	0.6	2.8
K-17	11.2-12.6	MC	12.0	14.9	53.7	22.7	59.5	7.1	1.8	1.3
K-16	11.2-10.7	MC	11.8	18.6	50.0	21.0	56.3	6.5	1.7	1.3
K-15	10.7-10.0	MC	11.3	29.2	43.6	17.4	47.7	4.8	1.4	1.6
K-14	10.0-9.2	MC	12.4	19.7	47.5	20.5	55.4	6.0	1.5	1.4
K-13	9.2-8.6	MC	10.9	26.2	45.5	19.0	50.8	5.5	1.3	1.5
K-11	8.1-8.4	XC	11.8	14.7	51.3	22.2	59.3	6.5	1.2	1.6
K-9	7.2-8.0	XC	11.2	16.4	50.6	21.7	58.1	6.4	1.4	2.1
K-8	6.9-6.1	XC	10.6	22.7	48.0	20.1	53.5	5.7	1.4	1.8
K-6	6.0-5.2	XC	11.4	17.6	50.5	20.6	56.4	5.6	1.2	1.9
K-5	5.0-3.6	XC	12.1	15.7	50.4	21.2	57.6	6.2	1.4	1.3
K-4	3.6-2.3	XC	12.0	12.6	51.7	22.9	61.0	6.3	1.3	1.5
K-3	2.3-0.6	XC	12.1	13.7	51.1	21.7	59.3	6.5	1.4	1.3
K-2	0.6-0.0	MR	6.7	49.8	33.3	11.2	31.3	3.0	0.5	3.0

4.3. Maceral composition

The coal-petrography analysis results show that huminite is the predominant maceral group in the Keles coal samples, while inertinite and liptinite display variable proportions (Table 3). Telohuminite is the dominant huminite maceral subgroup in the lower parts of the seam, and its proportion display a decreasing trend up the stratigraphic section (Fig. 5). In contrast, the detrohuminite subgroup is more common in the upper parts and increases upwards stratigraphically (Fig. 5). Textinite contents are generally more common in the xylite-rich coal lithotype samples, whereas ulminite is the most common telohuminite subgroup maceral in all the samples (Fig. 6a-b). Densinite is the predominant detrohuminite maceral with sporinite and liptodetrinite embedded within densinite (Fig. 6c-d). Aside from one sample (K-2), the proportion of attrinite on whole coal basis is less than 10 vol.%, and mostly associated with clays and liptodetrinite (Fig. 7c and e). Corpohuminite is mostly observed as cell-lumen infillings of textinite (Fig. 6e-f), and, in some cases, as resino-corpohuminite. Furthermore, levigelinite is more common in the upper parts of seam (Fig. 6b-c). Gelohuminite proportions are similar throughout the entire seam; nevertheless, levigelinite content increase upwards stratigraphically. Porigelinite occurs sporadically associated with telohuminite macerals. In some samples, telohuminite A variety and resino-corpohuminite display a brownish fluorescence, and this feature is related to the presence of H-rich compounds (e.g. resin, tannin, and cellulose) in telohuminite macerals and corpohuminite (Kus et al., 2020; Oskay et al. 2016; Querol et al. 1996).

Sporinite is the common liptinite maceral in the Keles samples (Figs. 6c-d and 7a-b), with liptodetrinite and resinite also being identified (Table 3). As mentioned above, sporinite and liptodetrinite are mostly associated with detrohuminite macerals and clays (Fig. 6c-d). Resinite is generally observed within cell-lumens of textinite, and fluorinite-type resinite was observed in some samples. Furthermore, in some samples from the upper parts of seam alginite (presumably *Botryococcus*) is observed within detrohuminite macerals and clays (Fig. 7b-c). Inertinite displays low proportions, with inertodetrinite, funginite, and fusinite being commonly identified (Figs. 6c-d and 7a).

The minerals identified under the microscope, are mainly clays, quartz, and pyrite (Figs. 6a, f and 7e). In addition, in some samples possible zeolite minerals were also identified (Fig. 7f). The mean random huminite reflectance (Rr) of the Keles coal varies between 0.29 and 0.31% (Table 3). Even though, no detailed organic-petrographical examination was conducted from roof rock (sample K-18) due to the high mineral content, sporinite and alginite are the most common macerals in this sample, and they are associated with clays, as in coal samples. Furthermore, in this sample diatom remains are commonly identified.

4.4. Mineralogy

The minerals identified by XRD from the raw and ashed coal samples and from sediment samples are clay minerals, quartz, feldspar, and gypsum (Table 4). Pyrite is detected in a few coal and inorganic samples by XRD. Furthermore, clinoptilolite/heulandite is detected in raw coal samples (K-13, -14, -15, -16 and -17) from the upper parts of seam. Cristobalite is detected from one coal (K-6) and one intercalation (K-12) sample. Anhydrite and szomolnokite are identified in coal ash. Clay minerals are generally the dominant to abundant phase in the coal samples from the lower seam part and feldspars are more abundant in the upper part. The XRD-CF data proved that smectite is the abundant clay mineral in the lower part of the seam, kaolinite and illite are also traced in the lower part, whilst zeolite minerals are only identified in the upper seam part (Table 4). In addition, apatite, barite, calcite, chalcopyrite, celestine, dolomite, Ti-oxides, and zircon in coal samples, and szomolnokite in roof rock sample (K-18) are identified as micron-size accessory mineral by SEM-EDX (Table 4). The SEM-EDX data from the roof rock sample (K-18) also show the common presence of diatom remains, suggesting the roof sample could be classified as carbonaceous clayey diatomite

4.5. FT-IR analysis

The representative FT-IR spectra of selected coal samples (K-2, -3, -15, and -17) are reported in Figure 8a and diatomite sample (K-18) in Figure 8b. The bands at 3700, 1010, 910, and 528 cm^{-1} originate from Si-O-Al^{VI} vibrations (Madejova, 2003). These bands could be attributed to clay minerals, and considering the XRD-CF results of selected coal samples, the band around 3700 cm^{-1} might be attributed to kaolinite and illite (Georgakopoulos et al. 2003; Madejova, 2003; Öztaş and Yürüm 2000). The bands around 1110 and 470 cm^{-1}, attributed to the Si-O-Si bending vibrations, could represent quartz in the studied coal and diatomite samples (Çetinkaya and Yürüm 2000; Georgakopoulos et al. 2003; Ilia et al. 2009).

The FT-IR spectra of Keles coal samples are characteristic for low-rank coals (Fig. 8a) (Baysal et al. 2016; Chen et al. 2015; Georgakopoulos et al. 2003; Oikonomopoulos et al., 2013). Although different coal lithotypes were logged at the sampling site, the FT-IR spectra of the bulk coal samples display similarities (Fig. 8). The only minor difference among coal samples is observed in the mineral-rich sample (K-2) where clay minerals display a relatively distinct peak at 1010 cm^{-1} (Fig. 8a). The sample K-18, on the other hand, demonstrates a distinct peak around 1100 cm^{-1} (Fig. 8b). This band could be attributed to Si–O_{apical} streching vibration; a similar intense peak around 1100 cm^{-1} was reported from FT-IR spectra of diatomites from northern Greece (Ilia et al. 2009). Therefore, the identified distinct peak could correspond to

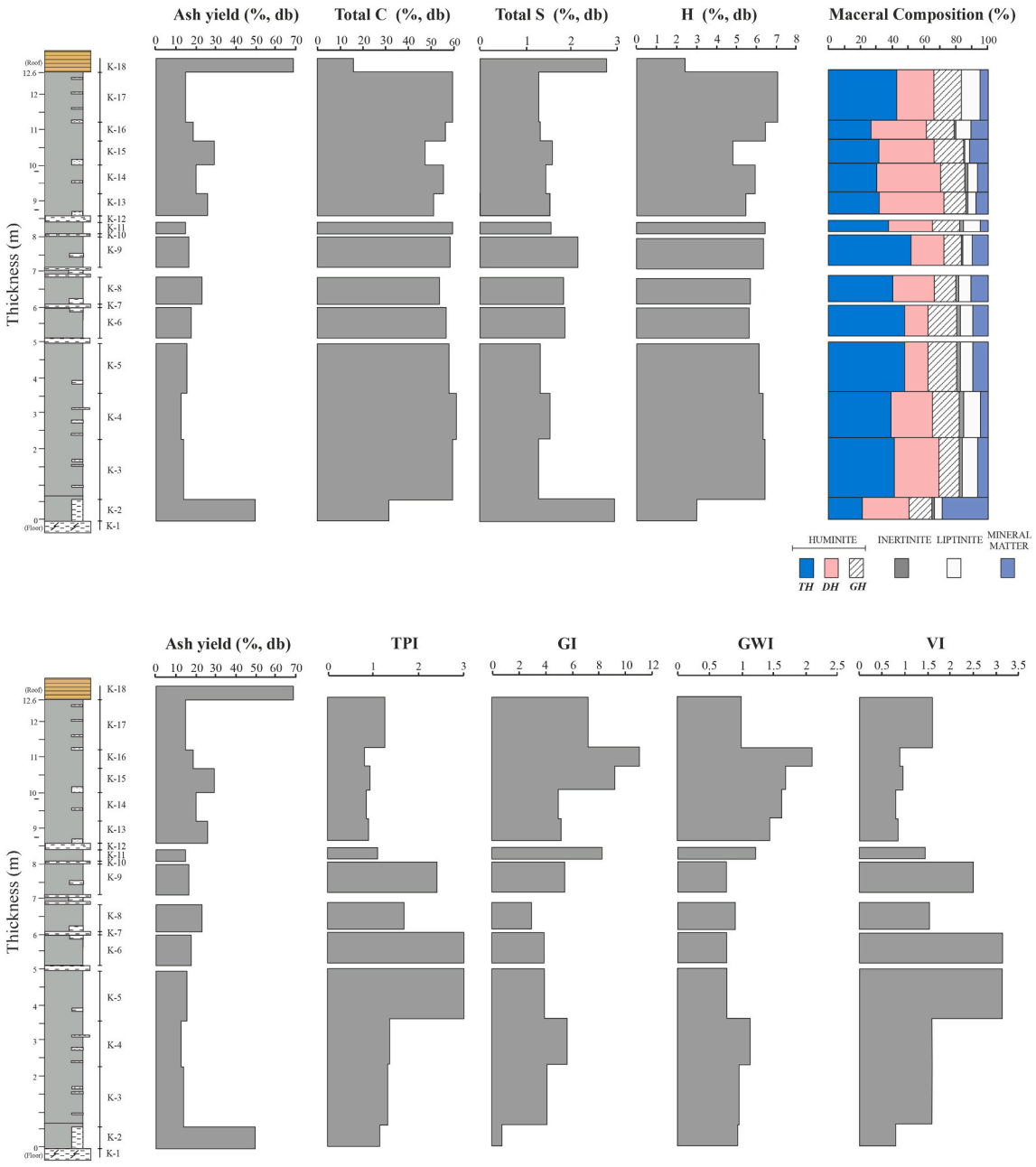

Fig. 5. Vertical distribution of ash yield, total C, H, S, and maceral contents as well as of the coal facies indices through the Keles coal profile (for legend of lithostratigraphic column, see Fig. 4).

diatoms included in sample K-18.

4.6. Rock-Eval pyrolysis and total organic carbon

The Rock-Eval pyrolysis analysis results show that the S_1, S_2, S_3, and TOC values of the studied coal samples are variable. Such variations are expectable for humic coals due to the heterogeneous nature of organic matter and variable ash yields (Petersen 2006). The S_1, S_2, and S_3 values of coal samples vary between 0.8 and 2.8 mg HC/g rock, 46.0 and 120.6 HC/g rock, and 20.1 and 39.8 CO_2/g rock (Table 5), respectively. The TOC contents display an upward decreasing trend, in parallel with ash yields, and range from 28.1 to 50.3 wt.% (Table 5). In addition, S_1, S_2, and S_3 values and TOC contents of the roof sample (K-18) are 2.5 HC/g rock, 89.9 HC/g rock, 6.2 CO_2/g rock, and 14.5 wt.% (Table 5), respectively. The T_{max} values show that the studied samples are mainly immature, and only one sample (K-17) has a T_{max} value (437°C) sufficient to pass the threshold for the early mature stage. In order to assess the kerogen types in the studied coal and roof rock samples, T_{max}, HI, and OI values were calculated from Rock-Eval pyrolysis results. The data on HI *vs* T_{max}, pseudo-van Krevelen, and S_2*vs* TOC diagrams are in agreement with maceral compositions. Type-III is also the most common kerogen in the coal samples (Figs. 9 and 10).

4.7. Elemental composition

The major elements in the studied samples on whole-coal basis are Si, Al, Fe, Mg, Ca, Na, and K, while the concentrations of Ba and Ti are higher than 1000 μg/g in certain samples (Table 6). The minor elements in coal samples (100–1000 μg/g) on whole-coal basis are B, Mn, Sr, and Ba, whereas concentration of P generally exceeds 100 μg/g in the middle part of seam. Beside V, Cr, Cu, Zn, Rb, Zr, Nb, and Ce, the average concentrations of trace elements in coal samples on whole-coal basis are

Table 3
Maceral composition (in vol.%) and reflectance (in %) of the Keles coal (MM: mineral matter, %Rr: random huminite reflectance, Stdev: standard deviation).

Maceral	Sample												
	K-17	K-16	K-15	K-14	K-13	K-11	K-9	K-8	K-6	K-5	K-4	K-3	K-2
Textinite	8.3	3.1	3.5	8.2	5.8	5.5	11.2	11.5	11.5	6.7	8.2	11.0	14.3
Ulminite	34.4	24.6	27.9	21.7	25.5	32.0	40.3	28.6	35.9	27.2	31.0	29.9	11.8
Telohuminite	42.7	27.7	31.4	29.9	31.3	37.5	51.5	40.1	47.4	33.9	39.2	40.9	26.1
Attrinite	1.8	2.6	4.7	5.1	7.3	1.6	1.6	7.9	3.4	6.1	1.6	4.6	33.2
Densinite	21.6	33.8	29.8	34.8	33.3	25.8	19.1	18.1	11.5	22.3	24.0	23.3	2.2
Detrohuminite	23.4	36.4	34.5	39.9	40.6	27.4	20.7	26.0	14.9	28.4	25.6	27.9	35.4
Levigelinite	13.3	8.5	9.7	5.8	4.0	11.0	3.8	3.7	5.0	6.5	8.1	7.2	1.5
Porigelinite				0.2	0.5	0.2		0.2	0.2	0.2	0.2	0.2	
Corpohuminite	3.9	9.9	9.9	9.6	9.7	6.2	7.4	10.2	13.1	8.3	8.8	6.7	16.6
Gelohuminite	17.2	18.4	19.6	15.6	14.2	17.4	11.2	14.1	18.2	15	17	14.1	18.1
Huminite	*83.3*	*82.5*	*85.4*	*85.3*	*86.2*	*82.2*	*83.3*	*80.1*	*80.6*	*77.3*	*81.9*	*83*	*79.7*
Fusinite					0.2	0.2		0.2	0.5	0.2	0.2		0.2
Inertodetrinite		1.0		0.7	0.4	0.9		0.2	0.3	0.3	1.4	0.5	0.5
Funginite		0.2	0.2	0.7	0.5	0.9	0.3	1.1	1.1	0.6	1.3	0.2	1.1
Inertinite		*1.2*	*0.2*	*1.4*	*1.1*	*2*	*0.3*	*1.4*	*1.9*	*1.1*	*2.9*	*0.7*	*1.8*
Sporinite	4.8	5.7	2.1	3.2	3.4	7.1	3.6	3.4	5.5	6.9	7.1	7.2	3.5
Cutinite		0.2				0.4					0.4		
Resinite	0.7	1.4	0.2	0.9	0.5	0.4	1.0	1.1	0.5		0.4	0.2	0.4
Suberinite					0.2			0.2	0.3			0.2	0.5
Alginite	4.3	0.3	0.3	0.2		1.2			0.3				
Liptodetrinite	2.1	2.1	0.5	2.4	0.9	2.1	1.9	3.0	1.5	3.4	2.4	2.1	1.3
Liptinite	*11.9*	*9.7*	*3.1*	*6.7*	*5.0*	*11.2*	*6.5*	*7.7*	*8.1*	*10.3*	*10.3*	*9.7*	*5.7*
MM	*4.8*	*11.5*	*11.7*	*6.5*	*7.7*	*4.6*	*9.8*	*10.7*	*9.5*	*11.3*	*4.9*	*6.7*	*35.8*
%Rr±Stdev	0.29±0.02	0.30±0.02	0.31±0.02	0.30±0.01	0.30±0.02	0.30±0.02	0.30±0.02	0.30±0.02	0.30±0.02	0.30±0.02	0.31±0.02	0.30±0.02	0.30±0.02

less than 10 μg/g (Table 6). Furthermore, the average concentrations of rare earth elements and yttrium (REY) on whole-coal basis are generally lower than 1 μg/g (Table 6).

The concentration coefficient (CC) of minor and trace elements in the Keles coal samples are calculated according to Dai et al. (2015a), i.e., the average concentrations of minor and trace elements are divided into their Clarke values for coal, as reported in Ketris and Yudovich (2009). The elements B (CC=9.7), Sr (CC=5.5), and Cs (CC= 6.6) are enriched elements, whereas Mn (CC=2.7), Se (CC=2.7), and Ba (CC=4.6) are slightly enriched elements in the Keles coal samples (Table 7). Furthermore, the elements Ge, Dy, Er, and Yb are depleted (CC<0.5) in coal in comparison with their Clarke values for low-rank coals (Dai et al., 2015a; Ketris and Yudovich 2009). The remaining minor and trace elements are close to corresponding Clarke values of low-rank coals. The vertical distributions of Si, Ti, Al, Fe, Mg, Ca, Na, and K are in parallel with ash yield, while enriched elements such as B, Mn, Sr, and Ba display increasing trends upwards (Fig. 11).

4.8. Palynological assemblages

The composition of Keles microflora includes 47 spore and pollen taxa, belonging to 38 genera and 37 families (Figs. 12 and 13). Three main palynomorph clusters (Cluster A, Cluster B2a, and Cluster B2a and B1), have been grouped in the palaeomires of the study area (Fig. 12). The first cluster (K-3, -4, -5 and -6 samples of the B2b subcluster in B2 cluster) is marked by high *Laevigatisporites hardti* (Polypodiaceae) (15-40%), Osmundaceae (10-15%) spores and *Pinus haploxylon* type (10-20%) pollen values (Fig. 12). Cupressaceae (*Inaperturopollenites concedipites*) and Cupressaceae-Taxodioideae-*Glyptostrobus* (*I. dubius*) display moderate values (3-10%) in this subcluster. The relative abundance of *Cathaya* and *Cedrus* ranges between 3% and 5%. The *Alnus* (2-10%) and *Castanea* (2-5%) pollen is represented by high values. The quantity of Typhaceae pollen is 2–4%, being the highest values in the B2b subcluster. *Carpinus*, Oleaceae, *Nyssa*, Acer, *Salix*, *Quercus* evergreen and deciduous types, *Juglans*, *Ulmus*, *Zelkova*, Asteraceae, *Pterocarya*, *Carya*, *Engelhardia*, *Myrica*, and Cyperaceae, are also registered with higher values (2-5%). In addition, the calculted average temperature values of the first palynomorph cluster were represented by the MAT 13.8 °C (*Engelhardtia* sp.)-21.3 °C (*Carya cordiformis*), CMT 0.9 °C (Sapotaceae) / 3.1 °C (*Engelhardtia* sp.) - 1.1 °C (*Pinus sylvestris*) / 13.3 °C (*Carya cordiformis*), WMT 20.7 °C (*Carya cordiformis*) - 28.1 °C (Cupressaceae) and MAP 740 mm (*Engelhardtia* sp.) - 1574 mm (Cupressaceae).

The second palynomorph cluster includes samples from the middle part of seam (sample K-9 of B2a subcluster in B2 cluster, and the K-11 samples of the B1 cluster) is characterized by the abundance of the woody gymnosperm and angiosperm pollen (Fig. 12). The percentage and diversity of the spores in the B2a subcluster are low. Although the relative abundanceof gymnosperm pollen (*Pinus haploxylon* type, Cupressaceae, Cupressaceae-Taxodioideae-*Glyptostrobus, Cathaya*, and *Cedrus*) generally decreases from the lower to middle part of seam, the values of these pollen grains (5-20%) are also the highest in the B2a subcluster (7.2-8.0 m). Relative abundances (2-5%) whitin B2a subcluster include Nymphaeaceae, Ephedraceae, *Myrica*, *Alnus*, *Tilia*, *Carya*, *Pterocarya*, *Ulmus*, *Zelkova*, *Quercus*, Oleaceae, and Cyrillaceae, which were predominant in the previous subcluster (B2b subcluster; 3-10%) (Fig. 12). In the B1 cluster (interval 8.1-8.4 m), spores have low values not exceeding 2%. The values of *Pinus haploxylon* type, Cupressaceae, Cupressaceae-Taxodioideae-*Glyptostrobus, Cathaya*, and *Cedrus* are significantly increased in the K-11 sample of the B1 cluster (5-40%). Besides, the *Abies* pollen is recorded in this sample. The relative abundance of the angiosperm pollen (*Myrica*, *Alnus*, *Engelhardia, Carya*, *Ulmus*, *Zelkova*, *Quercus*, *Fagus*, *Castanea*, Oleaceae, Sapotaceae, and Cyrillaceae) is 2-5%, and these values resemble the values of the B2a subcluster. In addition to, the calculated average temperature values of the second palynomorph cluster were represented by the MAT 13.8 °C (*Engelhardtia* sp.)- 21.3 °C (*Carya cordiformis*), CMT 3.1 °C (*Engelhardtia*

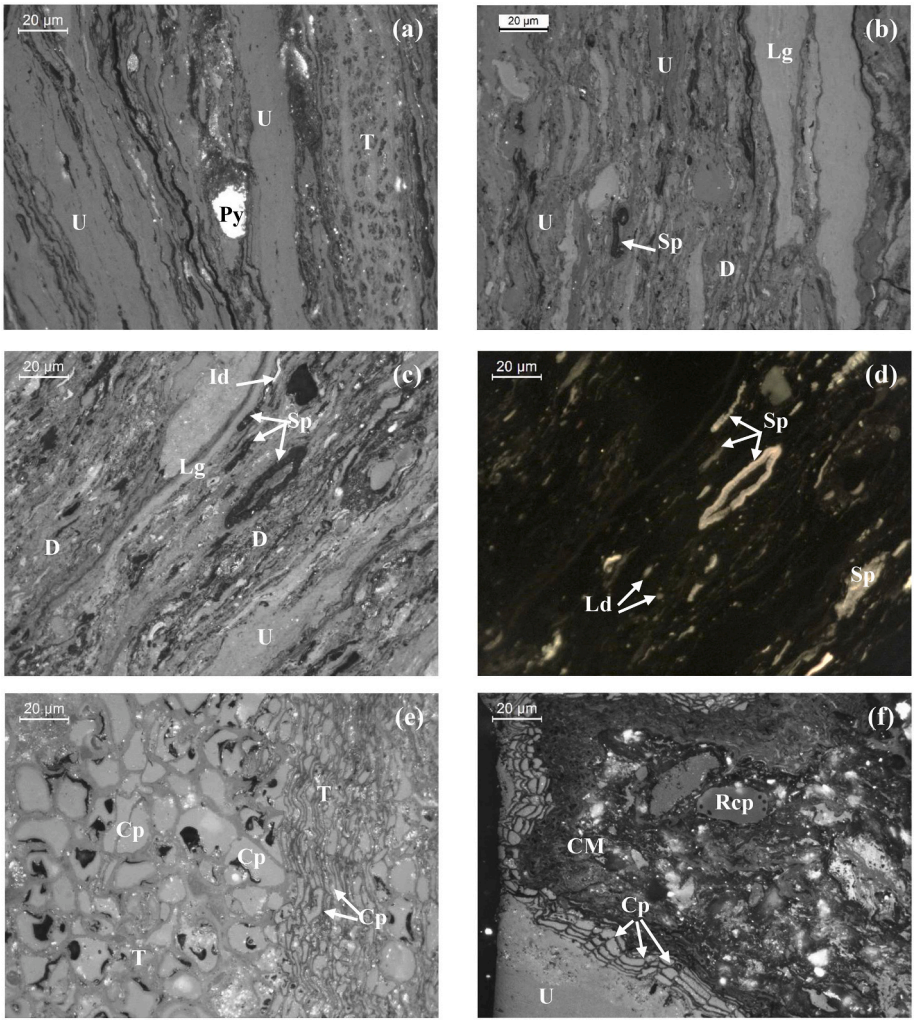

Fig. 6. Photomicrographs of the Keles coal. Textinite (T), eu-ulminite (U), densinite (D), corpohuminite (Cp), resinocorpohuminite (Rcp), levigelinite (Lg), inertodetrinite (Id), pyrite (Py), and clay minerals (CM). All photomicrographs are taken under incident white light (a, b, c, e, f) and blue-light excitation (d), oil immersion, 500 × total magnification.

sp.) - 13.3 °C (*Carya cordiformis*), WMT 20.7 °C (*Carya cordiformis*) - 28.1 °C (Cupressaceae) and MAP 740 (*Engelhardtia* sp.) – 1096 mm (*Ephedra* sp.) / 1574 mm (Cupressaceae).

The third palynomorphs cluster is defined between 10 and 12.6 m. The percentage of the spore species (*Laevigatisporites hardti* (Polypodiaceae) and Osmundaceae) increase in the lower part of cluster A (10-50%), while the percentages of spore species are low in the uppermost of the seam (K-17 sample) (3-5%). However, the highest percentage of spore species have been observed in the B2b subcluster of the lower part of the seam. The quantity and diversity of gymnosperm pollen (*Pinus haploxylon* and *P. silvesteris* types, Cupressaceae, Cupressaceae-Taxodioideae-*Glyptostrobus, Cathaya, Abies*, and *Cedrus*) drastically increase. cf. *Picea* and *Sequoia* are first recorded in this cluster. The angiosperm pollen (Poaceae, *Myrica*, *Alnus*, *Engelhardia, Carya*, *Ulmus*, *Zelkova*, *Quercus*, *Acer*, Onagraceae, *Fagus*, *Castanea*, Oleaceae, Sapotaceae, and Cyrillaceae) are represented by constant values ranging in between 2% and 6%. The percentage of Zygnemataceae significantly decreases, while *Botryococcus* values increase in the cluster A (Fig. 12). At the same time, the calculted average temperature values of the third palynomorph cluster were represented by the MAT 13.8 °C (*Engelhardtia* sp.) - 21.3 °C (*Carya cordiformis*), CMT 0.9 °C (Sapotaceae) / 3.1 °C (*Engelhardtia* sp.) - 1.1 °C (*Pinus sylvestris*) / 13.3 °C (*Carya cordiformis*), WMT 20.7 °C (*Carya cordiformis*) - 28.1 °C (Cupressaceae) and MAP 740 mm (*Engelhardia* sp.) - 1574 mm (Cupressaceae).

4.9. Diatom flora

Using SEM-BSE images, the identified diatom flora from the diatomite sample (K-18) comprises *Aulacoseria* sp., *Fragilaria* sp., *Pinnularia* sp., *Cymbella* sp., and *Gomphanea* sp. (Fig. 14).

5. Discussion

5.1. Coal rank

The use of a sole parameter for the rank determination of Cenozoic coals can be problematic; therefore, a combination of several parameters (e.g., moisture and gross calorific values) are applied for rank and grade determination of these coals (O'Keefe et al., 2013; Suggate, 1995, 2000). Nevertheless, the Rr value along with the gross calorific value and the ash yield of the Keles coal suggest that the studied samples could be classified as low- to medium-grade low-rank A-B (lignite) according to ECE-UN (1998) classification (Economic Commission for Europe-United Nations E.C.E.-U.N., 1988). Furthermore, samples K-2 and K-18 could be classified as carbonaceous rock due to their ash yields being higher than 50.0% (dry basis). The samples are also classified as medium- to high-ash low-rank B (lignite B) under ISO 11760 (2005) classification (International Standard Organisation ISO 11760, 2005). Furthermore, the studied samples are within bands for lignite according to Suggates' rank

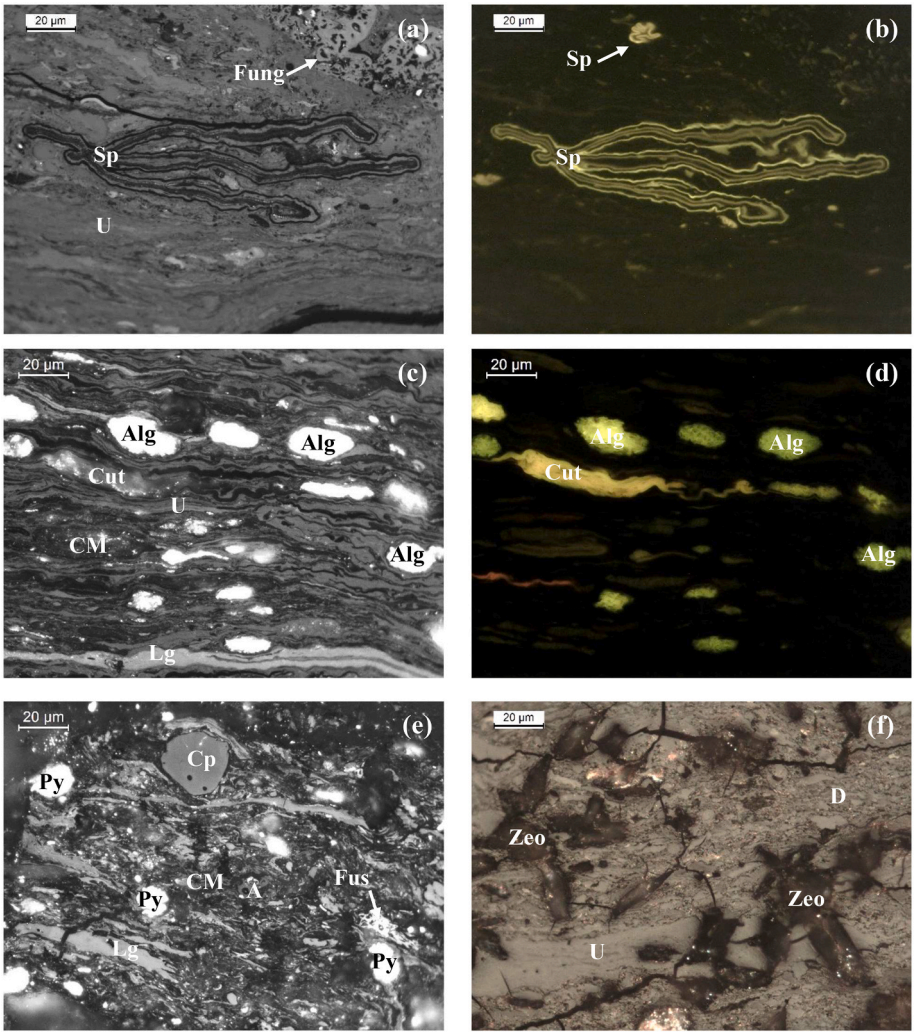

Fig. 7. Photomicrographs of the Keles coal. Eu-ulminite (U), densinite (D), attrinite (A), corpohuminite (Cp), sporinite (Sp), liptodetrinite (Ld), cutinite (Cut), alginite (Alg), fusinite (Fus), funginite (Fung), pyrite (Py), clay minerals (CM), zeolite (Zeo). All photomicrographs are taken under incident white light (a, c, d, e, f) and blue-light excitation (b), oil immersion, 500 × total magnification.

scale (Suggate, 1995, 2000). Besides, the Rr values of the Keles coals are similar to these of the Seyitömer coal (0.29%) and are slightly lower than these of the Tunçbilek coal (0.45%) (Celik and Karayigit 2004a; Karayigit and Celik 2003). Additionally, the presence of H-rich ulminite-A variety in the Keles and the Seyitömer coals, could supress the Rr values and cause reduction of measured %Rr from these coals (Kus et al., 2020; Oskay et al. 2016; Querol et al. 1996). A similar reason may also play a role for the relatively low Rr values of Miocene coal deposits in western Turkey and Spain (Bechtel et al. 2016; Büçkün et al. 2015; Karayigit et al., 2017a,b, 2020a,b, Querol et al. 1996).

5.2. Hydrocarbon generation potential

The hydrocarbon generation potential of humic coals of different rank and geological age has been widely investigated during the last three decades by several studies, and these studies have generally agreed that coal seams thicker than 0.5 m, with high vitrinite/huminite contents and liptinite contents exceeding 10–15% (on mineral matter-free basis) could display a hydrocarbon generation potential (Hunt 1991; Petersen 2006; Petersen et al., 2009; Sykes and Snowdon 2002; Wilkins and George 2002). Considering the thickness of Keles coal seam, the huminite and liptinite contents, and the H contents of the coal and the roof rock, the Keles coal seems to have hydrocarbon generation potential. Furthermore, previous studies also noted that roof rocks in the Seyitömer coalfield have hydrocarbon-generation potential (Dikmen and Yalçın 2020; Kara-Gülbay and Korkmaz 2008; Şener et al. 1995). For the determination of this potential, classical approaches are using HI-OI and HI-T_{max} diagrams (Fig. 9). The plotted data on these diagrams indicate that certain samples have oil-generation potential (K-18), and mixed hydrocarbon-generation potential (K-3 and K-17), whereas the remaining samples are gas-prone.

Humic coals with HI values higher than 200 mg HC/g TOC are generally considered as oil-prone, and the samples K-17 and K-18 have HI values higher than the threshold value for oil generation (Table 5 and Fig. 9). Nevertheless, hydrocarbon-generation potential and traditional source-rock determination parameters could be limited for humic coals due to their heterogeneous characteristics. In order to eliminate these problems, several parameters were proposed and, in this study, HI_{max} and effective HI parameters which were proposed by Petersen (2006) and Sykes and Snowdon (2002), respectively, were applied. For these calculations, samples K-17 and K-18 are excluded due to their slightly high HI values. The calculated HI_{max} values of the remaining coal samples vary between 200 and 250 mg HC/g TOC, and the effective HI values vary between 175 and 265 HC/g TOC (Fig. 15). These values show that the majority of the examined samples might be oil prone; however, their low T_{max}, PI, QI, and BI values, and the lack of exsudatinite implies that coal samples are not mature enough to generate liquid hydrocarbons.

Table 4
Minerals identified in the Keles coal and inorganic samples based on XRD and SEM-EDX analyses (+++ = dominant phase (> 20%), ++ = abundant phase (5–20%), + = minor phase (< 5%) by XRD, a: accessory mineral detected by SEM-EDX, Clp/Heu: clinoptilolite/ heulandite, Ill: ilite, Kln: kaolinite, Sm: smectite, $I0_I$-14_S: interstratified mixed-layer illite/smectite).

Sample	Quartz	Clay Minerals	Feldspars	Cristobalite	Clp/ Heu	Zircon	Calcite	Dolomite	Szomolnokite	Pyrite	Gypsum	Barite	Apatite	Ti-oxides
K-18	+	+++	++						+	+	+			
K-17	+		+++		++	a					++	a	a	a
K-16	++	++	+++		++									
K-15	+	++	+++		+++						++	a		
K-14	+		a		++						+++	a		
K-13	+	+++	++		++						+			
K-12		+++ (Sm ± Kln)	++	+						+	+			
K-11	++	+++	++								+	a		
K-10		+++ (Sm ± Kln)	++	+						+	++			
K-9	+	+++	+++								+			
K-8	+	++	+++								++	a	a	
K-7		+++ (Kln ± Ill)	+++											
K-6	+	+++	++	+							++	a		
K-5	+	+++	++							a	++			
K-4	++	+++	+								+	a		
K-3	++	+++	++					a		a	+	a		a
K-2	+++	+++ (Kln + $I0_I$-14_S + Ill)	+							+	+	a		a
K-1	++	+++ (Kln+$I0_I$-14_S+Ill)	+								+			

The relatively high HI values in humic coals are mostly related to H and total S contents, and more importantly with liptinite macerals (Oskay et al., 2019a; Petersen 2006; Petersen et al., 2009). Sporinite is commonly associated with clays in the samples K-18, whereas alginite displays the highest proportion in sample K-17and was also commonly observed in sample K-18. These data show that the relatively higher HI values from samples K-17 and K-18 seem to be controlled by liptinite macerals, particularly sporinite and alginite. Furthermore, relatively higher S_3 and OI values of humic coals are generally related to the presence of inertinite macerals and/or carbonate minerals which release additional CO_2 during pyrolysis (Bostick and Daws 1994); however, the inertinite contents of the studied coal samples are very low (<1.0 vol%., whole basis) and carbonate minerals were not detected from analysed coal samples by XRD. In Turkish Cenozoic low-rank coals (e.g., Soma and Yeniköy coal deposits), OI values are generally reported as being slightly high and these values are mostly explained by the presence of oxygen bearing organic compound (e.g., carboxyl and hydroxyl) due to low maturity of these coals (Çelik et al., 2017; Karayigit et al., 2017a; Oskay et al., 2019a). In addition, the intense and broad band at 3400 cm^{-1} could be attributed to −OH stretching vibrations of hydrogen-bonded hydroxyl groups of the water absorbed by clay minerals (Fig. 8). This band may also be related to the presence of -OH stretching vibrations of phenol groups at xylite-rich low-rank coals (Geng et al. 2009; Oikonomopoulos et al., 2013). As mentioned previously, fluorescent telohuminite A variety and resino-corpohuminite macerals may be the source of carboxyl and hydroxyl group-bearing compounds (e.g resin) in huminite macerals (Bechtel et al. 2016; Karayiğit et al., 2017b). The aliphatic C−H bands attributed to symmetric and asymmetric $-CH_2$ are distinct within the 2922–2850 cm^{-1} stretching region in coal and diatomite samples (Fig. 8a-b) (Georgakopoulos et al. 2003; Oikonomopoulos et al., 2013). The stretching vibrations around 1400 cm^{-1} are attributed to symmetric aliphatic C-H (Fig. 8a). The broad band around 1600 cm^{-1} is related to C=O aromatic ring stretching vibrations (Fig. 8a) (Bechtel et al. 2016; Mastalerz and Bustin, 1996; Oikonomopoulos et al., 2013). Thus, the FT-IR data show the presence of oxygenated organic compounds and, as with the carbonate minerals, their breakdown during pyrolysis could suppress S_2 peak and elevate the S_3 values (Bordenave et al. 1993; Vu et al., 2013). Thus, the S_3 and OI values of coal samples are relatively high.

The HI_{max} and effective HI values of samples K-17 and K-18 suggest that they experienced liquid hydrocarbon generation; however, their HI values are elevated due to the presence of sporinite and alginite dispersed within detrohuminite and clays rather than due to liquid hydrocarbon generation. Moreover, Rock-Eval pyrolysis of the roof rock, particularly the bituminous shale, in the Seyitömer coalfield was also subjected to studies about source potential (Dikmen and Yalçın 2020; Kara-Gülbay and Korkmaz 2008; Şener et al. 1995). In comparison with the results of these studies, the roof rock of the Keles coalfield displays relatively high TOC and HI values. The relatively high TOC values could simply be related to the presence of carbonaceous remains in K-18, while the common presence of sporinite and alginite in this sample could elevate HI values, as explained above. Although the studied coal and roof-rock samples have limited gas generation potential, further studies on their liquefaction potential should be conducted in the future. Overall, all these suggest that traditional and alternative parameters for hydrocarbon generation potential of humic coals should be applied with precautions.

5.3. Mineral assemblages

5.3.1. Quartz and feldspars

Quartz mostly occurs within clay mineral assemblages and/or as individual grains in raw coal samples, as deduced from SEM-EDX analysis (Figs. 16a-d and 17a). These grains have sharp and irregular edges indicating detrital input into the palaeomire from adjacent areas (Dai et al. 2012; Ward 2016). Although glass shards were not observed in the coal samples during SEM-EDX studies, the occurrence of cristobalite (as deduced by XRD analysis) in one coal sample might point to the precipitation of dissolved silica from the alteration of synchronous volcanic input within the palaeomire under weak alkaline conditions (Arbuzov et al. 2016; Karayigit et al., 2019b; Spears 2012). Furthermore, neither opal-A or opal-CT is detected by XRD in the diatomite roof rock sample, and the lack of opal-A and the associated hump in the XRD pattern of this sample could be related to the presence of well-preserved diatoms, and weak silica diagenesis in the study area (Koukouzas 2007).

The combination of XRD and SEM-EDX analyses indicate that

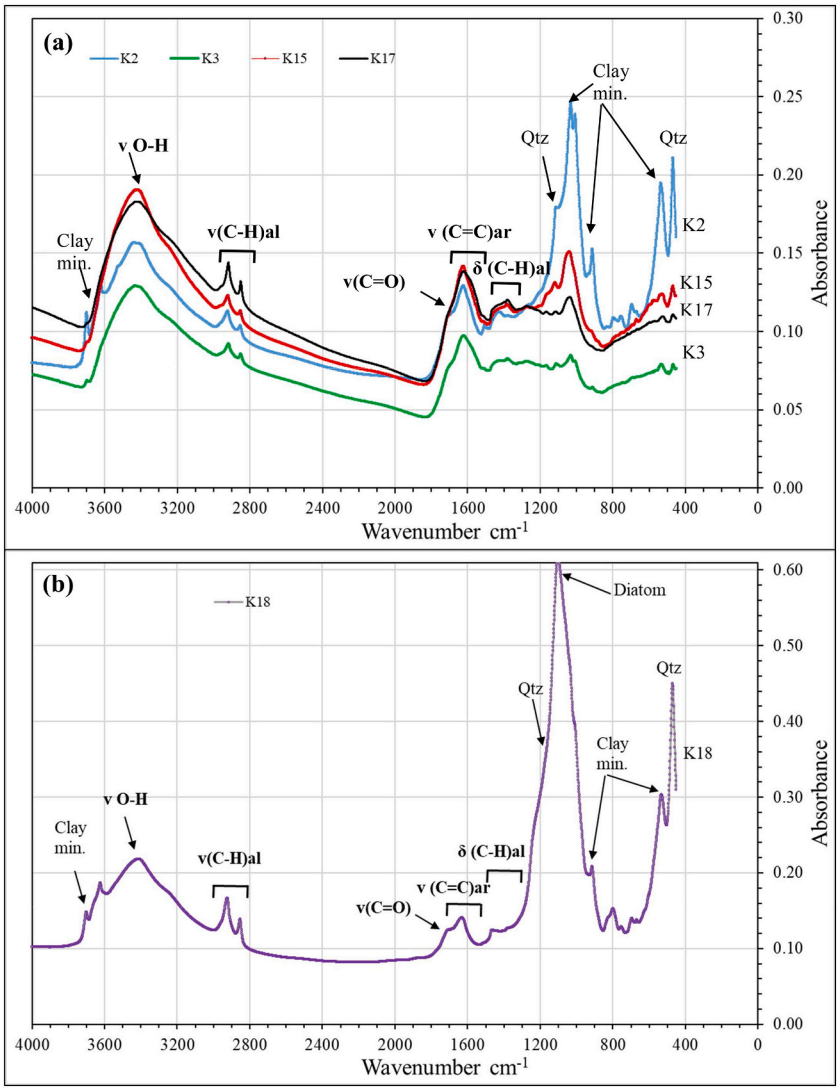

Fig. 8. FT-IR spectra of (a) selected coal samples and (b) roof rock (K-18) sample obtained from the Keles coal seam.

Table 5
The Rock-Eval pyrolysis parameters of the Keles coal and roof rock samples (TOC: total organic carbon, HI: hydrogen index, OI: oxygen index, RC: residual carbon, PC: pyrolyzed carbon, MINC: mineral carbon, PI: production index ($S_1/S_1 + S_2$); BI: bitumen index (S_1/TOC), and QI: quality index (($S_1 + S_2$)/TOC)).

Sample	TOC (wt.%)	S_1	S_2	S_3	T_{max} (°C)	OI (mg HC/g CO_2)	HI (mg HC/g TOC)	RC	PC	MINC	PI	BI	QI
		mg HC/g rock											
K-18	14.5	2.5	89.9	6.2	430	43	620	6.5	8.0	0.5	0.03	0.17	6.4
K-17	48.4	0.9	98.5	32.0	437	66	203	38.6	9.9	1.6	0.01	0.02	2.1
K-16	48.0	0.9	81.4	33.4	433	69	169	39.5	8.6	1.6	0.01	0.02	1.7
K-15	41.0	0.7	46.0	36.4	431	89	112	35.3	5.7	1.8	0.01	0.02	1.1
K-14	47.3	0.6	58.1	35.0	432	74	123	40.5	6.7	2.1	0.01	0.01	1.2
K-13	43.9	0.9	62.8	31.6	428	72	143	36.9	7.0	1.7	0.01	0.02	1.5
K-9	49.7	0.9	68.6	36.5	431	74	138	41.9	7.8	1.6	0.01	0.02	1.4
K-8	45.0	1.0	70.5	34.4	429	76	157	37.2	7.8	1.7	0.01	0.02	1.6
K-5	49.0	0.8	66.8	39.8	431	81	136	41.3	7.7	1.9	0.01	0.02	1.4
K-4	50.3	0.9	72.8	36.3	432	72	145	42.3	8.1	1.9	0.01	0.02	1.5
K-3	52.5	0.7	66.8	39.0	430	74	127	44.8	7.7	2.0	0.01	0.01	1.3
K-2	28.1	2.8	48.5	20.1	417	72	172	22.7	5.4	1.1	0.06	0.10	1.8

feldspars in the raw coal samples are mainly K-feldspars with trace amounts of Na, and less commonly plagioclase (Figs. 16e-f, 17b-c, and 18c-d). Considering the high-K calc-alkaline characteristics of synchronous volcanic rocks around the Harmancık Basin (Ersoy and Helvaci, 2016; Helvacı et al., 2017), the common presence of K-feldspar and plagioclase grains is expected. Further, feldspar grains are mostly associated with clay minerals, apatite, and Ti-oxides (Figs. 16e-f and 17b-c); thus, a volcanogenic origin of feldspars in the studied coal samples is determined, based on the same criteria from prior studies (Arbuzov et al. 2016; Bohor and Triplehorn 1993; Dai et al. 2017; Knight et al. 2000; Zhao et al. 2012). Similar associations were also reported from early-middle Miocene coal seams and altered tuff layers in

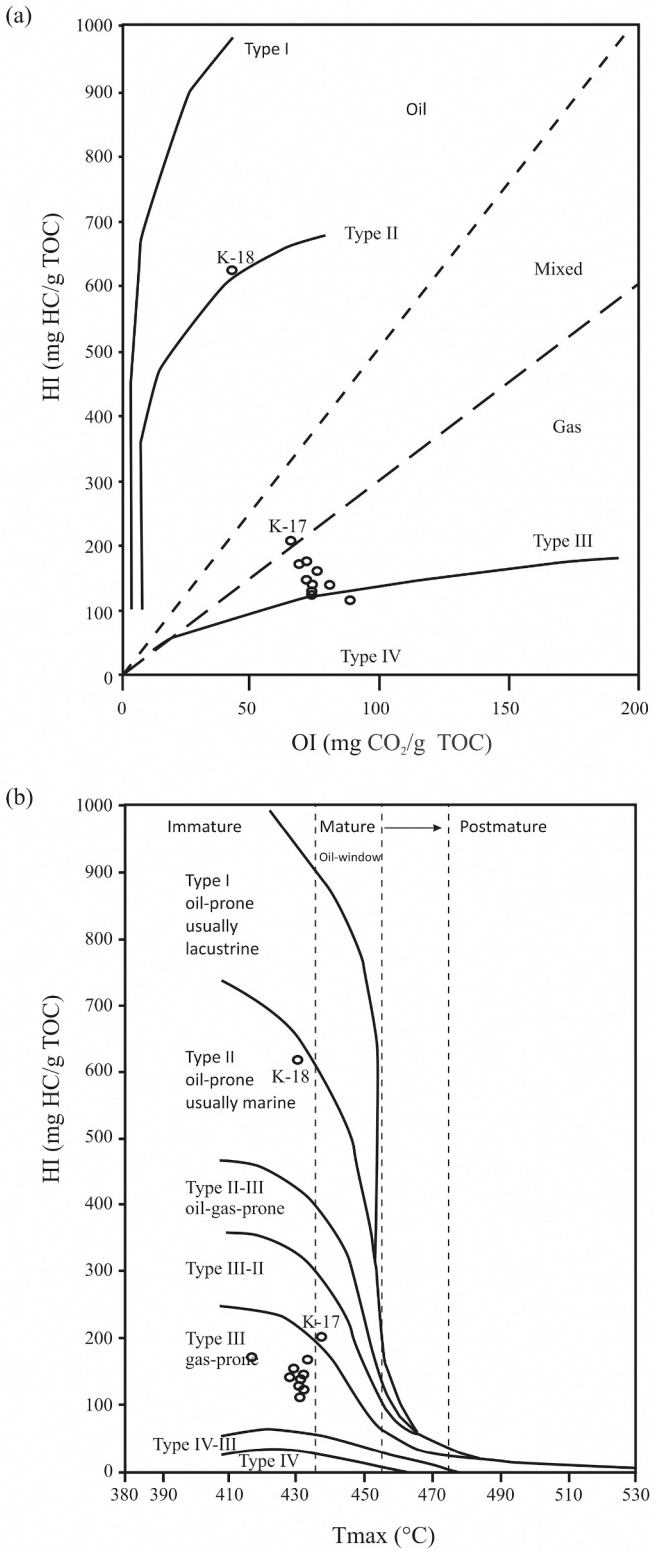

Fig. 9. The Keles coal and roof rock (K-18) samples projected on (a) the pseudo-van Krevelen diagram, (b) plot of HI against T_{max} of the coal samples (after Peters 1986).

Tunçbilek, Seyitömer, Soma, and Dursunbey coalfields (Erkoyun et al., 2017, 2019; Karayigit et al., 2017a,b, 2020b; Oskay et al., 2019a). The presence of a barite zone around feldspar grains in raw coal samples (Fig. 18c-d) indicates that feldspars altered within the palaeomire during and/or after deposition (Dai et al. 2017; Spears et al., 1988; Ward 2016).

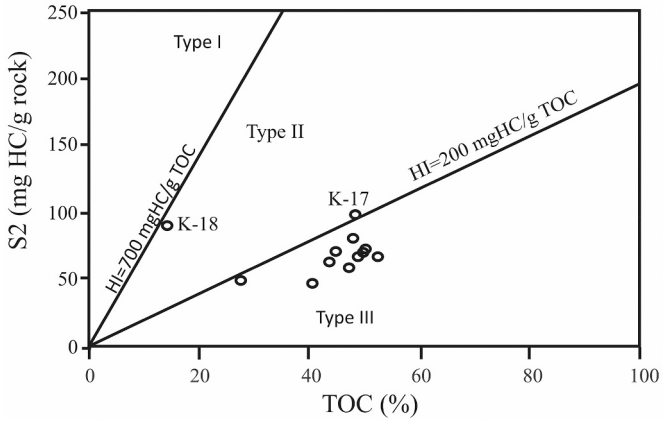

Fig. 10. The Keles coal and roof rock (K-18) samples projected on S_2 vs TOC diagram (after Langford and Blanc-Valleron 1990).

5.3.2. *Clay and zeolite minerals*

In the studied raw coal samples, quartz and aluminosilicate minerals are commonly identified (Table 4). Clay minerals in coal samples are generally associated with other mineral grains (e.g., quartz, feldspars, apatite, and zircon), and the matrices of these clay aggregates are mostly composed of smectite and kaolinite, and less commonly of illite (Fig. 16a-f). The latter case is commonly identified in mineral-rich coal lithotype indicating a detrital origin. The former cases are commonly reported from altered tuff and/or tonstein layers in coal seam, and mostly related to alteration of synchronous volcanic input during syngenetic and/or post-depositional stage (Bohor and Triplehorn 1993; Dai et al. 2017; Spears 2012; Zhou et al. 2000). In accordance similar smectite and kaolinitic matrices are commonly reported from Miocene coal seams hosting altered tuff layers (e.g., Soma and Dursunbey coalfields) in western Anatolia (Karayigit et al., 2017a,b, 2020b; Oskay et al., 2019a). Furthermore, smectite and kaolinite are also developed around feldspar grains in coal samples, implying that kaolinite and smectite are alteration by-products of feldspars (Fig. 16e-f). Similar feldspar-smectite associations and kaolinitized feldspars are also reported from coals and altered tuff layers in the Tunçbilek and Seyitömer coalfields (Erkoyun et al., 2017, 2019; Karayigit et al., 2019a). Even though altered tuff and/or tuffite layers were not observed within the Keles coal seam, several altered tuff and/or tuffite layers were reported in other parts of Harmancık Basin and in the synchronous Seyitömer coalfield (Celik and Karayigit 2004a; Erkoyun et al., 2017; Ersoy and Helvaci, 2016; Ersoy et al. 2014; Helvacı et al. 2017). Considering these layers and the intense volcanic activity during Middle Miocene around the Harmancık Basin, synchronous volcanic tephra was deposited into the Keles palaeomire. This synchronous input seems to be altered within the palaeomire and taking in account the abundance of smectite matrices in the studied samples, the alteration of the volcanic input is presumably developed in the hydrogeologically closed palaeomire system under weak acidic to neutral conditions (Bohor and Triplehorn 1993; Dai et al. 2017; Spears 2012). In addition, the presence of kaolinite in the floor rock and some intercalations samples suggest that synchronous input might also be kaolintized by pedogenic processes under acidic conditions (Korasidis et al., 2019).

Natural zeolite formation has not been reported up to date from Cenozoic coal seams with altered tuff layers from grabens in western Anatolia, even though several zeolite deposits associated with borate deposits are located in north-western Anatolia (Gündogdu et al., 1996; Karayigit et al. 2000, 2017a, 2020b; Oskay et al., 2019a; Querol et al. 1997). The lack of natural zeolite formation in western Anatolian coal deposits hosting altered tuff layers, could be related to the development of acidic to neutral conditions within these palaeomires (Celik and

Table 6
Major, minor, and trace element contents on whole coal basis (in μg/g, except otherwise cited) in Keles coal (bdl: below detection limit).

Elements	K-17	K-16	K-15	K-14	K-13	K-11	K-9	K-8	K-6	K-5	K-4	K-3	K-2
Si, %	2.8	3.7	6.8	3.8	5.8	2.7	3.3	4.1	3.8	3.0	2.0	2.6	14.6
Al, %	1.1	1.4	2.9	1.6	2.1	1.1	1.6	2.0	2.0	2.1	0.9	1.4	4.4
Ca, %	2.6	2.1	2.4	2.5	2.0	1.8	1.8	2.7	2.2	1.9	1.8	1.8	1.0
Fe, %	0.57	0.51	1.03	0.71	0.78	0.43	0.69	1.03	0.61	0.43	0.39	0.48	2.08
K, %	0.24	0.23	0.48	0.30	0.45	0.25	0.57	0.89	1.01	0.55	0.20	0.20	0.75
Mg, %	0.31	0.34	0.34	0.36	0.35	0.30	0.27	0.25	0.24	0.27	0.29	0.30	0.38
Na, %	0.21	0.14	0.48	0.17	0.19	0.07	0.23	0.27	0.23	0.08	0.06	0.06	0.20
Ti, %	0.03	0.03	0.08	0.05	0.07	0.06	0.05	0.06	0.04	0.04	0.03	0.04	0.18
P	183	46	168	49	50	49	144	179	105	109	49	49	45
Li	9.3	17	15	15	23	13	12	17	11	23	10	18	60
Be	bdl	bdl	1.2	bdl	1.3	0.8	2.1	1.9	0.9	bdl	bdl	bdl	1.1
B	850	492	465	452	433	616	521	459	503	543	607	570	194
Sc	3.2	3.4	4.4	3.3	5.1	5.4	7.5	5.9	2.9	2.8	2.0	3.1	4.9
V	13	15	30	17	32	47	60	66	17	18	11	21	51
Cr	7.3	8.8	6.4	10	15	16	11	12	8.7	10	8.9	11	44
Mn	315	344	284	307	277	275	257	242	232	258	271	260	138
Co	1.9	2.7	1.8	3.1	4.6	2.9	5.9	7.0	1.5	1.8	1.5	2.3	1.7
Ni	6.6	8.2	5.7	7.4	10.1	7.7	8.2	12.9	6.3	6.7	7.2	8.3	17
Cu	8.3	13	12	11	15	12	11	14	7.5	12	9.1	14	14
Zn	27	23	30	30	31	21	26	92	58	25	20	14	27
Ga	2.5	3.3	6.2	3.9	5.1	3.4	4.8	6.7	3.8	4.2	2.2	3.7	13
Ge	bdl	bdl	bdl	bdl	0.9	bdl	1.8	1.5	bdl	bdl	bdl	bdl	1.8
As	8.7	6.6	13	5.6	6.4	6.2	13	22	10	8.0	6.4	8.6	18
Se	2.7	2.4	3.2	2.8	3.0	2.6	3.1	3.3	2.7	2.9	1.8	2.3	3.0
Rb	10	11	16	14	21	10	18	25	23	14	7.3	12	68
Sr	826	793	843	795	731	618	626	706	569	581	598	571	364
Y	3.6	3.6	4.5	4.7	8.0	6.7	13	12	5.9	4.8	4.2	6.9	4.8
Zr	17	20	53	32	69	42	79	86	19	21	16	19	72
Nb	6.1	7.9	17	12	24	16	27	42	8.3	9.3	7.4	8.0	27
Mo	0.8	1.0	1.6	1.3	2.1	2.1	3.9	4.6	1.5	2.1	1.4	1.8	3.0
Sn	bdl	0.9	1.3	1.0	1.1	1.0	1.0	1.1	1.0	1.0	bdl	1.0	2.6
Sb	bdl	0.8	bdl	bdl	0.9	bdl	1.1	2.0	bdl	bdl	bdl	0.8	1.0
Cs	5.9	7.5	8.2	6.6	9.4	3.9	4.8	4.2	2.4	3.0	2.5	6.2	32
Ba	925	942	1180	958	972	476	668	683	509	492	467	588	429
La	7.4	6.4	8.0	8.7	10	7.2	10	13	7.2	6.5	5.5	6.4	14
Ce	17	15	19	20	21	16	22	29	16	16	13	17	38
Pr	1.3	1.1	1.5	1.5	1.8	1.4	2.1	2.8	1.4	1.3	1.1	1.5	2.9
Nd	5.5	4.9	6.4	6.5	7.9	6.7	9.4	12	6.3	6.1	5.1	7.1	12
Sm	0.9	0.9	1.2	1.2	1.6	1.4	1.9	2.4	1.2	1.3	1.1	1.8	2.1
Gd	1.0	0.9	1.2	1.2	1.6	1.5	2.1	2.5	1.3	1.3	1.1	1.7	1.9
Dy	bdl	bdl	bdl	bdl	1.1	1.0	1.6	1.6	0.8	bdl	bdl	1.1	0.8
Er	bdl	bdl	bdl	bdl	bdl	bdl	0.9	0.9	bdl	bdl	bdl	bdl	bdl
Yb	bdl	bdl	bdl	bdl	bdl	bdl	1.2	1.1	bdl	bdl	bdl	bdl	bdl
Hf	bdl	bdl	1.3	0.8	1.4	1.0	1.9	2.2	bdl	bdl	bdl	bdl	1.8
Hg	0.06	0.10	0.17	0.10	0.11	0.10	0.08	0.12	0.06	0.10	0.08	0.11	0.26
Pb	6.2	7.2	13	9.4	11	4.1	12	23	11	13	3.6	7.7	16
Th	3.8	4.6	7.3	5.9	6.6	2.8	5.7	9.0	4.0	7.1	2.4	6.0	11
U	1.3	2.0	4.3	3.5	5.2	2.1	6.0	8.3	2.8	2.2	1.9	2.3	3.1

Karayigit 2004a; Erkoyun et al. 2017, 2019; Karayigit et al., 2017a,b, 2019a, 2020b; Oskay et al., 2019a). In agreement, only authigenic kaolinite and smectite formation was reported from coals and altered tuff layers in the Tunçbilek and Seyitömer coalfields due to alteration of synchronous volcanic inputs under weak acidic to weak alkaline conditions in the palaeomires (Erkoyun et al., 2017, 2019; Karayigit et al., 2019a). Natural zeolite formation in the north-western central Anatolian coal deposits has been reported (Bechtel et al., 2014; Querol et al. 1997; Toprak et al. 2015; Whateley and Tuncali 1995; Whateley et al., 1996). In these basins (e.g., Beypazarı coalfield), syngenetic analcime was derived from altered Na-rich volcanic input and syngenetic clinoptilolite/heulandite formed due to alteration of Ca-rich volcanic input in alkaline palaeomires being hydrogeologically closed systems. Analcime was not detected by XRD and SEM-EDX in Keles coal; as mentioned previously, XRD analysis proves that clinoptilolite/heulandite appears as the dominant to abundant phase along with feldspars in the upper part of the coal seam (Table 3). A lower Na/Ca ratio of the glass activation solutions in the Keles coal compared to that of the Beypazari coal probably yields to the sole precipitation of heulandite/clinptilolite. Usually, NaOH alkalinity dissolves most of the Si and Al from the glass, but if the Ca content is high, clinoptilolite-type (Ca-Na-K) zeolites are crystallised instead of pure Na zeolites, such as analcime (Querol et al. 2002). The SEM-EDX data show that Si/Al ratios of identified zeolite grains in raw coal samples are around 3.9, implying that these grains are heulandite or transition between heulandite-clinoptilolite (Fig. 19); however, the peak at 8.99 Å in the coal ash obtained at 450°C (Fig. 20) indicates that these grains could be clinoptilolite (Armbrusteer and Gunter, 2001; Bish and Boak 2001). Moreover, Miocene volcanic rocks in the study area display a high K calc-alkaline composition (Ersoy and Helvaci, 2016; Helvacı et al. 2017); SEM-EDX analysis revealed that K-feldspars with traceable Na and plagioclases are often contained in the coal samples from the upper part of the seam. All these suggest that the K- and Ca-rich volcanic input was altered under alkaline conditions, which activated volcanic glass contained in the Keles coal/peat. The source of aluminosilicate gel was the alteration of volcanic glass, as it was for dissolved K^{+}, Ca^{2+} and Na^{2+}, together with the partial alteration of volcanic feldspars, particularly K-feldspars. Overall, the mineralogical differences throughout the seam could imply that weak acidic to neutral conditions were common during the initial stage of peat accumulation, while alkalinity was increased within the palaeomires and optimal conditions (e.g. high pH and/or lesser degree of flushing of ions from palaeomire) for natural zeolite formation were developed during the

Table 7
Weighted averages of the elements (in μg/g) for the Keles coal samples and their comparison with worldwide coals (CC: concentration coefficient; a: from (Swaine, 1990) Swaine, 1990; b: from Ketris and Yudovich 2009).

Element	Most World Coals[a]	Clarke Value For Low-Rank coals[b]	Average	CC
Li	1-80	10	20	2.0
Be	0.1-15	1.2	0.7	0.6
B	5-400	56	516	9.2
Sc	1-10	4.1	3.9	1.0
V	2-100	22	29	1.3
Cr	0.5-60	15	13	0.9
Mn	5-300	100	261	2.6
Co	0.5-30	4.2	2.8	0.7
Ni	0.5-50	9	8.8	1.0
Cu	0.5-50	15	12	0.8
Zn	5-300	18	35	2.0
Ga	1-20	5.5	5.1	0.9
Ge	1-50	2	0.5	0.2
As	0.5-80	7.6	11	1.4
Se	0.2-10	1.0	2.8	2.8
Rb	2-50	10	21	2.1
Sr	15-500	120	659	5.5
Y	2-50	8.6	6.0	0.7
Zr	5-200	35	41	1.2
Nb	3-30	11	16	1.5
Mo	0.1-10	2.2	2.1	0.9
Sn	1-10	0.79	1.0	1.3
Sb	0.5-10	0.84	0.5	0.6
Cs	0.1-5	0.98	7.8	8.0
Ba	20-1000	150	708	4.7
La	1-40	10	8.7	0.9
Ce	2-70	22	20	0.9
Pr	1-10	3.5	1.7	0.5
Nd	3-30	11	7.5	0.7
Sm	1-6	1.9	1.5	0.8
Gd	0.1-4	2.6	1.5	0.6
Dy	1-4	2	0.5	0.3
Er	1-3	0.85	0.1	0.1
Yb	0.3-3	1	0.2	0.2
Hf	0.4-5	1.2	0.8	0.6
Hg	0.02-1	0.1	0.11	1.1
Pb	2-80	6.6	11	1.7
Th	0.5-10	3.3	6.2	1.9
U	0.5-10	2.9	3.4	1.2

late stages. Thus, the Keles coalfield hosts the only known natural zeolite formation of Miocene age in western Anatolia.

5.3.3. Sulphides and sulphates

Pyrite is the only detected sulphide mineral by XRD in the raw coal (Table 3). Framboidal pyrite grains indicate its syngenetic origin (Figs. 16a and 17b). Nevertheless, the lack of pyrite in the XRD patterns, as well as its low proportion determined under the petrographic microscope could imply that redox conditions were not suitable for extensive syngenetic pyrite formation in the Keles palaeomire (Chou 2012; Dai et al., 2020b; Ward 2016). Chalcopyrite was detected within cavities of a feldspar grain in one coal sample during SEM studies, and such chalcopyrite cavity infillings of volcanogenic origin, were also reported from the İsaalan and Dursunbey coalfields (Karayigit et al., 2017b, 2020b); thus, chalcopyrite in the studied samples is presumably related to synchronous volcanic input.

The X-ray diffractograms reveal that gypsum is included in almost all raw coal samples, and anhydrite and szomolnokite in the coal ash (Table 4). Gypsum in coal is generally considered to be a by-product of pyrite during the late weathering stage or precipitation of pore water during storage (Dai et al. 2012; Oskay et al. 2016); however recent studies by Spiro et al. (2019) and Liu et al. (2021) found that gypsum can also be syngenetically deposited in low-rank coals. The lack of oxidized pyrite under the coal-petrography microscope suggests that former cases are less probable; the presence of gypsum flakes in the cleat/fracture of raw coal samples points to the formation from pore-water evaporation (Fig. 17f). Anhydrite, along with bassanite, is commonly reported from low-temperature ash due to dehydration of gypsum or reaction between CaO and SO_x during ashing (Finkelman et al. 2019; Ward, 2002). Considering the common occurrence of gypsum in raw coal samples, anhydrite is simply a dehydration product of gypsum during ashing. Szomolnokite is rarely reported in coal, and its dehydration product, melanterite, is identified in the coal seam; nevertheless, these Fe-sulphate minerals are generally considered as by-products of pyrite oxidization (Finkelman et al. 2019; Karayigit et al., 2020b; Kortenski and Sotirov 2004). Its presence in coal ash is related to either pyrite oxidization or reactions between FeO and SO_x during ashing. Nevertheless, its presence in the roof rock sample could imply that it might be derived from pyrite oxidiation during the late weathering stage (Fig. 21).

Barite is the most common sulphate mineral in raw coal samples identified through SEM-EDX analysis (Table 4) and is mostly observed around feldspar grains and/or associated with celestine and pyrite in raw coal (Figs. 16a, c, 18a-d, and 22). Barium and Sr liberated during alteration of volcanogenic feldspars in the palaeomire, could have reacted with sulphuric acid and precipitated within cavities of organic matter during late syngenetic stages and/or be reduced by bacteria in the palaeomire, and precipitated along with syngenetic framboidal pyrite grains (Karayigit et al., 2019b, 2020b). The calc-alkaline character of the volcanic activity along with the alkaline conditions within the palaeomire might suggest that liberated Ba and Sr could have reacted with phosphate and aluminosilicate gel in the Keles palaeomire (Brownfield et al., 2005; Dai et al., 2018, 2020a; Spears et al., 1988; Triplehorn et al. 1991; Ward et al. 1996). Nevertheless, the lack of Sr- and Ba-bearing aluminophosphates in the studied samples, and the presence of traceable Ba and Sr by SEM-EDX from analcime grains could suggest that either the decay of plant matter did not produce enough liberated P or the liberated Ba and Sr have been absorbed by syngenetic zeolites. Additionally, neutral to alkaline conditions might not also allow to reaction between Ca and phosphorus from organic matter during plant decay in palaeomire (Dai et al., 2015b).

5.3.4. Other minerals

Apatite, Ti-oxides, and zircon are mostly associated with clay mineral aggregates and feldspar grains in raw coal samples according to the SEM-EDX data (Figs. 16b and 17b-c), suggesting a volcanogenic origin (Bohor and Triplehorn 1993; Dai et al. 2017, 2018; Ward 2016). Furthermore, F and Cl traces from individual apatite grains (Fig. 17e) are another indicator of their volcanic origin (Spears 2012). As mentioned above, the presence of natural zeolite formation in the upper part of the seam due to development of alkaline conditions in the Keles palaeomire; however, carbonate minerals are not detected by XRD in the raw coal and ash samples. Carbonate minerals are only detected in a few samples during coal petrography and SEM studies (Fig. 17d). The SEM-EDX data show that calcite and dolomite are the only identified carbonate minerals and are presumably cleat/fracture infillings that possibly resulted from precipitation of dissolved Ca^{2+} and Mg^{2+} in pore water during late syngenetic or diagenetic stage. Syngenetic carbonates and fossil shell-bearing bands are commonly reported from Miocene coal seams within grabens (e.g. Seyitömer and Soma Basins) in western Anatolia (Celik and Karayigit 2004a; Karayigit et al., 2017a, 2019a). The lack of syngenetic carbonate minerals under alkaline conditions is not expected since the sedimentary sequence contains lacustrine carbonates. Nevertheless, this lack could be attributed to either Ca-poor groundwater supply, similarly to other coal-bearing basins in western Anatolia, and/or to the tendency of Ca^{2+} and Mg^{2+} dissolved in pore water to react with aluminosilicate gel in the palaeomire resulting in natural zeolite formation.

5.4. Abundance and mode of occurrence of elements

As mentioned above, the enriched elements in the studied coal

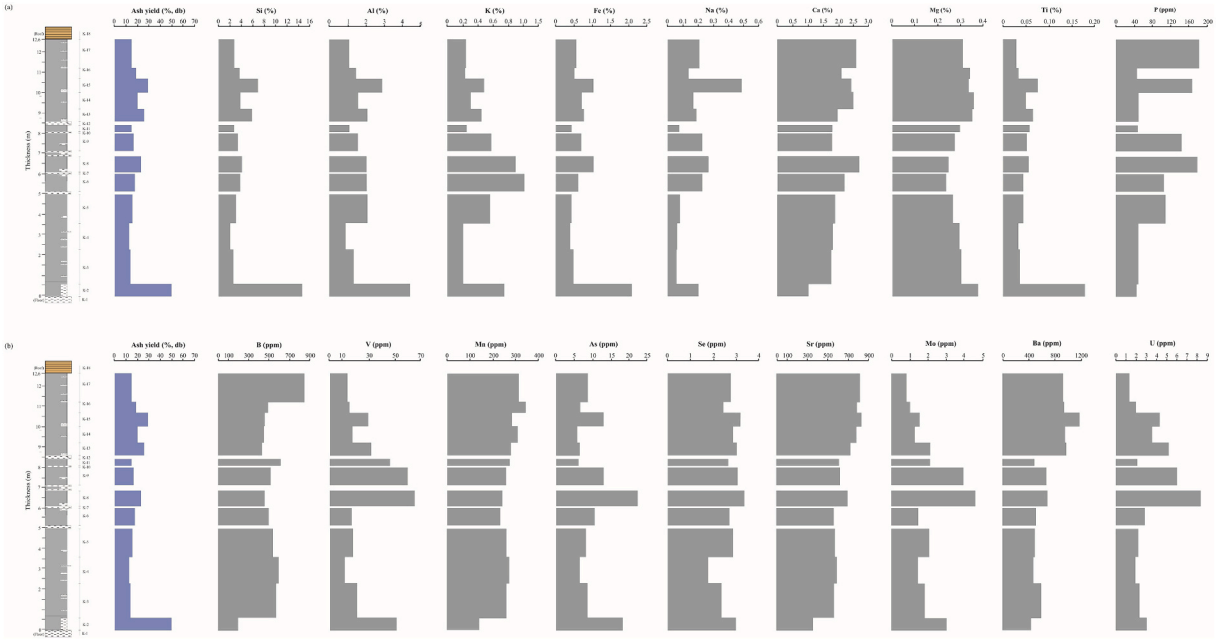

Fig. 11. Vertical distribution of (a) Si, Al, Fe, Mg, Ca, Na, K, Ti and P; (b) B, V, Mn, As, Se, Sr, Mo, Ba, and U through the Keles coal profile (for legend of lithostratigraphic column, see Fig. 4).

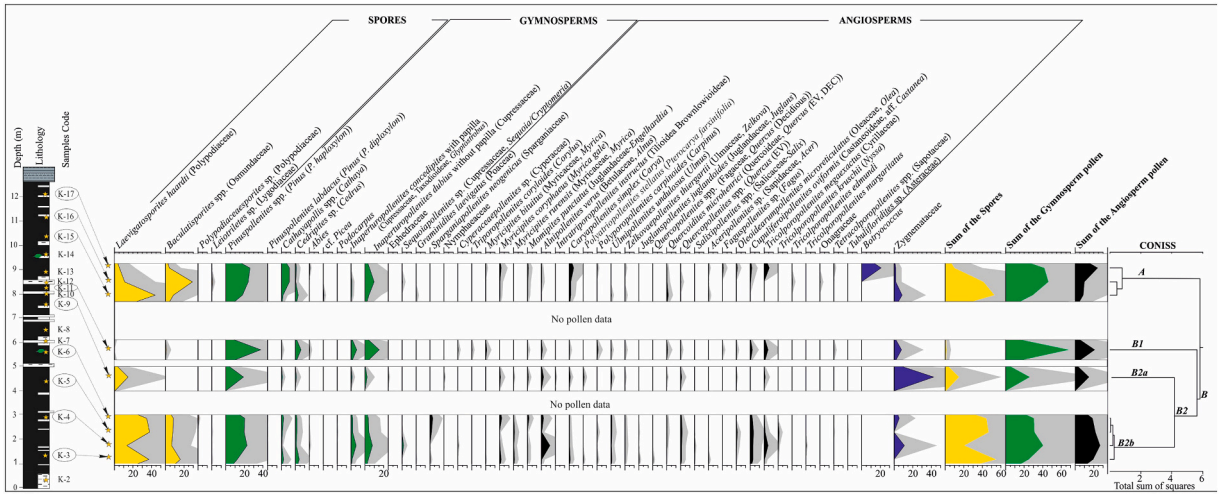

Fig. 12. Simplified pollen diagram showing the distribution of main pollen types for the studied Keles coal seam (for legend of lithostratigraphic column, see Fig. 4).

samples are B (CC=9.7), Cs (CC= 6.6), Mn (CC=2.7), Se (CC=2.7), Sr (CC=5.5), and Ba (CC=4.6) (Table 7). The average concentrations of the above enriched elements are generally higher than these in the neighbouring Tunçbilek and Seyitömer coals, while the average V, Cr, and Ni concentrations of the Keles coal are clearly lower than in these coalfields (Celik and Karayigit 2004a; Karayigit and Celik 2003; Karayigit et al., 2019a). Considering similar basement rocks and units in the margins of the Keles, Tunçbilek and Seyitömer coalfields, as noted in the discussion section, these differences could be related with either mineralogical compositions (e.g., the lack of certain accessory minerals) or redox conditions within the palaeomires. Furthermore, the B and Cs enrichments are commonly reported from Turkish Cenozoic coals, while Ba and Sr are generally enriched in altered tuff layer-bearing Cenozoic low-rank coals (Karayigit et al. 2000, 2017a, b, 2019b, 2020b; Querol et al. 1997; Palmer et al. 2004). Considering the regional volcanic activity in western and central Anatolia during Miocene and Pliocene times, the synchronous volcanic inputs into palaeomires seem to have caused elevated concentrations of these elements in the Cenozoic low-rank coals.

The affinities of elements in coal are a widely studied topic in coal geology, and statistical methods, such as Pearson's correlation coefficiencies and cluster methods have been applied. The sole usage of statistical methods could be inaccurate in some cases due to development of pseudo-affinities (Dai et al., 2020b; Drew et al. 2008; Eskenazy et al. 2010; Geboy et al. 2013; Xu et al. 2020); in order to eliminate this possibility, direct methods, such SEM-EDX and scanning proton microprobe, should be applied for more accurate interpretations (Dai et al. 2012, 2020b; Finkelman et al. 2018; Hower et al., 2008; Karayigit et al., 2017a, 2020a). In this study, the combination of Pearson's coefficiencies and SEM-EDX data is used for the determination of affinities of elements in coal samples. The Pearson's co-efficiencies show that the elements Al, Fe, Si, Mg, and Ti display strong to moderate positive correlations with the ash yield (Table 8). These correlations suggest that Al, Fe, Si, Mg, and Ti have inorganic affinities. Furthermore, Si and Al

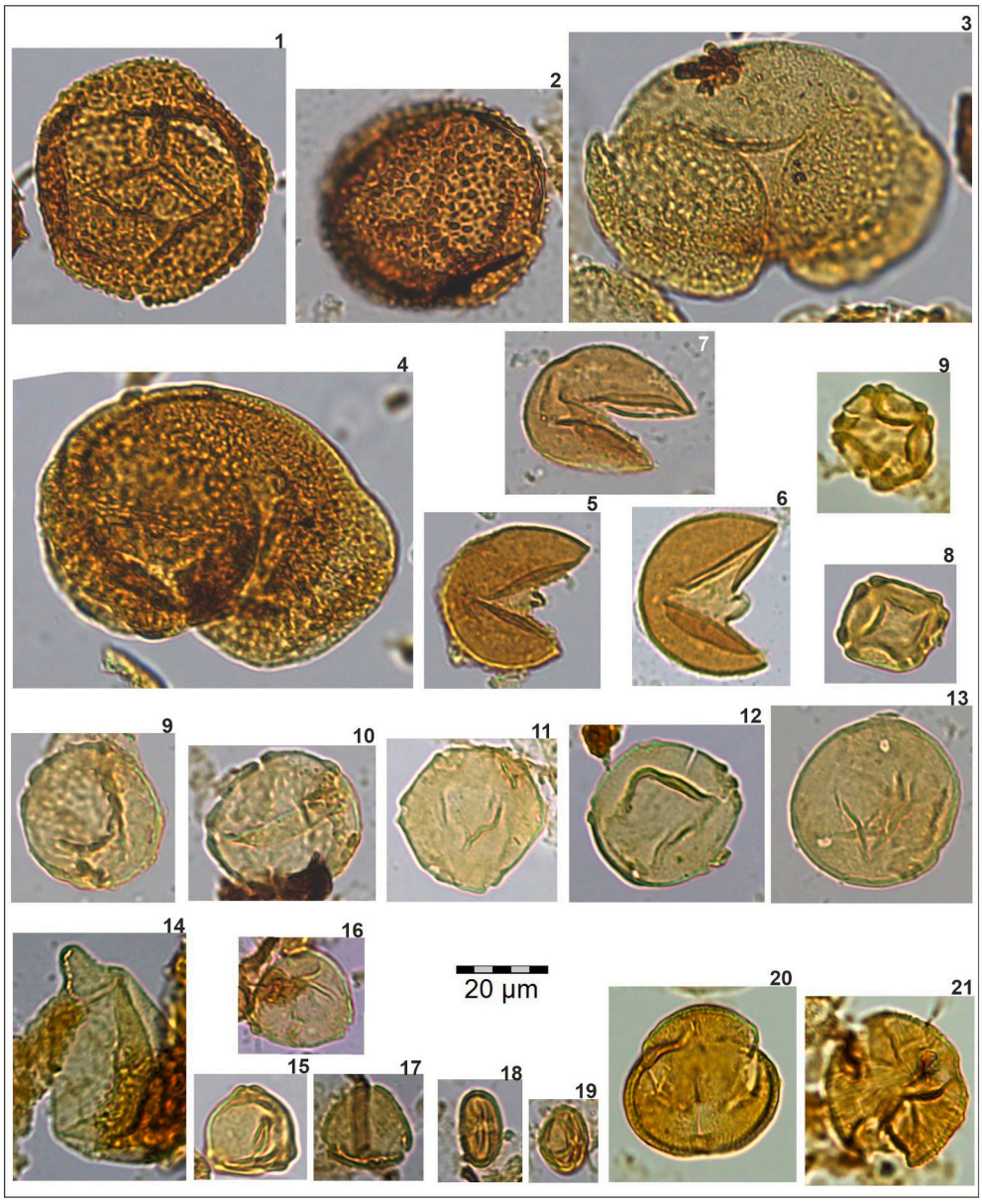

Fig. 13. Selected spores and pollen from the Keles coal seam (1,2. Osmundaceae; 3. Pinaceae-*Pinus*; 4. *Cedrus*; 5,6. Cupressaceae-Taxodioideae-*Glyptostrobus*; 7. Cupressaceae; 8,9. *Alnus*; 9,10. *Ulmus*; 11. *Pterocarya*; 12. *Carpinus*; 13. *Carya*; 14. Cyperaceae; 15. Myricaceae; 16, 17. *Engelhardia*; 18, 19. *Castanea* and 20,21. *Acer*).

display strong to moderate positive correlations with Fe, K, Mg, and Ti, indicating an aluminosilicate affinity for these elements. The SEM-EDX data show that Fe, K, Ti, and Mg are associated with illite and Mg is associated with smectite. The enrichment of Cs in Turkish Cenozoic coals is common and related to the aluminosilicate minerals, particularly clay minerals (Gürdal 2011; Karayigit et al. 2000, 2017a; Palmer et al. 2004). The Cs content of the coal samples is positively correlated with ash yield, Al and Si contents, indicating an aluminosilicate affinity, as in other Turkish Cenozoic coals. Furthermore, Si and Al contents of the studied samples also display positive correlation to several major and trace elements in the coal samples implying aluminosilicate affinity for these elements. Nevertheless, accessory, micron-sized minerals can display another affinity for these elements. For instance, Ti-oxides for Ti, and zircon for Zr.

Even though Ca and Na are traced from K-feldspars and clinoptilolite grains by SEM-EDX, these elements do not display any correlation with ash yield, Al, Si, and K contents, indicating intermediate affinity for Ca and Na. In agreement, Ca is traced from organic matter (maceral) by SEM-EDX data; however, Ca and Na show moderate positive correlations with Ba and P (Table 8). The SEM-EDX data show that accessory carbonate minerals could be a source for Ca, Mg and Mn in the studied samples. Furthermore, barite and celestine contain traceable amounts of Ca as SEM-EDX analysis proved, and Ca also correlates positively with Sr. Therefore, Ca could be affiliated with barite and celestine in the coal. In addition, Ca is partially affiliated with apatite according to the SEM-EDX data. In addition, Sr-bearing barite was identified around feldspar grains and celestine-pyrite and barite-pyrite associations were detected during SEM studies (Fig. 22). All of these indicate that Ba- and Sr-enrichments are controlled by Ba- and Sr-sulphates in the studied samples. Nevertheless, traceable amounts of Ba were also foundin clinoptilolite grains by SEM-EDX in the upper part of the seam. The zeolite affinity for Ba and Sr was reported from analcime-bearing Middle Miocene Beypazarı coal deposit where liberated Ba and Sr from the alteration of volcanic inputs were adsorbed by analcime (Querol et al. 1997). Similarly, in the Keles coal, the liberated Ba and Sr from alteration of feldspars were presumably absorbed by zeolite minerals. Hence,

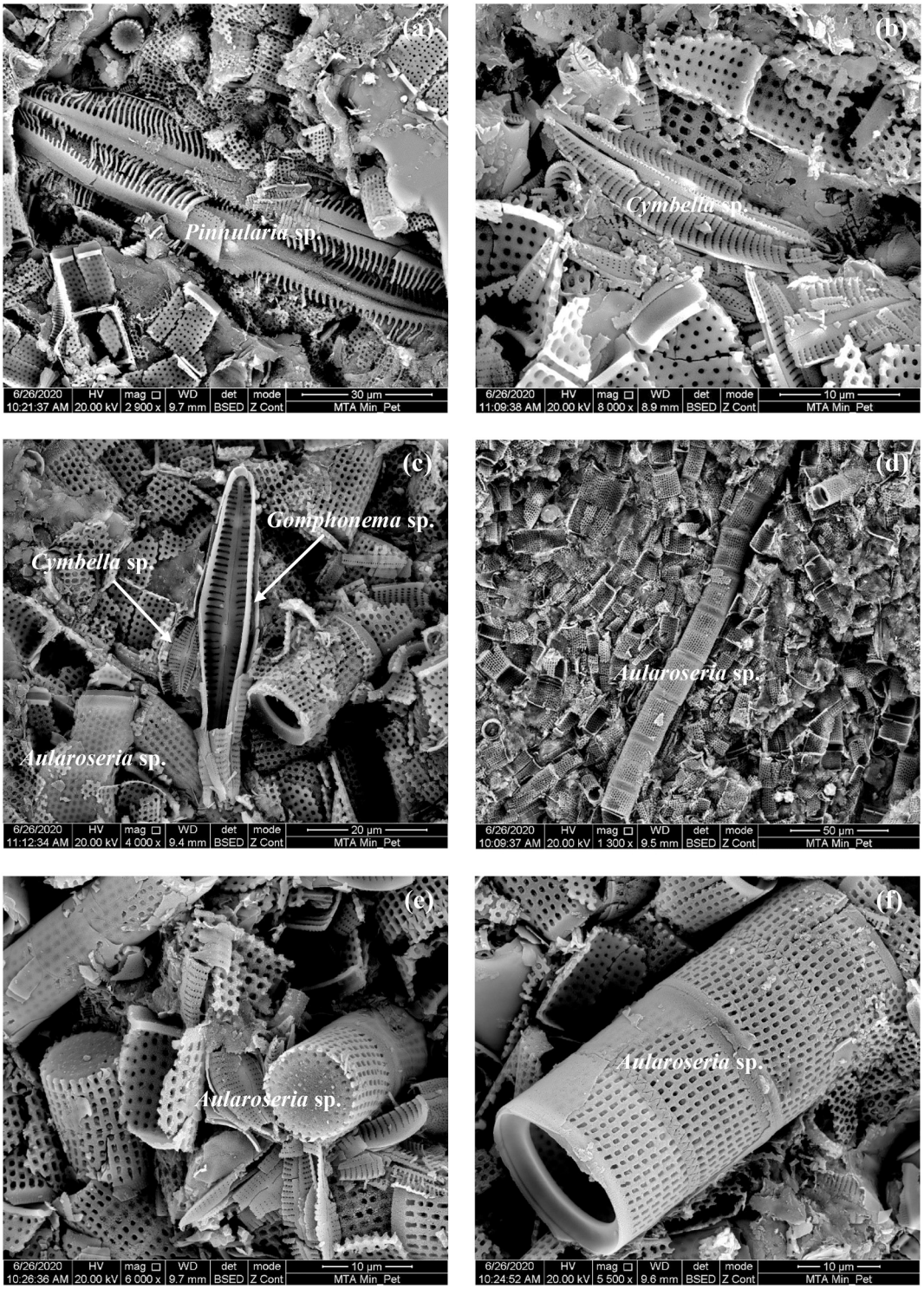

Fig. 14. SEM backscattered images of identified diatoms in the Keles roof rock (K-18) sample.

Ba and Sr might also have a partial zeolite affinity in the studied seam.

Selenium concentrations of Turkish Cenozoic coals are generally low, and Se-bearing epigenetic minerals (e.g., clausthalite) are rarely reported from Turkish Palaeozoic coals (Karayigit et al. 2000; Karayigit et al., 2018; Palmer et al. 2004). The element Se is affiliated with organic matter and sulphide minerals in coal (Bullock et al. 2018; Hower and Robertson 2003; Yudovich and Ketris 2006). Even though Se displays a weak positive correlation with ash yield, and no Se-bearing minerals (e.g., clausthalite) were identified by SEM-EDX. It is reported that certain microorganisms (e.g., algae) in palaeomires could also contain selenoproteins (Riley et al. 2007). The vertical distribution of Se is not variable throughout the seam, and there are not any notable differences in Se contents between alginite-bearing samples and other samples in the upper seam. Besides, Se displays moderate positive correlations with K and Na contents, suggesting possible aluminosilicate affinity. The alteration of synchronous volcanic input, on the other hand, could represent the source for Se ions in the palaeomires, and the adsorption of Se by minerals could be possible (Yudovich and Ketris 2006).

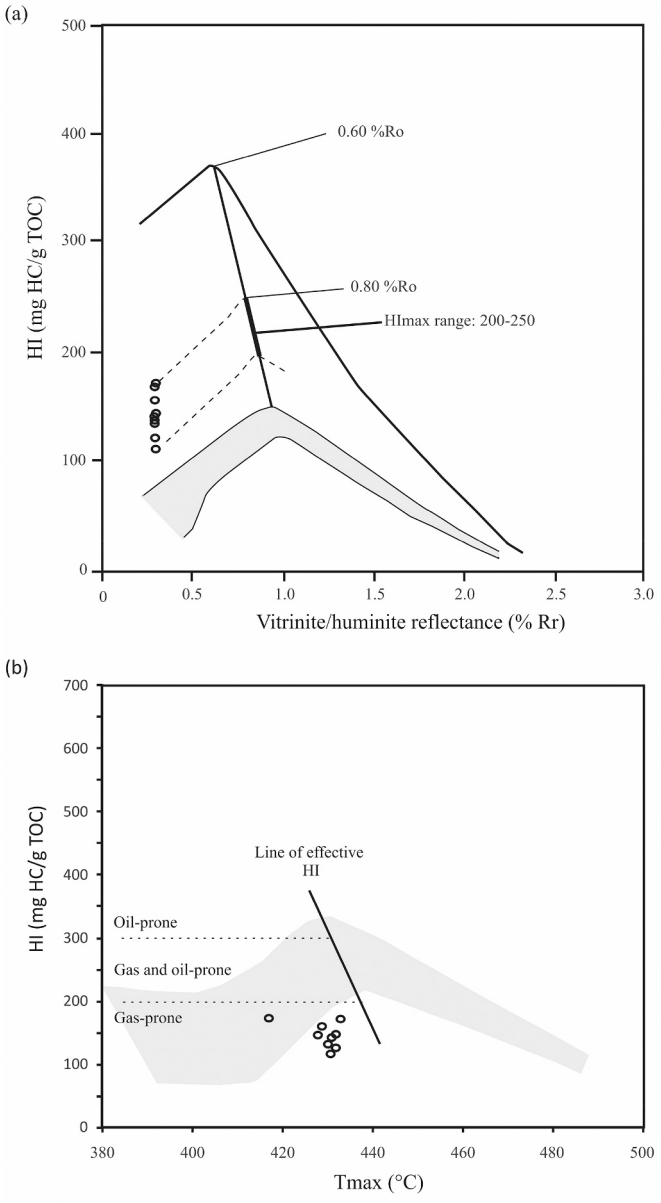

Fig. 15. (a) Plot of HI vs VR diagram (after Petersen 2006), and (b) HI vs T_{max} diagram (after Sykes and Snowdon 2002).

Considering that Na is mainly affiliated with clinoptilolite in the studied samples, clinoptilolite adsorption of Se, as with Ba and Sr, might have taken place in the Keles palaeomire.

Boron enrichment is in coals generally explained as synchronous and/or related to post-depositional marine influence onto palaeomires (Goodarzi and Swaine, 1994; Hower et al. 2002) or the presence of certain elements (e.g. clay minerals or tourmaline) in coal seams (Dai et al., 2020a, b; Eskenazy et al., 1994; Karayigit et al., 2020b). As mentioned earlier, high B contents could also developed in coal seams within non-marine sequences (Kear and Ross, 1961; Lynskey et al., 1984; Mackay and Wilson, 1978; Moore et al., 2005; Newman et al., 1997), bolstering with this, in Cenozoic Turkish coals, B enrichment is mostly related to synchronous volcanic input into palaeomires and the influence of hydrothermal solutions (Karayigit et al., 2017a, b; Querol et al. 1997). Considering the presence of freshwater palynoflora and the lack of any marine indicators in the Keles palaeomire, marine influence is not possible for B enrichment. Even though B displays negative correlations with ash yield, Al, K, and Ca suggest an organic affinity (Table 8), which could be pseudo-correlated with relatively high B concentrations in the upper part of the seam (Fig. 11b). Nevertheless, the source of B in coal, as well as in lacustrine deposits could be volcanic rocks and/or tuff layers leached by surface water (Karayigit et al., 2017a; Querol et al. 1997; Stamatakis 1989). In some coal-bearing Cenozoic grabens from western Turkey, B and zeolite deposits were reported where K-rich volcanic inputs into brine lakes represent the source for B and natural clinoptilolite formation (Gündogdu et al., 1989, 1996; Helvacı and Alonso, 2000). Considering the presence of altered K-feldspar grains in the Keles coal, liberated B ions from alteration of synchronous volcanic inputs in the palaeomires might be adsorbed by syngenetic clinoptilolite. Thus, B concentrations are elevated in the upper part of the seam (Fig. 11b).

In Tunçbilek and Seyitömer coalfields, Ni and Cr enrichments were also reported due to detrital chromite and pentlandite derived from ophiolites in the adjacent areas (Celik and Karayigit 2004a; Karayigit and Celik, 2003; Karayigit et al., 2019a). In contrast, in the Keles coal neither chromite nor pentlandite were identified by SEM-EDX studies, and Ni and Cr contents are close to the world low-rank Clarke values (Table 7) (Ketris and Yudovich 2009). These differences in elemental and mineralogical compositions could be related to the metamorphic rocks in the adjacent areas, while ore-grade Cr-bearing ophiolites are located in the adjacent areas of Tunçbilek and Seyitömer coalfields (Karayigit et al., 2019a). The palaeocurrent directions from the studied section in the Keles coalfield also imply that source of detrital input was the metamorphic rocks in the NE and E margins. The elements Ni and Cr in the Keles coalfield display positive correlations with the ash yield, and the Si and Al contents, suggesting possible aluminosilicate affinity for these elements.

Nickel, along with Fe, V, As, Mo, and Hg, show moderate to strong positive correlations with the total S contents of coal, implying a sulphide affinity for these elements. Pyrite is a minor phase in the studied samples and As, Ni, Mo, and Hg were not detected by SEM-EDX in framboidal pyrite grains. The lack of measureable chalcophile in syngenetic framboidal pyrite grains should not be interpreted as an absolute lack of an association due to their low concentrations or their possible mobilization from oxidized pyrite grains (Hower et al., 2008; Kolker 2012; de Joux and Moore, 2005). For example, while Hower et al. (2008) found significant concentrations of As in pyrite and marcasite over a wide order-of-magnitude range, a significant amount of Hg could only be detected in one marcasite grain only. Similarly, Weber et al. (2006) found Ni in a framboidal cluster using time-of-flight secondary ion mass spectrometry.

The elements As, Mo, and U are considered as redox-sensitive elements (Arbuzov et al. 2011; Dai et al., 2008), and generally display positive correlations with total S contents in Turkish Cenozoic coals due to alterations of synchronous volcanic inputs under anoxic conditions in palaeomires (Karayigit et al., 2019b, 2020a; Querol et al. 1997). Although U and total S contents do not display any correlation, U contents have moderate to strong positive correlations with V, As, and Mo, implying the development of anoxic conditions in the palaeomires. The development of alkaline conditions in palaeomires may also cause enrichment of As, Mo, and U (Querol et al. 1996); however, in the studied coal seam As, Mo, and U contents are relatively higher in the middle part of the seam (Fig. 11b). This part of the seam might have had anoxic and weak-acidic conditions developed in the palaeomire; these conditions resulted in a better preservation of the organic matter than in the upper part of the seam. Hence, the distribution of As, Mo, and U in the Keles coal section is related with the development of anoxic conditions in the palaeomire.

5.5. *Age of the Keles coalfield*

According to the palynological records of the Turkish and European Neogene Basins, the Miocene palynoflora has a unique palynofloral content (e.g. Bertini 2006; Biltekin et al. 2015; Fauquette et al. 2007;

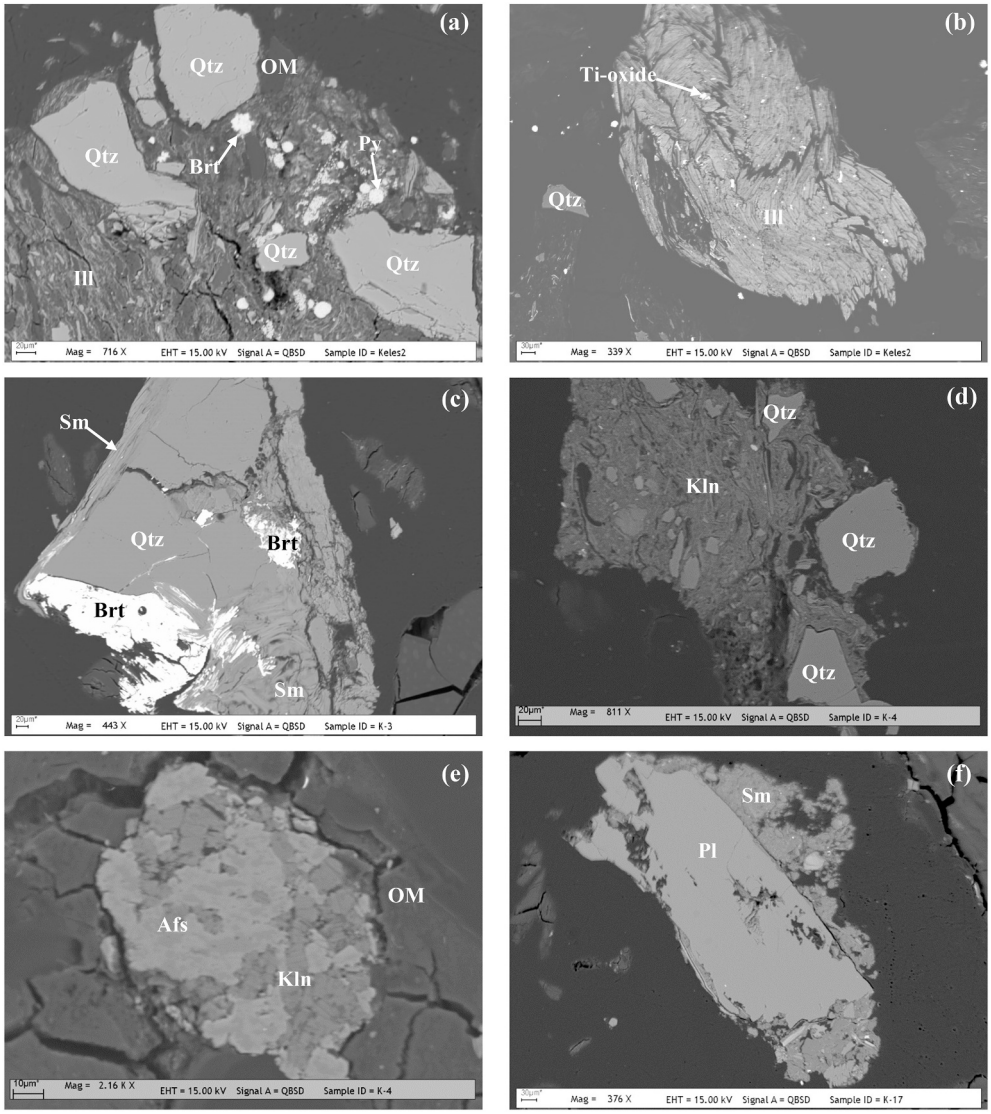

Fig. 16. SEM backscattered images in the Keles coal samples: a) quartz (Qtz), barite (Brt), pyrite (Py) and organic matter (OM) associated with illite (Ill) clay matrix; b) individual quartz (Qtz) grains, and Ti-oxide associated with illite (Ill) clay matrix; c) quartz (Qtz) associated with smectite (Smc) clay matrix, and epigenetic barite (Brt); d) quartz (Qtz) associated with kaolinite (Kln) clay matrix; e) kaolinite (Kln) associated with alkali feldspar (Afs); f) smectite (Smc) associated with plagioclase (Pl).

Ivanov 2015; Ivanov and Lazarova 2019; Ivanov and Worobiec 2017; Ivanov et al. 2007a, 2011, 2019; Jiménez-Moreno and Suc 2007; Karayigit et al. 1999; Kayseri and Akgün 2008; Jiménez-Moreno, 2006; Kayseri-Özer et al., 2014a, b; Popova et al. 2017; Uhl et al. 2007a, 2007b; Utescher et al., 2009a, 2009b, 2011a, 2011b, 2013, 2015; Yavuz et al. 2017). The existence and abundance of some spore species (e.g. *Leiotriletes adriennis, L. maxoides maxoides, Cicatricosisporites* sp.) significantly declined from the Oligocene to the Miocene, however some of the spores (e.g. *Leiotriletes microadriennis*) are observed during the Miocene. In addition, the presence of a high percentage of spores may be related to the deposition environment condition, and their abudance is useable for the age interpretation based on the palynological study (Akgün and Akyol 1999; Ivanov et al. 2002; Jiménez-Moreno and Suc, 2007; Kayseri and Akgün 2008). The pollen species *Plicatopollis pseudoexelsus, Plicapollis plicatus*, and *Momipites quietus* of the thermophilous plants are predominantly recorded in the Eocene, Oligocene, and early Miocene; the abundance of these pollen decreased during the Miocene (Akgün and Sözbilir 2001; Kayseri-Özer et al., 2014a,b; Stuchlik and Kvavadze, 1998). However, *Momipitespunctatus* was accompanied by the *M. quietus* during the Miocene (Akgün and Akyol 1999). In the Turkish middle Miocene palynoflora, *Caryapollenites simplex* (*Carya*) is abundant, but the abundance and diversity of some *Carya* species (e.g., *Subtriporopollentes anulatus nanus* and *S. constans*) is low from the middle to late Miocene. Diversity and percentage of the woody angiosperm pollen (Cyrillaceae, *Castanea*, *Quercus*, *Pterocarya*, *Carya*, *Alnus*, *Ulmus*, Oleaceae, *Salix/Platanus*, and *Nyssa*) were predominat in the middle Miocene due to palaeoclimatic and palaeonvironmental conditions. The abundance of the herbaceous pollen species (Amaranthaceae, Caryophyllaceae, Apiaceae, Asteraceae–Asteroideae, Asteraceae–Cichorioideae, Ephedraceae, and *Artemisia*) increases from Miocene to Pliocene in the western Anatolia (Kayseri-Özer 2014, 2017). According to the palynofloral composition, the studied samples from Keles coalfield represented by absence of the oldest spore species and less abundant herbaceous angiosperm pollen and the coal-bearing sediments were deposited during the middle Miocene. Furthermore, the fossil mammal fauna from Bursa-Orhaneli coalfield (MN6-7; 11.2-16.4 million years, Onar and Yıldız 2005) and Paşalar locatily (MN6, Pickford et al., 2020), which are located near to Harmancik Basin, are in aggrement with palynological data and imply middle Miocene age.

5.6. Coal depositional environment

5.6.1. Palaeovegetation during peat accumulation

Palynological studies enhance knowledge of depositional environments in the ancient terrestrial setting. Palaeoecological interpretations used the main palynoflora allows us to distinguish the main

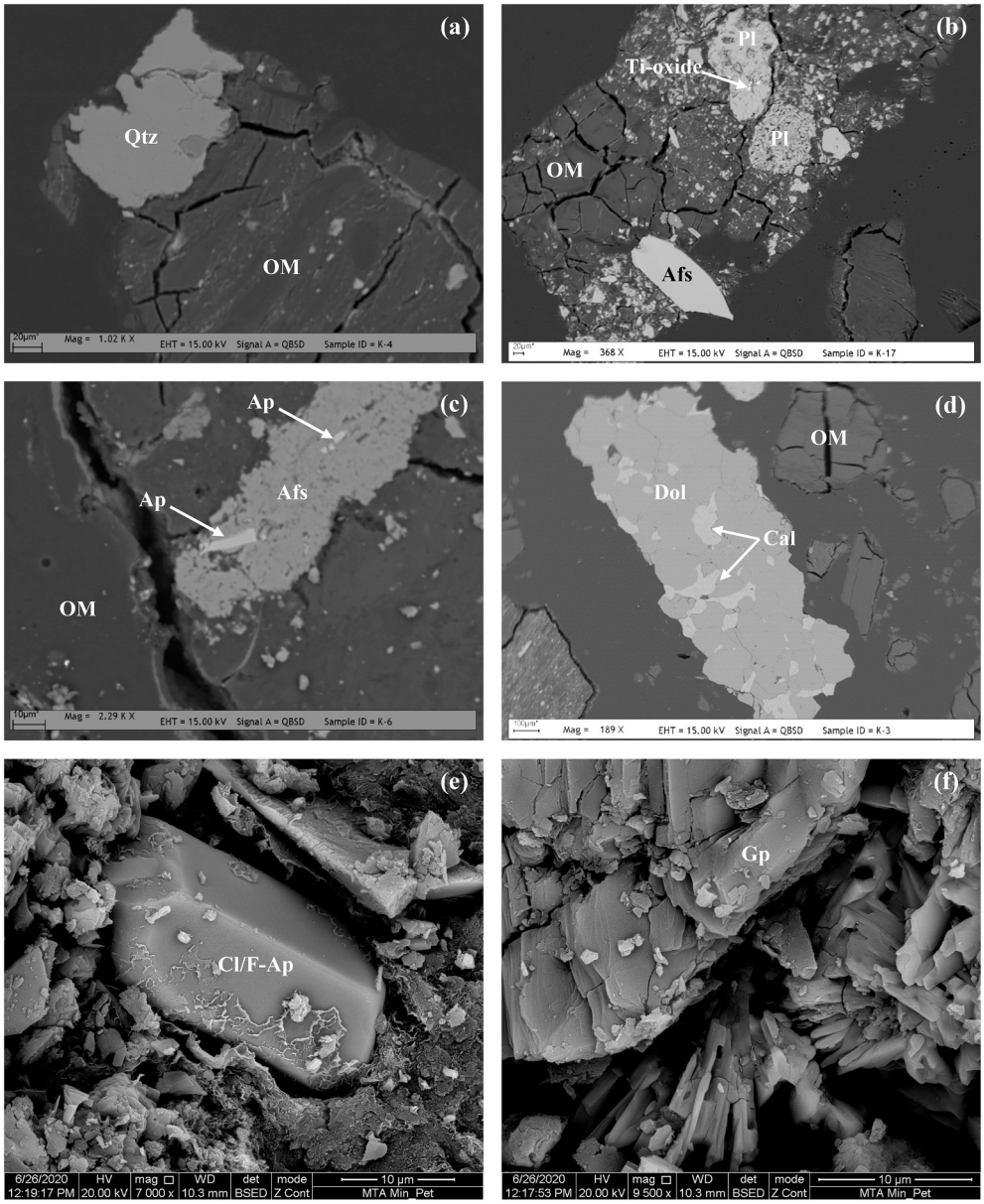

Fig. 17. SEM backscattered images in the Keles coal samples: a) individual quartz (Qtz) grain associated with organic matter (OM); b) Ti-oxide, plagioclase (Pl) and alkali feldspar (Afs) associated with organic matter (OM); c) apatite (Ap) associated with alkali feldspar (Afs); d) epigenetic calcite (Cal) and dolomite (Dol); e) individual chlor-/fluorapatite (Cl/F-Ap); f) gypsum (Gyp).

palaeovegetation type, developed in the middle Miocene palaeomires of the study area: mixed mesophytic forests, riparian forests, forested mire with ferns, mire and aquatic elements, and coniferous association. The most commonly identified fossil pollen belong to species of *Quercus,* Cyrillaceae*, Castanea, Ulmus, Zelkova,* Oleaceae-*Olea*, and *Carya*; the percentage of other pollen varies (*Carpinus, Corylus, Tilia, Acer, Pterocarya, Engelhardia*, *Juglans,* and others) within comparatively narrow ranges (generally between 1-5%). The co-occurence of these taxa is consitent with the establishment of the mixed mesophytic forest in the middle Miocene. In addition, sporadic occurrence of pollen types such as *Salix,* Mastixiaceae*,* Onagraceae, and others of the mixed mesophiytic and riparian forests are also recorded in the palynoflora. The herbaceous pollen of the non-arboreal pollen (NAP) is only represented by three pollen species (Poaceae, Ephedraceae, and Asteraceae-Tubuliflorea type), and these are less abundant and/or sporadic in the middle Miocene palynospectra of the Keles coals. As such, grassland areas were not widespread in the study area. Existence of the arboreal pollen (AP) species of the woody and shrub palaeovegetation elements (*Alnus*, *Myrica*, *Salix*, *Quercus*, Cyrillaceae, *Castanea*, *Ulmus*, *Zelkova*, Oleaceae-*Olea* evergreen and deciduous types, *Carpinus*, *Corylus*, *Tilia*, *Acer*, *Pterocarya*, *Engelhardia*, *Juglans*, and *Carya*) indicates the dominance of forest-type palaeovegetation represented by mixed mesophytic and riparian forests in the surrounding depositional area during the middle Miocene (Fig. 11).

The greater abundance of gymnosperm pollen in the palynospectra indicates palaeovegetational change in the middle Miocene. *Pinus haploxylon*-type pollen predominates over *Pinus silvestris*-type and *Cathaya*. These gymnosperms thrived at middle and high altitude areas and/or were generaly observed in the deciduous forest during the Neogene (e.g. Casas-Gallego et al., 2020; Ivanov and Lazarova 2019; Kayseri and Akgün 2008). Among the other coniferous pollen, *Cedrus* is predominant (between 5-10%), while *Tsuga, Picea*, and *Abies* are less common, usually in the range of 1-3%. The palynospectra shows the presence of coniferous plants (*Pinus haploxylon* and *silvestris*-types, *Cedrus, Tsuga, Picea*,

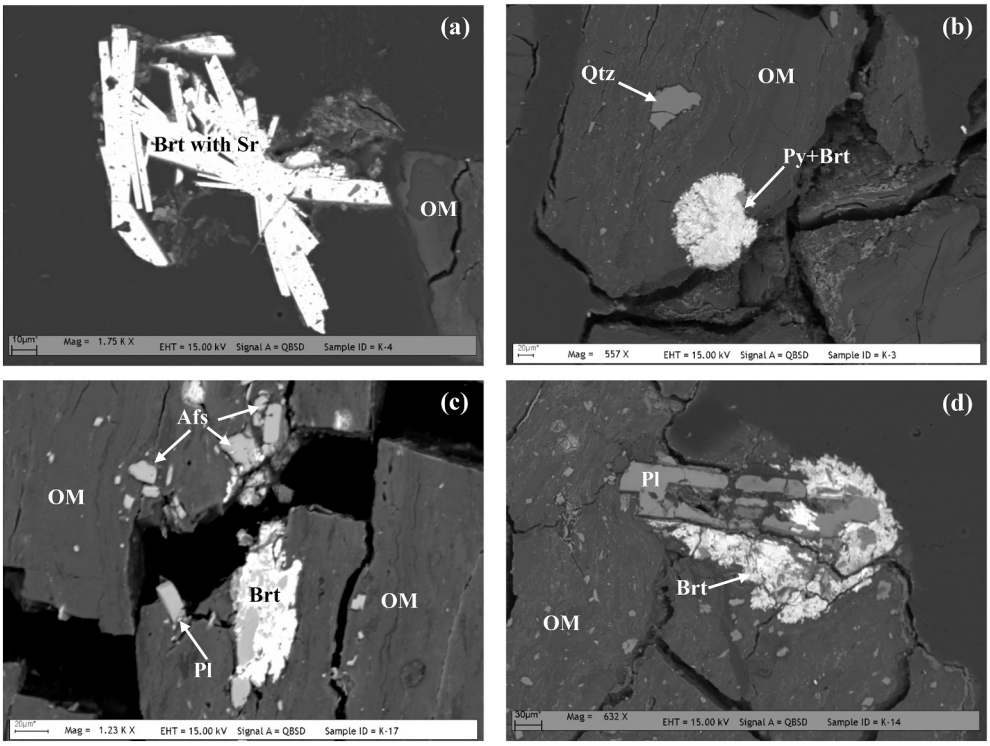

Fig. 18. SEM backscattered images in the Keles coal samples. a) epigenetic barite (Brt) with traceable strontium (Sr); b) framboidal pyrite (Py) grain associated with barite (Brt); c) alkali feldspar (Afs) associated with organic matter (OM), and barite (Brt) zone around plagioclase (Pl) grain; d) barite (Brt) zone around plagioclase (Pl) grain within organic matter (OM).

and *Abies)* and some angiosperms (*Corylus, Juglans, Fagus, Carpinus, Pterocarya*, etc.) which developed in low- to high-mountain plant communities during the middle Miocene (Fig. 11).

The riparian flora and mire palaeovegetation (e.g. *Alnus*, *Myrica*, *Salix*, *Ulmus, Zelkova,* Typhaceae, *Nyssa*, Osmundaceae, and Nymphaeaceae), developed on wet lowlands and coastal mire territories that provided the necessary water level for their development. Within the dominant elements of this palaeovegetation were representatives of Taxodioideae and *Alnus*. In conjunction with them, Cyperaceae, *Glyptostrobus, Nyssa*, Nymphaeaceae, Typhaceae, *Myrica, Sequoia*, and Osmundaceae were observed (Fig. 11).

The spore species have been defined with four taxa, and only representatives of *Baculatisporites* spp. (Osmundaceae-*Osmunda*) and *Laevigatosporites haardti* (Thelypteridaceae/ Polypodiaceae) have a higher abundance in the palynospectra of the study area. This common spore species peaks in the lowermost and upper parts of the seam indicating the presence of telmatic condition in the lacustrine palaeoenvironment. Additionally, other microfossils present in consist of the zygospores (*Spirogyra* sp. (Zygnemataceae)), fungal spores, and the green algae *Botryococcus*. Abundant *Spirogyra* sp. (Zygnemataceae) and the *Botryococcus,* which prefer to live in the freshwater and brackish ponds and lakes, peak in the uppermost portion of seam, beneath the diatomite roof rock supported the telmatic conditions (Fig. 11).

5.6.2. Palaeoclimate reconstruction

In this study, for the palaeoecological (e.g. palaeoclimate and paleoenvironment) interpretation, sporomorphs have been grouped based on the ecological preferences of the plants. The subtropical (megamesothermic: Cupressaceae, Cupressaceae-Taxodioideae-*Glyptostrobus*, *Engelhardia, Myrica,* Sapotaceae, *Castanea-Castanopsis* type, and Cyrillaceae-Clethraceae) and warm temperate (mesothermic: *Quercus*, *Carya*, *Pterocarya, Carpinus*, *Juglans*, *Zelkova*, *Ulmus*, *Tilia*, *Acer*, *Alnus, Salix*, *Nyssa*, *Sequoia*-type and *Fagus)* elements are abundant in the studied samples. The microthermic and meso-microthermic elements (high- and mid-altitude elements: *Abies*, *Picea* and *Cedrus*) are less abundant. The herbaceous plants representing the steppe elements are minor components (Fig. 23). Based on these climatic inferences and the palynomorph distributions, the palaeoclimate during the peat-accumulation is considered to have been humid subtropical during the middle Miocene. The occurrence of Typhaceae, *Sequoia*, Cyperaceae, Polypodiaceae, and Osmundaceae supports the development of mire conditions. The abundance of *Alnus* and *Myrica*, common riparian forest elements, suggests the palaeomire was fed with streams created by increased precipitation. The depositional environment in the middle part of the studied seam significantly changed with a notable decrease in the abundance of spores. This environmental change based on fluctuation of spore species and mire element values, could suggest seasonality during the middle Miocene in the study area due to precipitation change.

Continental climate records over the last 45 Ma have been reconstructed from micro-macrofloral data of Europe using the CoA, and also various climatic variables from European countries were obtained using this method (e.g. Barrón et al., 2010; Bruch et al. 2006, 2011; Ivanov et al. 2002, 2007a, 2007b; Mosbrugger and Utescher 1997; Syabryaj et al. 2007; Utescher et al. 2007a, 2007b, 2009). In Turkey based on the published palynologica studies, detailed palaeoclimatic interpretations were reconstructed for the Miocene by Akgün et al. (2007) and for the Eocene to Miocene interval by Kayseri-Özer (2014, 2017). In this study, numerical climatic values of middle Miocene coal samples in Keles coalfiled were obtained using the CoA method. The average CMT and MAP values of the lower part of the seam are 6.76 °C and 1216 mm, respectively. These values in the middle part of the seam are 8.2 °C and 1137.5 mm, and in the upper part one 9.28 °C and 1157 mm, respectively. According to these climatic values, the highest percipitation is recorded in the samples of the lower part seam in which riparian elements have been abundantly observed. Thus this abundance could be related to the high precipitation ratio (MAP: 1216 mm). Furthermore, fluctuations of the MAP and CMT values from the lower to upper part of the seam in this study could be attributed to seasonality. For the middle

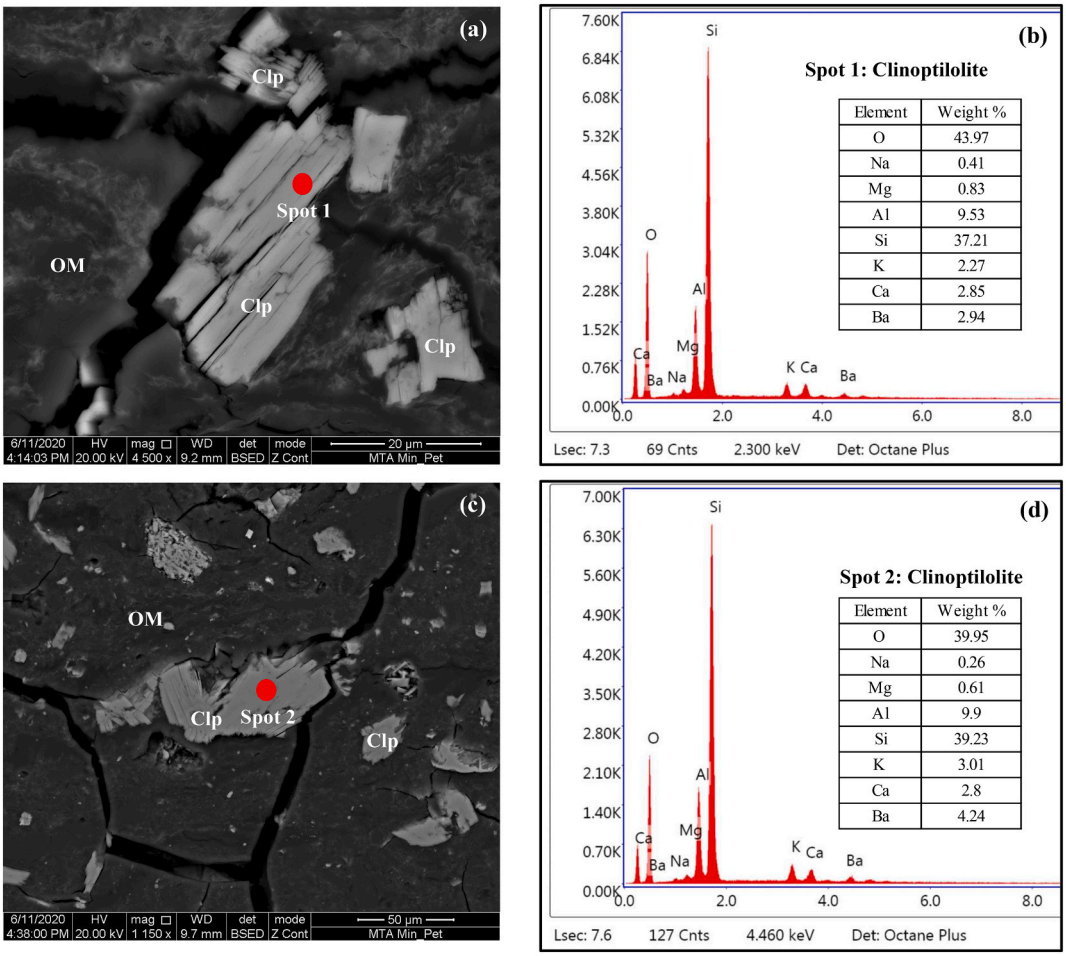

Fig. 19. SEM backscattered images (a, c) and SEM-EDX spectra (b, d) of clinoptilolite in the Keles coal samples.

Miocene, the average CMT and MAP values of other localities (Manisa-Akhisar (3.18°C and 1171 mm), Soma (5.21°C and 1112 mm); Aydın-İncirliova (2°C and 1135 mm), Hasköy (3.46°C and 1083 mm), Köşk (6°C and 1112 mm), Söke (5.3°C and 1068 mm), Şahinali (4.85°C and 1132 mm); İzmir-Kemalpaşa (5.6°C and 1116 mm)) have been calculated by CoA method Kayseri-Özer (2014, 2017), and the highest average CMT values belong to Keles coalfield (CMT 7.8°C). This warm climatic condition based on the CMT values of the study area could be related to the local climate, palaeotopography, deposition systems, and/or palaeogeography.

5.6.3. Coal facies

The merits of undertaking coal facies analysis has been long debated some critiques for coal facies indices and diagrams have been published since they were introduced to coal geology (Crosdale 1993; Dai et al., 2020b; Moore and Shearer 2003). These critiques are mainly based on transformation of organic matter from peat to coal during the early coalification stage, the origin of macerals (e.g., fire derived or allochthonous inertinite), processes within palaeomires (e.g., damages caused by fungi and by avian and other fauna), representative sampling interval corresponding to a short time of peat formation, and dispersion of arboreal pollen (AP) (e.g., bisaccate pollens) and leaves in the palaemires (Dai et al., 2020a). Therefore, coal facies analysis should be applied with caution and combined with other disciplines (e.g., mineralogy, sedimentology, and organic geochemistry) (Kus et al., 2020; Stock et al., 2016; Zdravkov et al., 2020; Zieger and Littke 2019). For instance, the published data from Turkish Cenozoic coals show that coal facies indices and diagrams, particularly using modification of Kalkreuth et al. (1991) and Kalaitzidis et al. (2004) for Cenozoic coals, could provide reasonable data when they are combined with mineralogical, palynological and/or organic geochemical data (Bechtel et al., 2014; Çelik et al., 2017; Karayigit et al., 2017a, b; Oskay et al., 2019a).

The studied coal samples, mainly from the upper parts of the seam, are mostly plotted in the area between apexes A and B of Mukhopadhyay's (1989) ternary diagram, while some samples (e.g., K-6 and -9) from lower and middle parts of seam projected closer to apex A (Fig. 24). These plotting data show that the contribution of woody peat-forming plants (e.g. Cupressaceae, Cupressaceae-Taxodioideae-*Glyptostrobus*) were high during the inital stages of peat accumulation, while herbaceous peat-forming plants (e.g., Osmundaceae, Polypodiaceae, and Nymphaeaceae) were common. Thus, mixed vegetation developed during the late stages of peat accumulation in middle Miocene. Furthermore, almost all samples were obtained from the lower seam suggesting that the palaeomire surface was constantly covered by the watertable. One sample (K-4) which has an inertinte content higher than the other samples, is located separately. This could suggest a lowering of the watertable and the formation of relatively suboxic conditions. In contrast, macrophyte and conifer palynomorphs were observed in this sample, and inertodetrinite and funginite are the predominant inertinite macerals. As mentioned earlier, the former maceral is associated with detrohuminite macerals and clays, and in such an association, inertodetrinite had an allochthonous origin (O'Keefe et al., 2013; Oskay et al., 2019b). In addition, funginite could imply that decay of organic matter took place in a humid environment, and the decay seems to develope after the plant death due to the lack of resinite-funginite association (Hower et al. 2010; Ogala et al. 2012).

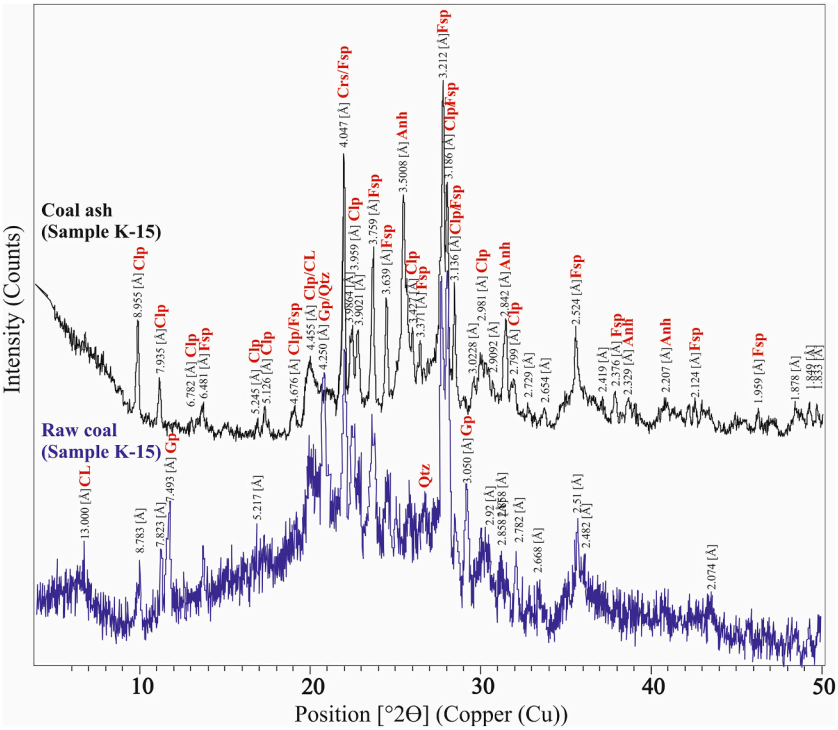

Fig. 20. X-ray diffraction patterns of raw coal and coal ash sample (K-15) (Anh: anhydrite, Cl: clay mineral, Clp: clinoptilolite, Fsp: feldspar, Gp: gypsum, Qtz: quartz).

The plotting data on TPI *vs.* GI and GWI *vs.* VI diagrams, which are based on the modification of Kalkreuth et al. (1991) and Kalaitzidis et al. (2004) for Cenozoic coals, also point out vegetation changes within the palaeomires during middle Miocene (Fig. 25). The TPI and VI values are slightly increased from the lower to middle parts of the seam, and ranges from 1.1-3.0, and 0.8-3.2, respectively (Figs. 4 and 25). These imply that the contribution of woody peat-forming vegetation was common during the initial stages of peat accumulation. These conditions are generally related with wet forest mire conditions (Oikonomopoulos et al., 2015; Omodeo-Salé et al., 2017; Kus et al., 2020; Mitrović et al. 2016; Oskay et al., 2019a); hence, a xylite-rich lithotype is identified from this part of the seam. This assumption is also supported by relatively higher proportions of Cupressaceae and Cupressaceae-Taxodioideae-*Glyptostrobus* pollen in this part of the seam. Under wet forest mire conditions, the preservation of organic matter could also be high due to development of anoxic conditions (Karayigit et al., 2017a; Korasidis et al., 2020; Omodeo-Salé et al., 2017). In such conditions, preservation of organic matter is high and detrital input ratios are low. Hence, relatively lower ash yields and higher TOC contents were obtained from the lower and middle parts. The low detrital input ratio into the palaeomire during initial stage could also explain the relatively low ash yield of the Keles coal than this of Seyitömer and Tunçbilek coals (Celik and Karayigit 2004a, 2004b; Karayigit and Celik 2003; Karayigit et al., 2019a). Furthermore, the anoxic conditions could be also manifested by the framboidal pyrite grains associated with Sr-bearing barite, and relatively higher concentrations of Mo and U in the middle seam part (Fig. 11b). The decreased ash yields from the lower to the middle seam part might indicate that detrital input was decreased, in turn, Al and Si concentrations were decreased. The TPI and VI values around 1.0could be an indicator of ferns (e.g. Osmundaceae-*Osmunda* and Thelypteridaceae/ Polypodiaceae) in the palaeomires (Omodeo-Salé et al., 2017; Oskay et al., 2019b). In agreement with the palynological data, the common presence of telohuminite A along with resino-corpohuminite and carboxyl/carbonyl and hydroxyl groups from the FT-IR present another evidence for the contribution of conifers in the palaeomires. Furthermore, the fluorinite-type resinite and *Myrica* pollen could also be source for carboxyl/carbonyl and hydroxyl groups in the studied samples (O'Keefe et al., 2013; Pickel et al., 2017). As mentioned above, resin-rich peat-forming plants (e.g. conifers) also could contain oxygen-rich compounds; thus, OI values of the lower and middle parts are generally higher than these of the upper part of the seam. The variable GI values (0.6-8.3) in the lower and central seam parts point to intense gelification of organic matter and unstable water-level; however, the relatively low GWI values (0.8-1.2) might be an indicator for watertable lowering. The relatively high telohuminite contents may have caused reduction of the GWI values which can easily be interpreted as a low watertable in the palaeomire. Such cases are generally reported from xylite-rich lithotype-bearing Cenozoic coals in south-eastern Europe and Miocene coal seams in western Turkey (e.g., Çelik et al., 2017; Kalaitzidis et al. 2004; Karayigit et al., 2017a; Mitrović et al. 2016; Oikonomopoulos et al., 2015). Therefore, the watertable constantly (i.e., was high) covered the mire surface during middle Miocene.

The TPI and VI values of the samples (except sample K-17) from the upper part of the seam are lower than 1.0, conversely with the lower and middle parts (Fig. 25). These values could be an indicator for low tissue preservation, which could explain the lower TOC contents of the upper part of the seam. The TPI, VI and GI values of the upper part of the seam are within the range for limno-telmatic palaeomires where the contribution of reeds and other macrophytes could be high (Omodeo-Salé et al., 2017; Oskay et al., 2019b). The relatively high GI values and Ca contents of the upper parts of the seam imply that alkaline conditions were developed within the palaeomire (Bechtel et al., 2014; Oikonomopoulos et al., 2015). The increased alkalinity could have enabled bacterial activity, thus reducing the preservation of organic matter and increase gelification of organic matter (Dehmer, 1989; Oikonomopoulos et al., 2015; Karayigit et al., 2017a). Such conditions could also result in natural zeolite formation from synchronous volcanic input at the late stages of peat accumulation. Barium and Sr concentrations in the upper part of the seamare higher than in the other parts; enrichment of these elements in coal is controlled by the marine influence within the peat-

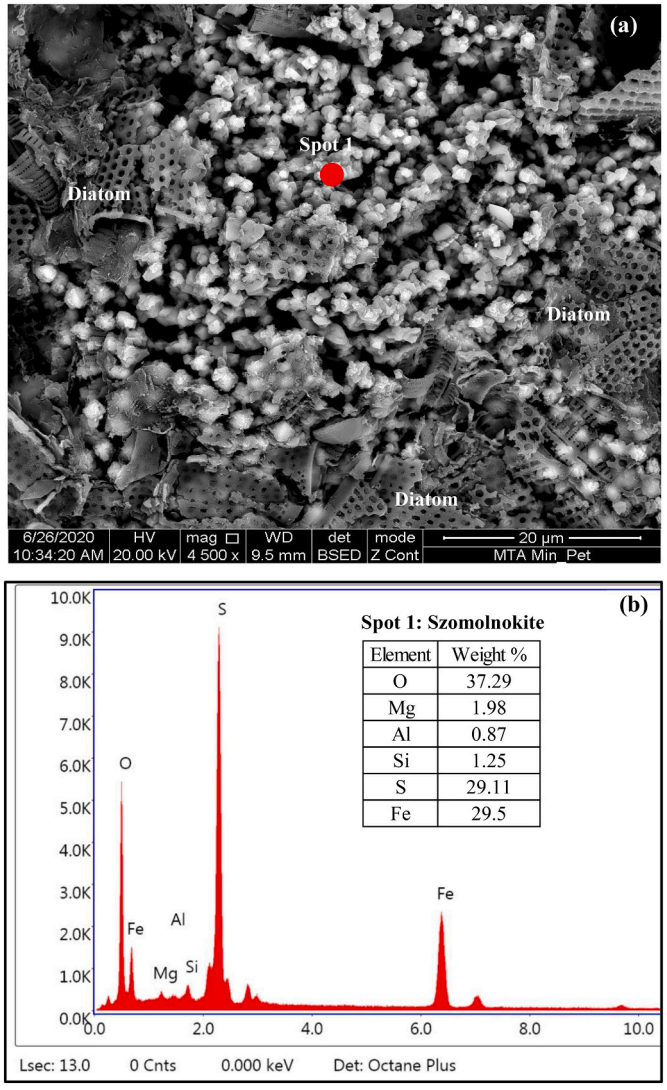

Fig. 21. SEM backscattered (a) image of the Keles roof rock (K-18) sample and (b) SEM-EDX spectra of szomolnokite at spot-1.

forming environment after deposition or by liberation from altered synchronous volcanic input (Dai et al., 2020a; Karayigit et al., 2020b; Spears et al., 1988; Spiro et al., 2019). The palynoflora of the coal seam and the diatomite flora from roof rock show that in the precursor palaeomire freshwater conditions were dominat without evidence of post-depositional marine influence. As noted above, the liberated Ba and Sr from the alteration of feldspar grains under neutral to alkaline conditions seem to have been adsorbed by syngenetic zeolites. Thus, Ba and Sr enrichments were developed in this part of the seam. Nevertheless, the common presence of macrophyte and herbaceous peat-forming plants in the palaeomire could result in lower TPI and VI values (Guo et al. 2020; Karayigit et al., 2017a; Oskay et al., 2019a, b; Zdravkov et al., 2020). In accordance with these values, the palynological data (palynomorph zone A) denotes an increased contribution of macrophytes and herbaceous peat-forming plants (e.g., Osmundaceae, Polypodiaceae, and Nymphaeaceae) and a decrease of woody peat-forming plants (e.g., Cupressaceae, Cupressaceae-Taxodioideae-*Glyptostrobus*) in the upper seam. This floral assemblage and coal facies data imply distinct changes in the vegetation of the palaeomire and in the depositional conditions. The underlying precursor peat presumably accumulated under limno-telmatic conditions during which the watertable was high. The humid conditions during the late stages of peat accumulation caused higher watertable than during the initial stages; in turn, the

Table 8
Element affinities with ash yield and total S (%, db) deduced from the calculation of Pearson's correlation coefficients.

Correlation with ash yield 0.70<r<1.0
Si, Al, Fe, Ti, Li, Cr, Ni, Ga, Rb, Sn, Cs, La, Ce, Pr, Hg, Th, total %S
Correlation with ash yield 0.40<r<0.70
Mg, Ge, As, Zr, Nd
Correlation with ash yield r ≥-0.40
B (−0.80), Mn (−0,66)
Correlation with Al content 0.70<r<1.0
Si, Fe, Ti, Li, Cr, Ga, Ge, Rb, Cs, Ce, Hg
Correlation with Al content 0.40<r<1.0
K, Ni, La, Pr, Nd, Pb
Correlation with Ca content 0.40<r<1.0
P (0.60), Mn (0.63), Sr (0.83), Ba (0.61)
Correlation with TS content 0.40<r<0.70
Fe (0.85), V (0.64), Ni (0.70), As (0.67), Mo (0.58), Sn (0.85), Hg (0.67)

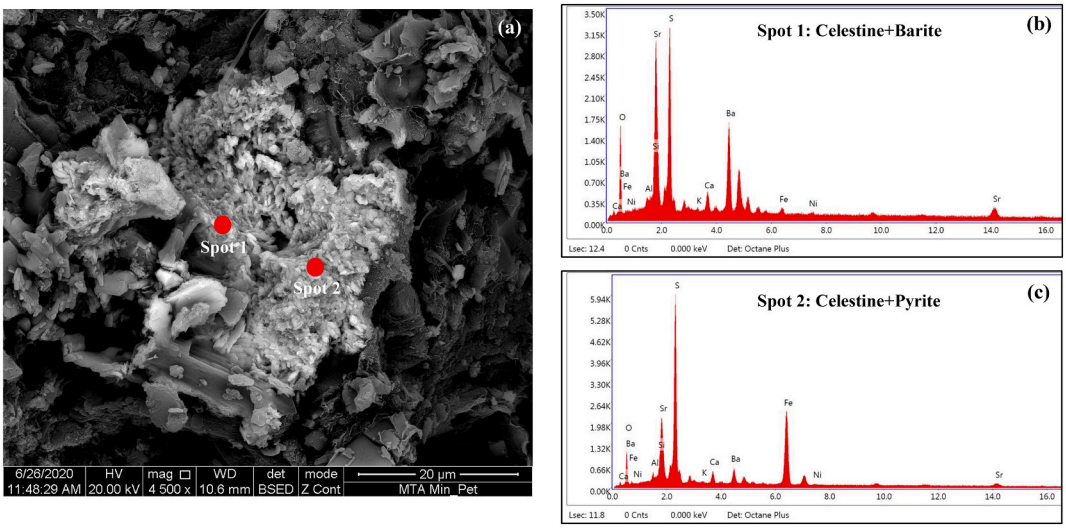

Fig. 22. SEM backscattered (a) image of barite-celestine-pyrite association in coal sample, and SEM-EDX spectra of (b) celestine+barite association at spot-1 and (c) celestine+pyrite association at spot-2.

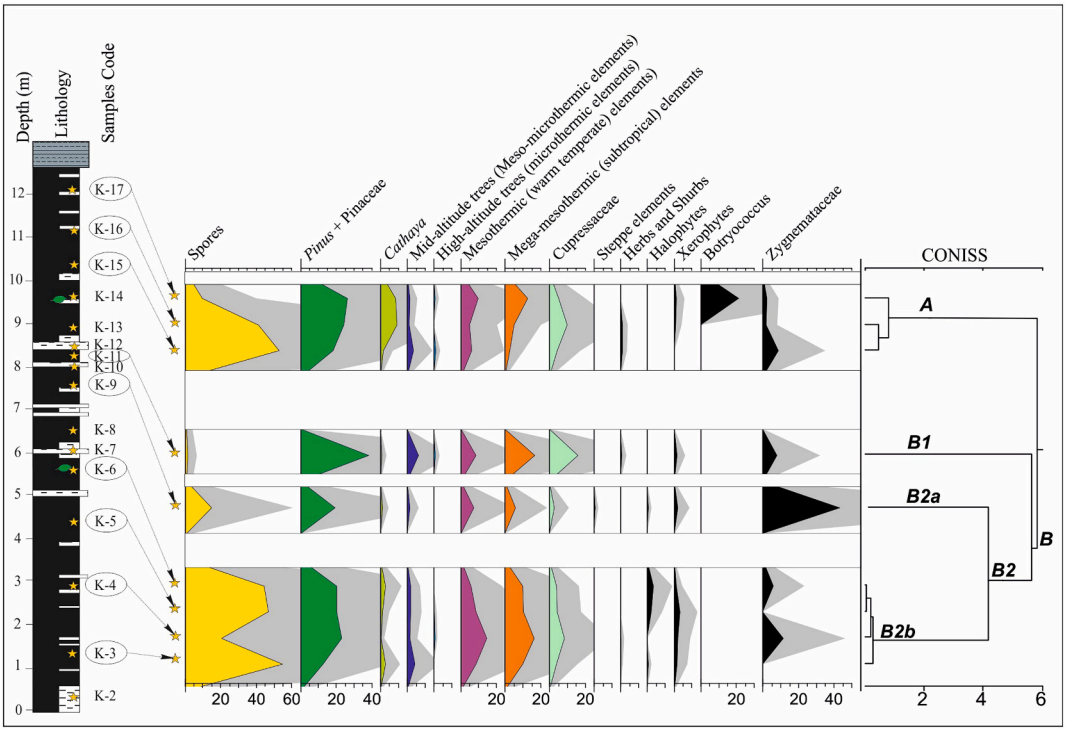

Fig. 23. The synthetic pollen diagram of the studied Keles coal seam (for legend of lithostratigraphic column, see Fig. 4).

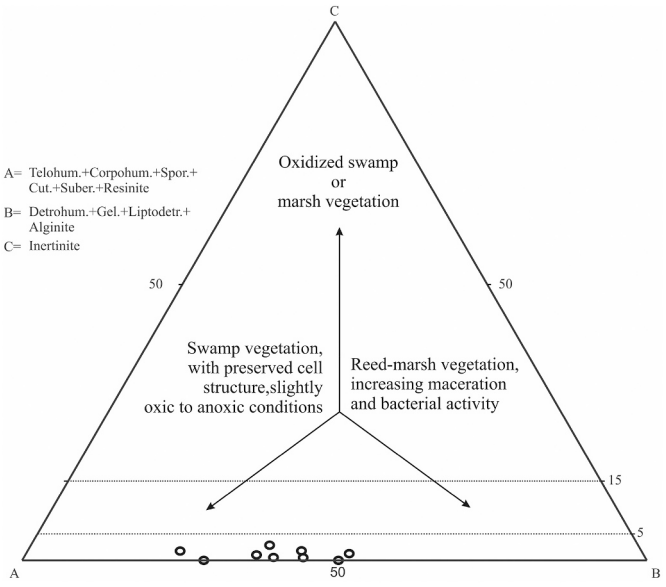

Fig. 24. ABC ternary plot of the Keles coal samples (after Mukhopadhyay 1989).

contribution of macrophytes (e.g., reeds and Nymphaeaceae) increased in the Keles palaeomire. Furthermore, the fluvial input along with synchronous volcanic input could provide nutrient-rich water into the palaeomire which allowed for the establishment of favorable conditions for algal activity (Burazer et al., 2020; Olgun et al., 2013; Simas et al., 2013). Hence, the contribution of *Botryococcus* increased, as observed in the palynoflora in the upper part, and the high proportions of alginite in the uppermost part of the seam.

In agreement with maceral and palynological data, the identified diatom flora from the roof rock sample (K-18) consists of planktonic elements and is characteristic for neutral to alkaline freshwater conditions (Owen et al. 2010). The common presence of *Aulacoseria* sp. and *Fragilaria* sp. could be an indicator for eutrophic shallow water conditions. Considering the presence of coal fragments and plant remains in the studied diatomite sample, nutrient-rich water with plant-litter supplied the depositional environment (Koukouzas 2007; Owen et al. 2010). The presence of coal fragments and plant remains could also explain the functional groups of organic matter identified in the FT-IR analysis from this sample (Fig. 8b). In addition, this nutrient-rich water with plant-litter and high watertable could also be favourable for algal growth (Kumar et al. 2017), which explains co-occurrence of diatoms and *Botryococcus* in the roof rock sample. The formation of anoxic conditions during deposition of the roof rock may also have caused sulphur-reduction, promoting the formation of framboidal pyrite grains and celestine-pyrite and celestine-barite associations (Figs. 17b and 22). Moreover, increased waterlevel and alkalinity caused the cessation of peat accumulation during middle Miocene followed by the deposition of the lacustrine carbonates common in the broad study area.

6. Conclusions

Variable vegetation and depositional conditions were established during the middle Miocene in the Keles palaeomires. The precursor peat of the lower and middle seam parts was accumulated under telmatic conditions and is derived from mainly woody peat-forming plants (e.g., Cupressaceae-Taxodioideae-*Glyptostrobus*). The anoxic conditions resulted in relatively higher V, Mo, and U concentrations than in the upper part of the seam, whereas the included smectite and kaolinite aggregates originate from the alteration of synchronous volcanic inputs. The development of humid conditions and the consequent increase of surface water supply into the Keles palaeomire during the late stages of peat accumulation resulted in the waterlevel rising and the increased contribution of macrophytes and herbaceous peat-forming plants (e.g., Osmundaceae, Polypodiaceae, and Nymphaeaceae). Thus, the precursor peat of the upper part of the seam accumulated under limno-telmatic and more alkaline conditions; under these conditions the glass of the volcanic input was altered to Ca-K-Na-bearing zeolites (heulandite-

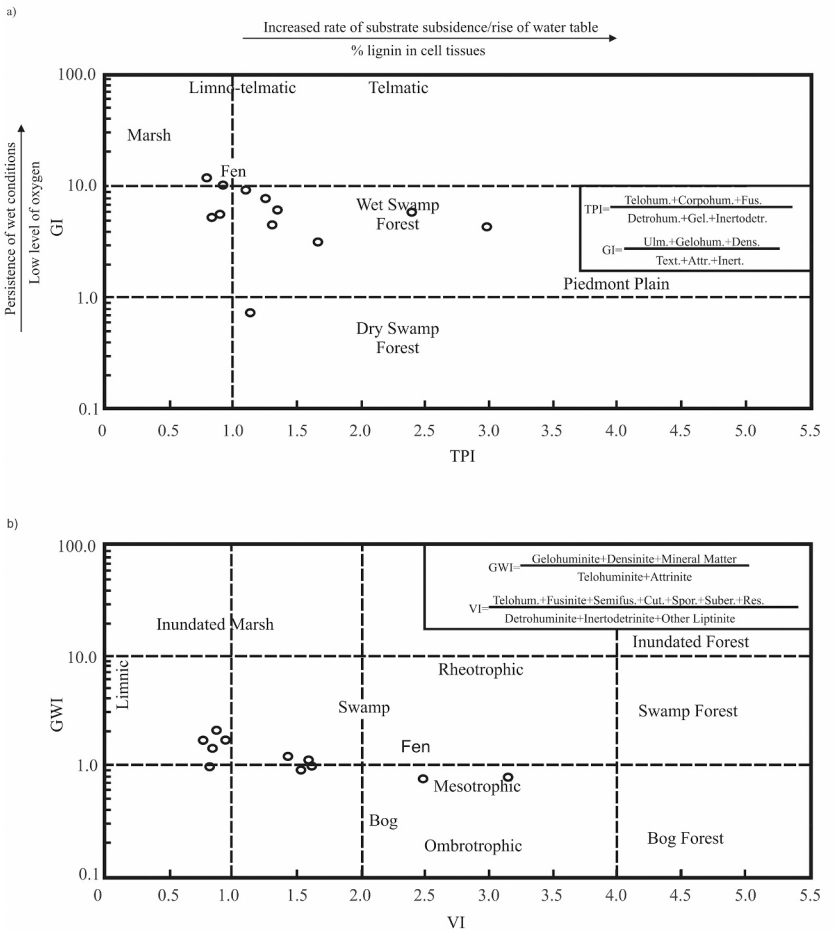

Fig. 25. (a) GI vs. TPI plot of the Keles coal samples (after Diessel, 1992, as modified by Kalaitzidis et al. 2004); (b) VI vs. GWI plot of the Keles coal samples (after Calder et al., 1991, as modified by Kalaitzidis et al. 2004).

clinoptolite). Finally, increased nutrient-rich water supply raised the watertable in the palaeomire during the very late stages of peat accumulation, caused formation of limnic conditions suitable for intense algal activity. Overall, changes in climatic conditions during middle Miocene caused changes in the waterlevel and the water chemistry, and thus, in the vegetation in the Keles palaeomire. These changes are fingerprinted in the maceral, mineralogical and elemental compositions, as well as in all the coal features.

Author contributions

The first author, Y. Çelik, collected coal samples from Keles coalfield and performed sedimentalogical interpretation, A.I. Karayigit together with R.G. Oskay and K. Christanis conducted proximate, ultimate, coal petrography, and XRD analyses, and interpreted Rock-Eval analysis, J. Hower was responsible for the XRF and Hg measurements, X. Querol performed ICP-MS analysis, and M.S. Kayseri-Özer investigated palynological compositions of coal samples. The manuscript was written through contributions of all authors.

Declaration of Competing Interest

The authors declare that they have no known competing financial interests or personal relationships that could have appeared to influence the work reported in this paper.

Acknowledgments

A part of this study is supported by Scientific Research Projects Coordination Unit of İstanbul University (Turkey) under project number 554. The authors would like to thank Prof. Dr. Y. Ersoy for his suggesting about regional volcanic activity data, Prof. Dr. A. Akbulut for his assistance in determining the diatom flora, Dr. Maria Mastalerz for her assistance on the interpretation of FT-IR data and Dr. E. Cicioğlu-Sütçü and Bülent Başara for their help during analyses. Finally, the authors thank Prof. Dr. Shifeng Dai, Editor-in-Chief of the Journal, Dr. T. Moore and anonymous reviewer are thanked for their comments and suggestions.

References

Akgün, F., Akyol, E., 1999. Palynostratigraphy of the coal–bearing Neogene deposits Graben in Büyük Menderes Western Anatolia. Geobios 32, 367–383.
Akgün, F., Sözbilir, H., 2001. A palynostratigraphic approach to the SW Anatolian molasse basin: Kale–Tavas molasse and Denizli molasse. Geodin. Acta 14, 71–93.
Akgün, F., Kayseri, M.S., Akkiraz, M.S., 2007. Palaeoclimatic evolution and vegetational changes during the Late Oligocene-Miocene period in Western and Central Anatolia (Turkey). Palaeogeogr. Palaeoclimatol. Palaeoecol. 253, 56–90.
American Society for Testing and Materials (ASTM) D2797/D2797M, 2011. Standard Practice for Preparing Coal Samples for Microscopical Analysis by Reflected Light ASTM International, West Conshohocken, PA, p. 5.
American Society for Testing and Materials (ASTM) D4326, 2011. Standard Test Method for Major and Minor Elements in Coal and Coke Ash by X-ray Fluorescence. ASTM International, West Conshohocken, PA, p. 4.
Arbuzov, S.I., Volostnov, A.V., Rikhvanov, L.P., Mezhibor, A.M., Ilenok, S.S., 2011. Geochemistry of radioactive elements (U, Th) in coal and peat of northern Asia (Siberia, Russian Far East, Kazakhstan, and Mongolia). Int. J. Coal Geol. 86, 318–328.

Arbuzov, S.I., Mezhibor, A.M., Spears, D.A., Ilenok, S.S., Shaldybin, M.V., Belaya, E.V., 2016. Nature of tonsteins in the Azeisk deposit of the Irkutsk Coal Basin (Siberia, Russia). Int. J. Coal Geol. 153, 99–111.
Armbrusteer, T., Gunter, M.E., 2001. Crystal structructures of natural zeolites. In: Bish, D.L., Ming, D.W. (Eds.), Natural Zeolites: Occurrence, Properties, Applications. Reviews in Mineralogy and Geochemistry, vol. 45, pp. 1–68.
Barrón, E., Rivas-Carballo, R., Postigo Mijarra, J.M., Alcalde-Olivares, C., Vieira, M., Castro, L., Pais, J., Valle-Hernández, M., 2010. The Cenozoic vegetation of the Iberian Peninsula: a synthesis. Rev. Palaeobot. Palynol. 162, 382–402.
Baş, H., 1986. Tertiary geology of the Domaniç-Tavşanlı-Kütahya-Gediz region. Geol. Eng. Turk. 11-18 (in Turkish with English abstract), 27.
Baysal, M., Yürüm, A., Yıldız, B., Yürüm, Y., 2016. Structure of some western Anatolia coals investigated by FTIR, Raman, ^{13}C solid state NMR spectroscopy and X-ray diffraction. Int. J. Coal Geol. 163, 166–176.
Bechtel, A., Karayiğit, A.I., Sachsenhofer, R.F., İnaner, H., Christanis, K., Gratzer, R., 2014. Spatial and temporal variability in vegetation and coal facies as reflected by organic petrological and geochemical data in the Middle Miocene Çayirhan coal field (Turkey). Int. J. Coal Geol. 134-135, 46–60.
Bechtel, A., Karayigit, A.I., Bulut, Y., Mastalerz, M., Sachsenhofer, R.F., 2016. Coal characteristics and biomarker investigations of Dombayova coals of Late Miocene-Pliocene age (Afyonkarahisar-Turkey). Org. Geochem. 94, 52–67.
Bertini, A., 2006. The northern Apennines palynological record as a contribute for the reconstruction of the Messinian palaeoenvironments. Sediment. Geol. 188-189, 235–258.
Biltekin, D., Popescu, S.-M., Suc, J.-P., Quézel, P., Jiménez-Moreno, G., Yavuz, N., Çağatay, M.N., 2015. Anatolia: a long-time plant refuge area documented by pollen records over the last 23million years. Rev. Palaeobot. Palynol. 215, 1–22.
Bish, D.L., Boak, J.M., 2001. Clinoptilolite-heulandite nomenclature. In: Bish, D.L., Ming, D.W. (Eds.), Natural Zeolites: Occurrence, Properties, Applications. Rev. Mineral. Geochem, 45, pp. 207–216.
Bohor, B.F., Triplehorn, D.M., 1993. Tonstein: altered volcanic ash layers in coal-bearing sequences. Geol. Soc. Am. Spec. Pap. 285, 40.
Bordenave, M.L., Espitalié, L., Leplat, P., Oudin, J.L., Vandenbroucke, M., 1993. Screening techniques for source rock evaluation. In: Bordenave, M.L. (Ed.), Applied Petroleum Geochemistry. Editions Technip, Paris, pp. 217–278.
Bostick, N.H., Daws, T.A., 1994. Relationships between data from Rock-Eval pyrolysis and proximate, ultimate, petrographic, and physical analyses of 142 diverse U.S coal samples. Org. Geochem. 21, 35–49.
Bouchal, J.M., Mayda, S., Grímsson, F., Akgün, F., Zetter, R., Denk, T., 2017. Miocene palynofloras of the Tınaz lignite mine, Muğla, southwest Anatolia: taxonomy, palaeoecology and local vegetation change. Rev. Palaeobot. Palynol. 243, 1–36.
Brownfield, M.E., Affolter, R.H., Cathcart, J.D., Johnson, S.Y., Brownfield, I.K., Rice, C. A., 2005. Geologic setting and characterization of coals and the modes of occurrence of selected elements from the Franklin coal zone, Puget Group, John Henry No. 1 mine, King County, Washington, USA. Int. J. Coal Geol. 63, 247–275.
Bruch, A.A., Gabrielyan, I., 2002. Quantitative data of the Neogene climatic development in Armenia and Nakhichevan. Acta Univ. Carol. Geol. 46, 41–48.
Bruch, A.A., Fauquette, S., Bertini, A., 2002. Quantitative climate reconstructions on Miocene palynofloras of the Velona Basin (Tuscany, Italy). Acta Univ. Carol. Geol. 46, 27–37.
Bruch, A.A., Utescher, T., Olivares, C.A., Dolakova, N., Ivanov, D., Mosbrugger, V., 2004. Middle and Late Miocene spatial temperature patterns and gradients in Europe -Preliminary results based on palaeobotanical climate reconstructions. CFS 249, 15–27.
Bruch, A.A., Utescher, T., Mosbrugger, V., Gabrielyan, I., Ivanov, D.A., 2006. Late Miocene climate in the circum-alpine realm - A quantitative analysis of terrestrial palaeofloras. Palaeogeogr. Palaeoclimatol. Palaeoecol. 238, 270–280.
Bruch, A.A., Utescher, T., Mosbrugger, V., NECLIME members, 2011. Precipitation patterns in the Miocene of Central Europe and the development of continentality. Palaeogeogr. Palaeoclimatol. Palaeoecol. 304, 202–211.
Büçkün, Z., İnaner, H., Oskay, R.G., Christanis, K., 2015. Palaeoenvironmental reconstruction of Hüsamlar coal seam, SW Turkey. J. Earth Syst. Sci. 124, 729–746.
Bullock, L.A., Parnell, J., Perez, M., Armstrong, J.G., Feldmann, J., Boyce, A.J., 2018. High selenium in the carboniferous coal measures of Northumberland, North East England. Int. J. Coal Geol. 195, 61–74.
Burazer, N., Šajnović, A., Vasić, N., Kašanin-Grubin, M., Životić, D., Mendonça Filho, J. G., Vulić, P., Jovančićević, B., 2020. Influence of paleoenvironmental conditions on distribution and relative abundance of saturated and aromatic hydrocarbons in sediments from the NW part of the Toplica basin, Serbia. Mar. Pet. Geol. 115, 104252.
Calder, J., Gibling, M., Mukhopadhyay, P., 1991. Peat formation in a Westphalian B piedmont setting, Cumberland Basin, Nova Scotia. Bull. Soc. Géol. Fr. 162, 238–298.
Casas-Gallego, M., Marza, A., Tudor, E., 2020. Palaeovegetation and palaeoclimate evolution during the Late Miocene to Early Pliocene of SE Romania. Geol. J. https://doi.org/10.1002/gj.3734.
Celik, Y., 2005. In: Coal Geology and Depositional Environment of Miocene Lignite-Bearing Sediments in the Harmancik-Keles (Bursa) Basin, Western Turkey. 6th European Coal Conference, Book of Proceidings. Coal 05, Belgrade, pp. 405–410.
Celik, Y., Karayigit, A.I., 2004a. Chemical Properties and petrographic composition of the lacustrine Seyitomer lignites (Miocene), Kutahya, Turkey. Energy Sources 26, 339–352.
Celik, Y., Karayigit, A.I., 2004b. Geological setting and quality of the lignite seams in the Seyitomer Basin, Kutahya, Turkey. Geol. Belg. 7, 259–265.
Çelik, Y., Karayigit, A.I., Querol, X., Oskay, R.G., Mastarlerz, M., Kayseri Özer, M.S., 2017. Coal characteristics, palynology, and palaeoenvironmental interpretation of the Yeniköy coal of Late Oligocene age in the Thrace Basin (NW Turkey). Int. J. Coal Geol. 181, 103–123.
Çetinkaya, S., Yürüm, Y., 2000. Oxidative pyrolysis of Turkish lignites in air up to 500°C. Fuel Process. Technol. 67, 177–189.
Chen, Y., Zou, C., Mastalerz, M., Hu, S., Gasaway, C., Tao, X., 2015. Applications of micro- Fourier transform infrared spectroscopy (FTIR) in the geological sciences-a review. Int. J. Mol. Sci. 16, 30223–30250.
Chou, C.-L., 2012. Sulfur in coals: a review of geochemistry and origins. Int. J. Coal Geol. 100, 1–13.
Christanis, K., Georgakopoulos, K., Fernández-Turiel, J.L., Bouzinos, A., 1998. Geological factors influencing the concentration of trace elements in the Philippi peatland, eastern Macedonia, Greece. Int. J. Coal Geol. 36, 295–313.
Crosdale, P.J., 1993. Coal maceral ratios as indicators of environment of deposition: do they work for ombrogenous mires? An example from the Miocene of New Zealand. Org. Geochem. 20, 797–809.
Dai, S., Finkelman, R.B., 2018. Coal as a promising source of critical elements: progress and future prospects. Int. J. Coal Geol. 186, 155–164.
Dai, S., Ren, D., Zhou, Y., Chou, C.L., Wang, X., Zhao, L., Zhu, X., 2008. Mineralogy and geochemistry of a superhigh-organic-sulfur coal, Yanshan Coalfield, Yunnan, China: evidence for a volcanic ash component and influence by submarine exhalation. Chem. Geol. 255, 182–194.
Dai, S., Ren, D., Chou, C.-L., Finkelman, R.B., Seredin, V.V., Zhou, Y., 2012. Geochemistry of trace elements in Chinese coals: a review of abundances, genetic types, impacts on human health, and industrial utilization. Int. J. Coal Geol. 94, 3–21.
Dai, S., Seredin, V.V., Ward, C.R., Hower, J.C., Xing, Y., Zhang, W., Song, W., Wang, P., 2015a. Enrichment of U-Se-Mo-Re-V in coals preserved within marine carbonate successions: geochemical and mineralogical data from the Late Permian Guiding Coalfield, Guizhou, China. Mineral. Deposita 50, 159–186.
Dai, S., Hower, J.C., Ward, C.R., Guo, W., Song, H., O'Keefe, J.M.K., Xie, P., Hood, M.M., Yan, X., 2015b. Elements and phosphorus minerals in the middle Jurassic inertinite-rich coals of the Muli Coalfield on the Tibetan Plateau. Int. J. Coal Geol. 144-145, 23–47.
Dai, S., Ward, C.R., Graham, I.T., French, D., Hower, J.C., Zhao, L., Wang, X., 2017. Altered volcanic ashes in coal and coal-bearing sequences: a review of their nature and significance. Earth-Sci. Rev. 175, 44–74.
Dai, S., Nechaev, V.P., Chekryzhov, I.Y., Zhao, L., Vysotskiy, S.V., Graham, I., Ward, C.R., Ignatiev, A.V., Velivetskaya, T.A., Zhao, L., French, D., Hower, J.C., 2018. A model for Nb–Zr–REE–Ga enrichment in Lopingian altered alkaline volcanic ashes: key evidence of H-O isotopes. Lithos 302-303, 359–369.
Dai, S., Hower, J.C., Finkelman, R.B., Graham, I.T., French, D., Ward, C.R., Eskenazy, G., Wei, Q., Zhao, L., 2020a. Organic associations of non-mineral elements in coal: a review. Int. J. Coal Geol. 218, 103347.
Dai, S., Bechtel, A., Eble, C.F., Flores, R.M., French, D., Graham, I.T., Hood, M.M., Hower, J.C., Korasidis, V.A., Moore, T.A., Püttmann, W., Wei, Q., Zhao, L., O'Keefe, J.M.K., 2020b. Recognition of peat depositional environments in coal: a review. Int. J. Coal Geol. 219, 103383.
de Joux, A., Moore, T.A., 2005. Geological controls on the source and occurrence of nickel in Rapid Stream, South Island, New Zealand. In: Metals in New Zealand. Resolutionz press ltd., Christchurch, pp. 261–276.
Dehmer, J., 1989. Petrological and organic geochemical investigation of recent peats with known environments of deposition. Int. J. Coal Geol. 28, 111–138.
Diessel, C.F.K, 1992. Coal-Bearing Depositional Systems. Springer, Berlin, p. 721.
Dikmen, D., Yalçın, M.N., 2020. Depositional environment and organic facies of coal-bituminous marl association in Seyitömer (Kütahya) region. Geol. Bull. Turk. 63, 303–328.
Drew, L.J., Grunsky, E.C., Schuenemeyer, J.H., 2008. Investigation of the structure of geological process through multivariate statistical analysis-the creation of a coal. Math. Geosci. 789–811.
Economic Commission for Europe-United Nations (E.C.E.-U.N.), 1988. International classification of in-seam coals, Energy/19. ECE, Geneva, p. 41.
Ercan, E., Satır, M., Sevin, D., Türkecan, A., 1997. Interpretation of the new radiometric age determinations from the Tertiary and Quaternary volcanic rocks in western Anatolia. Bull. Min. Res. Expl. 119, 103–112 (in Turkish with English abstract).
Erdtman, G., 1966. Pollen morphology and plant taxonomy. Angiosperms. Hafner Publishing Company, N.Y., p. 539
Erkoyun, H., Kadir, S., Külah, T., Huggett, J., 2017. Mineralogy, geochemistry and genesis of clays interlayered coal seams succession in the Neogene lacustrine Seyitömer coal deposit, Kütahya, western Turkey. Int. J. Coal Geol. 172, 112–133.
Erkoyun, H., Kadir, S., Huggett, J., 2019. Occurrence and genesis of tonsteins in the Miocene lignite, Tunçbilek Basin, Kütahya, western Turkey. Int. J. Coal Geol. 202, 46–68.
Ersoy, E.Y., Helvaci, C., 2016. Geochemistry and petrology of the lower Miocene bimodal volcanic units in the Tunçbilek-Domaniç basin, western Anatolia. Int. Geol. Rev. 58, 1234–1252.
Ersoy, E.Y., Çemen, I., Helvaci, C., Billor, Z., 2014. Tectono-stratigraphy of the Neogene basins in Western Turkey: Implications for tectonic evolution of the Aegean Extended Region. Tectonophysics 635, 33–58.
Esenlik, S., Karayigit, A.I., Bulut, Y., Querol, X., Alastuey, A., Font, O., 2006. Element behaviour during combustion in coal-fired Orhaneli power plant, Bursa-Turkey. Geol. Acta 4, 439–449.
Eskenazy, G., Delibaltova, D., Mincheva, E., 1994. Geochemistry of boron in Bulgarian coals. Int. J. Coal Geol. 25, 93–110.
Eskenazy, G., Finkelman, R.B., Chattarjee, S., 2010. Some considerations concerning the use of correlation coefficients and cluster analysis in interpreting coal geochemistry data. Int. J. Coal Geol. 83, 491–493.

Espitalié, J., Laporte, J.L., Madec, M., Marquis, F., Leplat, P., Paulet, J., Boutefeu, A., 1977a. Méthode rapide de caractérisation des roches mères de leur potentiel pétrolier et de leur degré d'évolution. Revue de L'Institut Français du Pétrole 32, 23–42.

Espitalié, J., Madec, M., Tissot, B., 1977b. Source rock characterization method for petroleum exploration. In: Proceedings 9th Offshore Technology Conference, vol. 3. Offshore Technology Conference, Houston, pp. 439–444.

Fauquette, S., Suc, J.-P., Jiménez-Moreno, G., Micheels, A., Jost, A., Favre, E., Bachiri-Taoufiq, N., Bertini, A., Clet-Pellerin, M., Diniz, F., Farjanel, G., Feddi, N., Zheng, Z., 2007. Latitudinal climatic gradients in the Western European and Mediterranean regions from the Mid-Miocene (c. 15 Ma) to the Mid-Pliocene (c. 3.5 Ma) as quantified from pollen data. In: Williams, M., Haywood, A.M., Gregory, F.J., Schmidt, D.N. (Eds.), Deep-Time Perspectives on Climate Change: Marrying the Signal from Computer Models and Biological Proxies. The Micropalaeontological Society, Spec. Publ, 2, pp. 481–502.

Finkelman, R.B., Belkin, H.E., Zheng, B., 1999. Health impacts of domestic coal use in China. Proc. Natl. Acad. Sci. U. S. A. 96, 3427–3431.

Finkelman, R.B., Palmer, C.A., Wang, P., 2018. Quantification of the modes of occurrence of 42 elements in coal. Int. J. Coal Geol. 185, 138–160.

Finkelman, R.B., Dai, S., French, D., 2019. The importance of minerals in coal as the hosts of chemical elements: a review. Int. J. Coal Geol. 212, 103251.

Geboy, N.J., Engle, M.A., Hower, J.C., 2013. Whole-coal versus ash basis in coal geochemistry: a mathematical approach to consistent interpretations. Int. J. Coal Geol. 113, 41–49.

Geng, W., Nakajima, T., Takanashi, H., Ohki, A., 2009. Analysis of carboxyl group in coal and coal aromaticity by Fourier transforminfrared (FT-IR) spectrometry. Fuel 88, 139–144.

Georgakopoulos, A., Iordanidis, A., Kapina, V., 2003. Study of low rank Greek coals using FTIR spectroscopy. Energy Sources 25, 995–1005.

Goodarzi, F., Swaine, D.J., 1994. The influence of geological factors on the concentration of boron in Australian and Canadian coals. Chem. Geol. 118, 301–318.7.

Grimm, E., 1987. CONISS: a Fortran 77 program for stratigraphically constrained cluster analyses by the method of incremental sum of squares. Comput. Geosci. 13, 13–35.

Grimm, E., 1991. TILIA 2.0.b.4 (Software). Illinois State Museum. Springfield, Illinois, USA.

Grimm, E., 2004. TG View 2.0.2 (software). Illinois State Museum. Springfield, Illinois, USA.

Gündogdu, M.N., Bonot-Coutois, C., Clauer, N., 1989. Isotopic and chemical signatures of sedimentary smectite and diagenetic clinoptiloite of a lacustrine Neogene basin near Bigadiç, western Turkey. Appl. Geochem. 4, 635–644.

Gündogdu, M.N., Yalçin, H., Temel, A., Clauer, N., 1996. Geological, mineralogical and geochemical characteristics of zeolite deposits associated with borates in the Bigadiç, Emet and Kirka Neogene lacustrine basins, western Turkey. Mineral. Deposita 31, 492–513.

Güner, H.T., Bouchal, J.M., Köse, N., Göktaş, F., Mayda, S., Denk, T., 2017. Landscape heterogeneity in the Yataǧan Basin (southwestern Turkey) during the middle Miocene inferred from plant macrofossils. Palaeontogr. Abt. B 296, 113–171.

Guo, Q., Littke, R., Sun, Y., Zieger, L., 2020. Depositional history of low-mature coals from the Puyang Basin, Yunnan Province, China. Int. J. Coal Geol. 221, 103428.

Gürdal, G., 2011. Abundances and modes of occurrence of trace elements in the Çan coals (Miocene), Çanakkale-Turkey. Int. J. Coal Geol. 87, 157–173.

Helvacı, C., Alonso, R.N., 2000. Borate deposits of Turkey and Argentina; a summary and geological comparison. Turk. J. Earth Sci. 24, 1–27.

Helvacı, C., Ersoy, E.Y., Billor, M.Z., 2017. Stratigraphy and Ar/Ar geochronology of the Miocene lignite-bearing Tunçbilek-Domaniç Basin, western Anatolia. Int. J. Earth Sci. 106, 1797–1814.

Hower, J.C., Robertson, J.D., 2003. Clausthalite in coal. Int. J. Coal Geol. 53, 219–225.

Hower, J.C., Ruppert, L.F., Eble, C.F., 1999. Lanthanide, yttrium, and zirconium anomalies in the Fire Clay coal bed, eastern Kentucky. Int. J. Coal Geol. 39, 141–153.

Hower, J.C., Ruppert, L.F., Williams, D.A., 2002. Controls on boron and germanium distribution in the low-sulfur Amos coal bed, Western Kentucky coalfield, USA. Int. J. Coal Geol. 53, 27–42.

Hower, J.C., Campbell, J.L.I., Teesdale, W.J., Nejedly, Z., Robertson, J.D., 2008. Scanning proton microprobe analysis of mercury and other trace elements in Fe-sulfides from a Kentucky coal. Int. J. Coal Geol. 75, 88–92.

Hower, J.C., O'Keefe, J.M.K., Volk, T.J., Watt, M.A., 2010. Funginite-resinite associations in coal. Int. J. Coal Geol. 83, 64–72.

Hower, J.C., Qian, D., Briot, N.J., Hood, M., Eble, C.F., 2020a. Mineralogy of a rare earth element-rich Manchester coal lithotype, Clay County, Kentucky. Int. J. Coal Geol. 220, 103413.

Hower, J.C., Eble, C.F., Backus, J.S., Xie, P., Liu, J., Fu, B., Hood, M., 2020b. Aspects of rare earth element enrichment in Central Appalachian coals. Appl. Geochem. 120, 104676.

Hunt, J.M., 1991. Generation of gas and oil from coal and other terrestrial organic matter. Org. Geochem. 17, 673–680.

Ilia, I.K., Stamatakis, M.G., Perraki, T.S., 2009. Mineralogy and technical properties of clayey diatomites from north and central Greece. Cent. Eur. J. Geosci. 1, 393–403.

International Committee for Coal Petrology (ICCP), 1993. International Handbook of Coal Petrography, 2nd ed. Centre National de la Recherche Scientifique, Paris, France.

International Committee for Coal Petrology (ICCP), 2001. The new inertinite classification (ICCP System 1994). Fuel 80, 459–470.

International Organization for Standardization (ISO) 7404–5, 2009. Methods for the Petrographic Analysis of Coal—Part 5: Method of Determining Microscopically the Reflectance of Vitrinite. International Organization for Standardization, Geneva, Switzerland, p. 4.

International Standard Organisation (ISO) 11760, 2005. Classification of Coals. International Organization for Standardization, Geneva, p. 9.

Ivanov, D., 2015. Climate and vegetation change during the late Miocene in Southwest Bulgaria based on pollen data from the Sandanski Basin. Rev. Palaeobot. Palynol. 221, 128–137.

Ivanov, D., Lazarova, M., 2005. Late Miocene flora from Tundzha Basin. Preliminary palynological data. CR Acad. Bulg. Sci. 58, 799–804.

Ivanov, D., Lazarova, M., 2019. Past climate and vegetation in Southeast Bulgaria - a study based on the late Miocene pollen record from the Tundzha Basin. J. Palaeogeogr. 8, 43–67.

Ivanov, D., Worobiec, E., 2017. Middle Miocene (Badenian) vegetation and climate dynamics in Bulgaria and Poland based on pollen data. Palaeogeogr. Palaeoclimatol. Palaeoecol. 467, 83–94.

Ivanov, D., Ashraf, A.R., Mosbrugger, V., Palamarev, E., 2002. Palynological evidence for Miocene climate change in the Forecarpathian Basin (central Paratethys, NW Bulgaria). Palaeogeogr. Palaeoclimatol. Palaeoecol. 178, 19–37.

Ivanov, D., Ashraf, A.R., Mosbrugger, V., 2007a. Late Oligocene and Miocene climate and vegetation in the eastern Paratethys area (Northeast Bulgaria), based on pollen data. Palaeogeogr. Palaeoclimatol. Palaeoecol. 255, 342–360.

Ivanov, D., Ashraf, A.R., Utescher, T., Mosbrugger, V., Ivanov, D., Slavomirova, E., 2007b. Late Miocene vegetation and climate of the Balkan region: palynology of the Beli Breg Coal Basin sediments. Geol. Carpath. 58, 367–381.

Ivanov, D., Djorgova, N., Slavomirova, E., 2010. Palynological subdivision of Late Miocene sediments from Karlovo Basin, Central Bulgaria. Phytol. Balcan. 16, 23–42.

Ivanov, D., Utescher, T., Mosbrugger, V., Syabryaj, S., Djordjević-Milutinović, D., Molchanoff, S., 2011. Miocene vegetation and climate dynamics in eastern and central Paratethys (southeastern Europe). Palaeogeogr. Palaeoclimatol. Palaeoecol. 304, 262–275.

Ivanov, D., Tsenov, B., Utescher, T., Kováčová, M., Mosbrugger, V., Ashraf, A.R., 2019. Climate reconstructions based on Miocene leaf flora from NW Bulgaria: comparing leaf physiognomy and nearest living relative approach. Phytol. Balcan. 25 (2), 137–146.

Jiménez-Moreno, G., 2006. Progressive substitution of a subtropical forest for a temperate one during the middle Miocene climate cooling in Central Europe according to palynological data from cores Tengelic-2 and Hidas-53 (Pannonian Basin, Hungary). Rev. Palaeobot. Palynol. 142, 1–14.

Jiménez-Moreno, G., Suc, J.-P., 2007. Middle Miocene latitudinal climatic gradient in Western Europe: evidence from pollen records. Palaeogeogr. Palaeoclimatol. Palaeoecol. 253, 208–225.

Jiménez-Moreno, G., Rodriguez-Tovar, F.J., Pardo-Iguzquiza, E., Fauquette, S., Suc, J.-P., Muller, P., 2005. High-resolution palynological analysis in late early-middle Miocene core from the Pannonian Basin, Hungary: climatic changes, astronomical forcing and eustatic fluctuations in the Central Paratethys. Palaeogeogr. Palaeoclimatol. Palaeoecol. 216, 73–97.

Jiménez-Moreno, G., Fauquette, S., Suc, J.-P., Aziz, H.A., 2007a. Early Miocene repetitive vegetation and climatic changes in the lacustrine deposits of the Rubielos de Mora Basin (Teruel, NE Spain). Palaeogeogr. Palaeoclimatol. Palaeoecol. 250, 101–113.

Jiménez-Moreno, G., Popescu, S.-M., Ivanov, D., Suc, J.-P., 2007b. Neogene flora, vegetation and climate dynamics in southeastern Europe and the northeastern Mediterranean. In: Williams, M., Haywood, A.M., Gregory, F.J., Schmidt, D.N. (Eds.), Deep-Time Perspectives on Climate Change: Marrying the Signal from Computer Models and Biological Proxies. The Micropalaeontological Society, Spec. Publ, 2, pp. 503–516.

Jiménez-Moreno, G., Mandic, O., Harzhauser, M., Pavelic, D., Vranjkovic, A., 2008b. Vegetation and climate dynamics during the early middle Miocene from Lake Sinj (Dinaride Lake system, SE Croatia). Rev. Palaeobot. Palynol. 152, 270–278.

Kalaitzidis, S., Bouzinos, A., Papazisimou, S., Christanis, K., 2004. A short-term establishment of forest fen habitat during Pliocene lignite formation in the Ptolemais Basin, NW Macedonia, Greece. Int. J. Coal Geol. 57, 243–263.

Kalkreuth, W.D., Marchioni, D.L., Calder, J.H., Lamberson, M.N., Naylor, R.D., Paul, J., 1991. The relationship between coal petrography and depositional environments from selected coal basins in Canada. Int. J. Coal Geol. 19, 21–76.

Kara-Gülbay, R., Korkmaz, S., 2008. Element contents and organic matter-element relationship of the Tertiary oil shale deposits in northwest Anatolia, Turkey. Energy Fuel 22, 3164–3173.

Karayigit, A.I., Celik, Y., 2003. Mineral matter and trace elements in Miocene coals of the Tuncbilek-Domanic basin, Kutahya, Turkey. Energy Sources 25, 339–355.

Karayigit, A.I., Gayer, R.A., 2000. Trace elements in a Pliocene-Pleistocene lignite profile from the Afsin-Elbistan field, eastern Turkey. Energy Sources 22, 13–21.

Karayigit, A.I., Akgun, F., Gayer, R.A., Temel, A., 1999. Quality, palynology, and palaeoenvironmental interpretation of the Ilgin lignite, Turkey. Int. J. Coal Geol. 38, 219–236.

Karayigit, A.I., Gayer, R.A., Querol, X., Onacak, T., 2000. Contents of major and trace elements in feed coals from Turkish coal-fired power plants. Int. J. Coal Geol. 44, 169–184.

Karayigit, A.I., Littke, R., Querol, X., Jones, T., Oskay, R.G., Christanis, K., 2017a. The Miocene coal seams in the Soma Basin (W. Turkey): Insights from coal petrography, mineralogy and geochemistry. Int. J. Coal Geol. 173, 110–128.

Karayigit, A.I., Bircan, C., Mastalerz, M., Oskay, R.G., Querol, X., Lieberman, N.R., Türkmen, I., 2017b. Coal characteristics, elemental composition and modes of occurrence of some elements in the İsaalan coal (Balıkesir, NW Turkey). Int. J. Coal Geol. 172, 43–59.

Karayigit, A.I., Yiğitler, Ö., İşerli, S., Querol, X., Mastalerz, M., Oskay, R.G., Hower, J.C., 2019a. Mineralogy and geochemistry of feed coals and combustion residues from tunçbilek and Seyitömer coal-fired power plants in western Turkey. Coal Combust. Gasif. Prod. 11, 18–31.

Karayigit, A.I., Mastalerz, M., Oskay, R.G., Gayer, R.A., 2018. Coal petrography, mineralogy, elemental compositions and palaeoenvironmental interpretation of Late Carboniferous coal seams in three wells from the Kozlu coalfield (Zonguldak Basin, NW Turkey). Int. J. Coal. Geol. 187, 54–70.
Karayigit, A.I., Oskay, R.G., Gayer, R.A., 2019b. Mineralogy and geochemistry of feed coals and combustion residues of the Kangal power plant (Sivas, Turkey). Turk. J. Earth Sci. 28, 438–456.
Karayigit, A.I., Bircan, C., Oskay, R.G., Türkmen, İ., Querol, X., 2020a. The geology, mineralogy, petrography, and geochemistry of the Miocene Dursunbey coal within fluvio-lacustrine deposits, Balıkesir (Western Turkey). Int. J. Coal Geol. 218, 103548.
Karayigit, A.I., Atalay, M., Oskay, R.G., Córdoba, P., Querol, X., Bulut, Y., 2020b. Variations in elemental and mineralogical compositions of Late Oligocene, Early and Middle Miocene coal seams in the Kale-Tavas Molasse sub-basin, SW Turkey. Int. J. Coal Geol. 218, 103366.
Kayseri, M.S., Akgün, F., 2008. Palynostratigraphic, palaeovegetational and palaeoclimatic investigations on the Miocene deposits in Central Anatolia (Çorum Region and Sivas Basin). Turk. J. Earth Sci. 17, 361–403.
Kayseri-Özer, M.S., 2014. Spatial distribution of climatic conditions from the Middle Eocene to Late Miocene based on palynoflora in Central, Eastern and Western Anatolia. Geodin. Acta 26, 122–157.
Kayseri-Özer, M.S., 2017. Cenozoic vegetation and climate change in Anatolia-A study based on the IPR-vegetation analysis. Palaeogeogr. Palaeoclimatol. Palaeoecol. 467, 37–68.
Kayseri-Özer, M.S., Akgün, F., Mayda, S., Kaya, T., 2014a. Palynofloras and Vertebrates from Muğla-Ören region (SW Turkey) and Palaeoclimate of the Middle Burdigalian-Langhian period in Turkey. Bull. Geosci. 89, 137–162.
Kayseri-Özer, M.S., Sözbilir, H., Akgün, F., 2014b. Miocene palynoflora of the Kocaçay and Cumaovası Basins: a contribution to the synthesis of Miocene palynology, palaeoclimate, and palaeovegetation in Western Turkey, Turk. J. Earth Sci. 23, 233–259.
Kear, D., Ross, J.B., 1961. Boron in New Zealand coal ashes. N. Z. J. Sci. 4, 360–380.
Ketris, M.P., Yudovich, Ya.E., 2009. Estimations of Clarkes for Carbonaceous biolithes: world averages for trace element contents in black shales and coals. Int. J. Coal Geol. 78, 135–148.
Knight, J.A., Burger, K., Bieg, G., 2000. The pyroclastic tonsteins of the Sabero Coalfield, north-western Spain, and their relationship to the stratigraphy and structural geology. Int. J. Coal Geol. 44, 187–226.
Kolker, A., 2012. Minor element distribution in iron disulfides in coal: a geochemical review. Int. J. Coal Geol. 94, 32–43.
Korasidis, V.A., Wallace, M.W., Dickinson, J.A., Hoffman, N., 2019. Depositional setting for Eocene seat earths and related facies of the Gippsland Basin, Australia. Sediment. Geol. 390, 100–113.
Korasidis, V.A., Wallace, M.W., Tosolini, A.-M.P., Hill, R.S., 2020. The origin of floral Lagerstätten in coals. Palaios 35, 22–36.
Kortenski, J., Sotirov, A., 2004. Petrography of the Neogene lignite from the Sofia basin, Bulgaria. Int. J. Coal Geol. 57, 117–126.
Koukouzas, N., 2007. Mineralogy and geochemistry of diatomite associated with lignite seams in the Komnina Lignite Basin, Ptolemais, Northern Greece. Int. J. Coal Geol. 71, 276–286.
Kumar, M., Monga, P., Shukla, A., Mehrotra, R.C., 2017. Botryococcus from the early Eocene lignite mines of western India: inferences on morphology, taphonomy and palaeoenvironment. Palynology 41, 462–471.
Kus, J., Dolezych, M., Schneider, W., Hofmann, T., Visiné Rajczi, E., 2020. Coal petrological and xylotomical characterization of Miocene lignites and in-situ fossil tree stumps and trunks from Lusatia region, Germany: palaeoenvironment and taphonomy assessment. Int. J. Coal Geol. 217, 103283.
Langford, F.F., Blanc-Valleron, M.-M., 1990. Interpreting Rock-Eval pyrolysis data using graphs of pyrolizable hydrocarbons vs. total organic carbon. AAPG Bull. 74, 799–804.
Li, B., Zhuang, X., Querol, X., Li, J., Moreno, N., Córdoba, P., Shangguan, Y., Zhou, J., Ma, X., Liu, S., 2019. Geological controls on enrichment of Mn, Nb (Ta), Zr (Hf), and REY within the Early Permian coals of the Jimunai Depression, Xinjiang Province, NW China. Int. J. Coal Geol. 215, 103298.
Liu, J., Spiro, B.F., Dai, S., French, D., Graham, I.T., Wang, X., Zhao, L., Zhao, J., Zeng, R., 2021. Strontium isotopes in high- and low-Ge coals from the Shengli Coalfield, Inner Mongolia, northern China: new indicators for Ge source. Int. J. Coal Geol. 233, 103642.
Lynskey, J., Gainsford, A.R., Hunt, J.L., 1984. Trace and major element analyses of Waikato coals: an interlaboratory study. N. Z. J. Sci. 27, 443–464.
Mackay, A.M., Wilson, B.I., 1978. Borate in Waikato coal. N. Z. J. Sci. 21, 611–614.
Madejova, J., 2003. FTIR techniques in clay mineral studies. Vib. Spectrosc. 944, 1–10.
Mastalerz, M., Bustin, R.M., 1996. Application of reflectance micro-Fourier transform infrared analysis to the study of coal macerals: An example from the late Jurassic to early Cretaceous coals of the Mist Mountain Formation, British Columbia, Canada. Int. J. Coal Geol. 32, 55–67.
Miall, A.D., 1977. A review of the braided-river depositional environment. Earth-Sci. Rev. 13, 1–62.
Miall, A.D., Miall, A.D., 1978. Lithofacies types and vertical profile models in braided river deposits: a summary. In: Fluvial Sedimentology, 5. Canadian Society of Petroleum Geologists, Memoir, pp. 597–604.
Miall, A.D., 1985. Architectural-element analysis: a new method of facies analysis applied to fluvial deposits. Earth-Sci. Rev. 22, 261–308.
Miall, A.D., Walker, R.G., James, N.P., 1992. Alluvial deposits. In: Facies models: response to sea-level change. Geol. Assoc, Canada, pp. 119–142.
Miall, A.D., 1996. The Geology of Fluvial Deposits. Sedimentary Facies, Basin Analysis and Petroleum Geology. Springer, Berlin, p. 582.
Mitrović, D., Đoković, N., Životić, D., Bechtel, A., Šajnović, A., Stojanović, K., 2016. Petrographical and organic geochemical study of the Kovin lignite deposit, Serbia. Int. J. Coal Geol. 168, 80–107.
Moore, T.A, Li, Z., Nelson, C.M., Finkelman, R.B., Boyd, R., 2005. Concentration of trace elements in coal beds. In: Moore, T.A., Black, A., Centeno, J.A., Harding, J.S., Trumm, D.A. (Eds.), Metal Contaminants in New Zealand. Resolutionz press ltd., Christchurch, pp. 81–113.
Moore, T.A., Shearer, J.C., 2003. Peat/coal type and depositional environment - Are they related. Int. J. Coal Geol. 56, 233–252.
Mosbrugger, V., Utescher, T., 1997. The coexistence approach- a method for quantitative reconstructions of tertiary terrestrial palaeoclimate data using plant fossils. Palaeogeogr. Palaeoclimatol. Palaeoecol. 134, 61–86.
Mukhopadhyay, P., 1989. Organic Petrography and Organic Geochemistry of Tertiary Coals from Texas in Relation to Depositional Environment and Hydrocarbon Generation. Report of Investigations. Bureau of Economic Geology, Texas, p. 118.
Newman, N.A., Moore, T.A., Esterle, J.S., 1997. Geochemistry and petrography of the Taupiri and Kupakupa coal beds (Eocene), North Island, New Zealand. Int. J. Coal Geol. 33, 103–133.
Nix, H., 1982. Environmental determinants of biogeography and evolution in Terra Australis. In: Barker, W.R., Greenslade, P.J.M. (Eds.), Evolution of the Flora and fauna of Arid Australia. Peacock Publishing, Frewville, pp. 47–66.
Ogala, J., Siavalas, G., Christanis, K., 2012. Coal petrography, mineralogy and geochemistry of lignite samples from the Ogwashi–Asaba Formation, Nigeria. J. Afr. Earth Sci. 66–67, 35–45.
Oikonomopoulos, I.K., Perraki, M., Tougiannidis, N., Perraki, T., Frey, M.J., Antoniadis, P., Ricken, W., 2013. A comparative study on structural differences of xylite and matrix lignite lithotypes by means of FT-IR, XRD, SEM and TGA analyses: an example from the Neogene Greek lignite deposits. Int. J. Coal Geol. 115, 1–12.
Oikonomopoulos, I.K., Kaouras, G., Tougiannidis, N., Ricken, W., Gurk, M., Antoniadis, P., 2015. The depositional conditions and the palaeoenvironment of the Achlada xylite-dominated lignite in western Makedonia, Greece. Palaeogeogr. Palaeoclimatol. Palaeoecol. 440, 777–792.
Okay, A.I., Harris, N.B.W., Kelley, S.P., 1998. Exhumation of blueschists along a Tethyan suture in northwest Turkey. Tectonophysics 285, 275–299.
O'Keefe, J.M.K., Bechtel, A., Christanis, K., Dai, S., DiMichele, W.A., Eble, C.F., Esterle, J. S., Mastalerz, M., Raymond, A.L., Valentim, B.V., Wagner, N.J., Ward, C.R., Hower, J.C., 2013. On the fundamental difference between coal rank and coal type. Int. J. Coal Geol. 118, 58–87.
Olgun, N., Duggen, S., Andronico, D., Kutterolf, S., Croot, P.L., Giammanco, S., Censi, P., Randazzo, L., 2013. Possible impacts of volcanic ash emissions of Mount Etna on the primary productivity in the oligotrophic Mediterranean Sea: results from nutrient-release experiments in seawater. Mar. Chem. 152, 32–42.
Omodeo-Salé, S., Deschamps, R., Michel, P., Chauveau, B., Suárez-Ruiz, I., 2017. The coal-bearing strata of the Lower Cretaceous Mannville Group (Western Canadian Sedimentary Basin, South Central Alberta), Part 2: factors controlling the composition of organic matter accumulations. Int. J. Coal Geol. 179, 219–241.
Onar, V., Yıldız, B., 2005. New Chalicotheriidae (Perissodactyla-Mammalia) fossil from the Middle Miocene of Turkey (Bursa-Orhaneli), Uludag Univ. J. Fac. Vet. Med. 24, 65–68.
Oskay, R.G., Inaner, H., Karayigit, A.I., Christanis, K., 2013. Coal deposits of Turkey: properties and importance on energy demand. Bull. Geol. Soc. Greece 2111–2120.
Oskay, R.G., Christanis, K., Inaner, H., Salman, M., Taka, M., 2016. Palaeoenvironmental reconstruction of the eastern part of the Karapınar-Ayrancı coal deposit (Central Turkey). Int. J. Coal Geol. 163, 100–111.
Oskay, R.G., Bechtel, A., Karayigit, A.I., 2019a. Mineralogy, petrography and organic geochemistry of Miocene coal seams in the Kınık coalfield (Soma Basin-Western Turkey): Insights into depositional environment and palaeovegetation. Int. J. Coal Geol. 210, 103205.
Oskay, R.G., Christanis, K., Salman, M., 2019b. Coal features and depositional environment of the Northern Karapinar-Ayranci coal deposit (Konya, Central Turkey). Turk. J. Earth Sci. 28, 260–274.
Owen, R.B., Reanut, R.W., Stamatakis, M.G., 2010. Diatomaceous sedimentation in late Neogene lacustrine basins of western Macedonia, Greece. J. Paleolimnol. 44, 343–359.
Öztaş, N.A., Yürüm, Y., 2000. Pyrolysis of Turkish Zonguldak bituminous coal. Part 1. Effect of mineral matter. Fuel 79, 1221–1227.
Palmer, C.A., Tuncali, E., Dennen, K.O., Coburn, T.C., Finkelman, R.B., 2004. Characterization of Turkish coals: a nationwide perspective. Int. J. Coal Geol. 60, 85–115.
Peters, K.E., 1986. Guidelines for evaluating petroleum source rock using programmed pyrolysis. AAPG Bull. 70, 318–329.
Petersen, H.I., 2006. The petroleum generation potential and effective oil window of humic coals related to coal composition and age. Int. J. Coal Geol. 67, 221–248.
Petersen, H.I., Lindström, S., Nytoft, H.P., Rosenberg, P., 2009. Composition, peat-forming vegetation and kerogen paraffinicity of Cenozoic coals: relationship to variations in the petroleum generation potential (Hydrogen Index). Int. J. Coal Geol. 78, 119–134.
Pickel, W., Kus, J., Flores, D., Kalaitzidis, S., Christanis, K., Cardott, B.J., Misz-Kennan, M.F., Rodrigues, S., Hentschel, A., Hamor-Vido, M., Crosdale, P., Wagner, N., ICCP, 2017. Classification of liptinite – ICCP System 1994. Int. J. Coal Geol. 169, 40–61.
Pickford, M., Mayda, S., Alpagut, B., Demirel, F.A., Şarbak, A., Kaya, T.T., 2020. Hyracoidea from the Middle Miocene hominoid locality of Paşalar (NW Turkey). Turk. J. Earth Sci. 29, 1114–1124.

Popova, S., Utescher, T., Gromyko, D.V., Bruch, A.A., Henrot, A.-J., Mosbrugger, V., 2017. Cenozoic vegetation gradients in the mid- and higher latitudes of Central Eurasia and climatic implications. Palaeogeogr. Palaeoclimatol. Palaeoecol. 467, 69–82.

Poppe, L.J., Paskevich, V.F., Hathaway, J.C., Blackwood, D.S., 2001. A laboratory manual for X-ray powder diffraction. U.S. Geological Survey Open-File Report 01-041 (2001). Available at. https://pubs.usgs.gov/of/2001/of01-041/index.htm. Accessed 24th July 2020.

Querol, X., Cabrera, Ll., Pickel, W., López-Soler, A., Hagemann, H.W., Fernández-Turiel, J.L., 1996. Geological controls on the coal quality of the Mequinenza subbituminous coal deposit, northeast Spain. Int. J. Coal Geol. 29, 67–91.

Querol, X., Whateley, M.K.G., Fernández-Turiel, J.L., Tuncali, E., 1997. Geological controls on the mineralogy and geochemistry of the Beypazari lignite, central Anatolia, Turkey. Int. J. Coal Geol. 33, 255–271.

Querol, X., Moreno, N., Umaa, J.C., Alastuey, A., Hernández, E., López-Soler, A., Plana, F., 2002. Synthesis of zeolites from coal fly ash: an overview. Int. J. Coal Geol. 50, 413–423.

Reading, H.G., 1996. Sedimentary Environments: Processes, Facies and Stratigraphy. Blackwell, Oxford, p. 689.

Riley, K.W., French, D.H., Lambropoulos, N.A., Farrell, O.P., Wood, R.A., Huggins, F.E., 2007. Origin and occurrence of selenium in some Australian coals. Int. J. Coal Geol. 72, 72–80.

Rust, B.R., 1982. Sedimentation in fluvial and lacustrine environments. Hydrobiologia 91, 59–70.

Şener, M., Şengüler, I., Kök, M.V., 1995. Geological considerations for the economic evaluation of oil shale deposits in Turkey. Fuel 74, 999–1003.

Seredin, V.V., Dai, S., Sun, Y., Chekryzhov, I.Y., 2013. Coal deposits as promising sources of rare metals for alternative power and energy-efficient technologies. Appl. Geochem. 31, 1–11.

Simas, M.W., Guerra-Sommer, M., MendonÇa Filho, J.G., Cazzulo-Klepzig, M., Formoso, M.L.L., Degani-Schmidt, I., 2013. An accurate record of volcanic ash fall deposition as characterized by dispersed organic matter in a lower permian tonstein layer (Faxinal Coalfield, Paraná Basin, Brazil). Geol. Acta 11, 45–57.

Spears, D.A., 2012. The origin of tonsteins, an overview, and links with seat earths, fireclays and fragmental clay rocks. Int. J. Coal Geol. 94, 22–31.

Spears, D.A., Arbuzov, S.I., 2019. A geochemical and mineralogical update on two major tonsteins in the UK Carboniferous Coal Measures. Int. J. Coal Geol. 210, 103199.

Spears, D.A., Zheng, Y., 1999. Geochemistry and origin of elements in some UK coals. Int. J. Coal Geol. 38, 161–179.

Spears, D.A., Duff, P.McL.D., Caine, P.M., 1988. The West Waterberg tonstein, South Africa. Int. J. Coal Geol. 9, 221–233.

Spiro, F.B., Liu, J., Dai, S., Zeng, R., Large, D., French, D., 2019. Marine derived 87Sr/86Sr in coal, a new key to geochronology and palaeoenvironment: elucidation of the India-Eurasia and China-Indochina collisions in Yunnan, China. Int. J. Coal Geol. 215, 103304.

Stamatakis, M.G., 1989. A boron-bearing potassium feldspar in volcanic ash and tuffaceous rocks from Miocene lake deposits, Samos Island Greece. Amer. Miner. 74, 230–235.

Stock, A.T., Littke, R., Lücke, A., Zieger, L., Thielemann, T., 2016. International Journal of Coal Geology Miocene depositional environment and climate in western Europe: the lignite deposits of the Lower Rhine Basin, Germany. Int. J. Coal Geol. 157, 2–18.

Stuchlik, L., Kvavadze, E., 1998. Subfossil pollen spectra of flood-plain forest of *Pterocarya* pterocarpa in the Alazani Valley (East Georgia). Acta Palaeobot. 38, 217–222.

Suc, J.-P., 1984. Origin and evolution of the Mediterranean vegetation and climate in Europe. Nature 307, 429–432.

Suggate, R.P., 1995. Coal type and rank variation in Tatu Mine, New Zealand. Int. J. Coal Geol. 27, 33–57.

Suggate, R.P., 2000. The rank(Sr) scale: its basis and its applicability as a maturity index for all coals. New Zealand J. Geol. Geophys. 43, 521–553.

Swaine, D.J., 1990. Trace Elements in Coal. Butterworths, London, p. 278.

Syabryaj, S., Utescher, T., Molchanoff, S., Bruch, A., 2007. Vegetation and palaeoclimate in the Miocene of Ukraine. Palaeogeogr. Palaeoclimatol. Palaeoecol. 253, 169–184.

Sykes, R., Snowdon, L.R., 2002. Guidelines for assessing the petroleum potential of coaly source rocks using Rock-Eval pyrolysis. Org. Geochem. 33, 1441–1455.

Sýkorová, I., Pickel, W., Christanis, K., Wolf, M., Taylor, G.H., Flores, D., 2005. Classification of huminite - ICCP System 1994. Int. J. Coal Geol. 62, 85–106.

Toprak, S., Sutcu, E.C., Senguler, I., 2015. A fault controlled, newly discovered Eskişehir Alpu coal basin in Turkey, its petrographical properties and depositional environment. Int. J. Coal Geol. 138, 127–144.

Triplehorn, D.M., Stanton, R.W., Ruppert, L.F., Crowley, S.S., 1991. Volcanic ash dispersed in the Wyodak-Anderson coal bed, Powder River Basin, Wyoming. Org. Geochem. 17, 567–575.

Uhl, D., Mosbrugger, V., Bruch, A., Utescher, T., 2003. Reconstructing palaeotemperatures using leaf floras — Case studies for a comparison of leaf margin analysis and the coexistence approach. Rev. Palaeobot. Palynol. 126, 49–64.

Uhl, D., Traiser, C., Griesser, U., Denk, T., 2007a. Fossil leaves as palaeoclimate proxies in the Palaeogene of Spitsbergen (Svalbard). Acta Palaeobot. 47, 89–107.

Uhl, D., Klotz, S., Traiser, C., Thiel, C., Utescher, T., Kowalski, E., Dilcher, D.L., 2007b. Cenozoic paleotemperatures and leaf physiognomy- a European perspective. Palaeogeogr. Palaeoclimatol. Palaeoecol. 248, 24–31.

Utescher, T., Djordjevic-Milutinovic, D., Bruch, A., Mosbrugger, V., 2007a. Palaeoclimate and vegetation change in Serbia during the last 30 Ma. Palaeogeogr. Palaeoclimatol. Palaeoecol. 253, 141–152.

Utescher, T., Erdei, B., François, L., Mosbrugger, V., 2007b. Tree diversity in the Miocene forests of Western Eurasia. Palaeogeogr. Palaeoclimatol. Palaeoecol. 253, 226–250.

Utescher, T., Mosbrugger, V., Ivanov, D., Dilcher, D.L., 2009a. Present-day climatic equivalents of European Cenozoic climates. Earth Planet. Sci. Lett. 284, 544–552.

Utescher, T., Ivanov, D., Harzhauser, M., Bozukov, V., Ashraf, A.R., Rolf, C., Urbat, M., Mosbrugger, V., 2009b. Cyclic climate and vegetation change in the late Miocene of Western Bulgaria. Palaeogeogr. Palaeoclimatol. Palaeoecol. 272, 99–114.

Utescher, T., Böhme, M., Mosbrugger, V., 2011a. The Neogene of Eurasia: spatial gradients and temporal trends-the second synthesis of NECLIME. Palaeogeogr. Palaeoclimatol. Palaeoecol. 304, 196–201.

Utescher, T., Bruch, A.A., Micheels, A., Mosbrugger, V., Popova, S., 2011b. Cenozoic climate gradients in Eurasia — A palaeo-perspective on future climate change? Palaeogeogr. Palaeoclimatol. Palaeoecol. 304, 351–358.

Utescher, T., Böhme, M., Hickler, T., Liu, Y., Mosbrugger, V., Portmann, F., 2013. Continental climate and vegetation patterns in North America and Western Eurasia before and after the closure of the central American seaway. In: GSA 125th Anniversary Annual Meeting, 7. Geological Society of America, Denver 45, p. 302.

Utescher, T., Bruch, A.A., Erdei, B., François, L., Ivanov, D., Jacques, F.M.B., Kern, A.K., Liu, Y., Mosbrugger, V., Spicer, R.A., 2014. The coexistence approach. Theoretical background and practical considerations of using plant fossils for climate quantification. Palaeogeogr. Palaeoclimatol. Palaeoecol. 410, 58–73.

Utescher, T., Bondarenko, O.V., Mosbrugger, V., 2015. The Cenozoic cooling continental signals from the Atlantic and Pacific side of Eurasia. Earth Planet. Sci. Lett. 415, 121–133.

Vu, T.T.A., Horsfield, B., Mahlstedt, N., Schenk, H.J., Kelemen, S.R., Walters, C.C., Kwiatek, P.J., Sykes, R., 2013. The structural evolution of organic matter during maturation of coals and its impact on petroleum potential and feedstock for the deep biosphere. Org. Geochem. 62, 17–27.

Ward, C.R., 2002. Analysis and significance of mineral matter in coal seams. Int. J. Coal Geol. 50, 135–168.

Ward, C.R., 2016. Analysis, origin and significance of mineral matter in coal: an updated review. Int. J. Coal Geol. 165, 1–27.

Ward, C.R., Corcoran, J.F., Saxby, J.D., Read, H.W., 1996. Occurrence of phosphorus minerals in Australian coal seams. Int. J. Coal Geol. 30, 185–210.

Whateley, M.K.G., Tuncali, E., 1995. Quality variations in the high-sulphur lignite of the Neogene Beypazari Basin, Central Anatolia, Turkey. Int. J. Coal Geol. 27, 131–151.

Weber, P.A., Skinner, W.M., Hughes, J.B., Linsday, P., Moore, T.A., 2006. Source of Ni in coal mine acid rock drainage, West Coast, New Zealand. Int. J. Coal Geol. 67, 214–220.

Whateley, M.K.G., Querol, X., Fernández-Turiel, J.L., Tuncali, E., 1996. Zeolites in Tertiary coal from the Çayirhan mine, Beypazari, Turkey. Mineral. Deposita 31, 529–538.

Wilkins, R.W.T., George, S.C., 2002. Coal as a source rock for oil: a review. Int. J. Coal Geol. 50, 317–361.

Xu, N., Finkelman, R.B., Xu, C., Dai, S., 2020. What do coal geochemistry statistics really mean? Fuel 267, 117084.

Yavuz, N., Culha, G., Demirer, Ş.S., Utescher, T., Aydın, A., 2017. Pollen, ostracod and stable isotope records of palaeoenvironment and climate: Upper Miocene and Pliocene of the Çankırı basin (Central Anatolia, Turkey). Palaeogeogr. Palaeoclimatol. Palaeoecol. 467, 149–165.

Yudovich, Ya.E., Ketris, M.P., 2006. Selenium in coal: a review. Int. J. Coal Geol. 67, 112–126.

Zdravkov, A., Stefanova, M., Worobiec, E., Bechtel, A., Marinov, S., Kortenski, J., 2020. International Journal of Coal Geology Implications for peat formation in Maritsa-West Basin, SE Bulgaria: insights from organic petrology, palynology and biomarker assemblage. Int. J. Coal Geol. 222, 103447.

Zhao, L., Ward, C.R., French, D., Graham, I.T., 2012. Mineralogy of the volcanic-influenced Great Northern coal seam in the Sydney Basin, Australia. Int. J. Coal Geol. 113, 94–110.

Zhou, Y., Bohor, B.F., Ren, Y., 2000. Trace element geochemistry of altered volcanic ash layers (tonsteins) in late Permian coal-bearing formations of eastern Yunnan and western Guizhou Provinces. China. Int. J. Coal Geol. 44, 305–324.

Zieger, L., Littke, R., 2019. Bolsovian (Pennsylvanian) tropical peat depositional environments: the example of the Ruhr Basin, Germany. Int. J. Coal Geol. 211, 103209.